AN ANALYTICAL FRAMEWORK TO PRICE LONG-DATED CLIMATE-EXPOSED ASSETS

PAULINE CHIKHANI AND JEAN-PAUL RENNE

ABSTRACT. This paper uses a tractable stochastic integrated-assessment model to analyze the influence of climate change on asset returns across time and maturity. Analytical formulas allow to price various long-dated assets, including fixed-income products, derivatives, and equities. We find that climate risks will increasingly drive down long-term risk-free yields, reducing them by about 40 basis points by the end of the century, reflecting lower growth and increased uncertainty. We illustrate the concept of climate risk premiums—the excess returns asked by investors exposed to climate risks—by examining model-implied prices of long-term assets vulnerable to sea level rise or temperatures. Climate risk premiums are particularly sensitive to damage assumptions.

JEL: Q54, C32, E43, G12, H43.

Keywords: Integrated Assessment Model, term structure model, temperature risk premium, climate linkers.

This version: December, 2023.

Renne: University of Lausanne, Quartier Chamberonne, CH-1015 Lausanne, Switzerland (email: jean-paul.renne@unil.ch); Chikhani: University of Lausanne (email: pauline.chikhani@unil.ch). This paper has circulated under two other titles: "Climate Linkers: Rationale and Pricing," and "Pricing Climate Linkers." We are grateful to Stefano Battiston, Heiner Beckmeyer (discussant), Darrell Duffie, Adrian Fernandez-Perez, Aleksandra Friedl, Stefano Giglio, Elise Gourier, Patrick Grüning (discussant), Christian Gouriéroux, Christian Heyerdahl Larsen (discussant), Larry Kotlikoff, Hanno Lustig, Alain Monfort, Sarah Mouabbi, Marcelo Ochoa, Riccardo Rebonato, Guillaume Roussellet, Julien Royer (discussant), Patrick Saner, Simon Scheidegger, Chris Smith, James Stock, Roméo Tédongap, Dieter Wang, and Frederica Zeni (discussant) for useful comments. We also thank seminar participants at the 11th RCEA Money-Macro-Finance Conference, the 2021 ACFR-AUT Derivative Markets Conference, the 7th Annual Volatility Institute Conference at NYU Shanghai, the Virtual Seminar on Climate Economics, the 15th Financial Risks International Forum, the 8th International Symposium on Environment and Energy Finance Issues (ISEFI 2022), the 2022 North America Summer Meeting of the Econometric Society, the 2022 Annual meeting of the Society for Financial Econometrics, the 3rd Long-Term Investors Banca d'Italia Workshop, the Sciences Po 1st Summer Workshop in Sustainable Finance, the University of Zurich Workshop on Climate Economics, the 11th Bundesbank term structure workshop, the 2022 AFFI annual meeting, the 2023 IBEFA meeting (ASSA), the 2023 King's College London Climate Finance Workshop, and seminars at EDF R&D, McGill university (brownbag), ECON-GSW, ACPR, CIRED, the Federal Reserve Board Climate-related Risks, the Economy, and financial STability (CREST virtual brown bag), e-axes forum. We hereby declare that we have no known competing financial interests or personal relationships that could have appeared to influence the work reported in this paper. R codes for full reproduction of results are available here; a web interface is available here.

1. Introduction

Climate change introduces a pervasive and multifaceted set of challenges that impact virtually every sector of the global economy. It poses a profound risk to long-term assets, threatening the value and sustainability of investments over extended periods. Increasing environmental volatility and the fast-evolving awareness of investors regarding climate risks are reshaping the financial landscape, necessitating a fundamental reevaluation of how long-term assets are priced.

We develop a modeling framework aimed to price long-dated assets whose payoffs are exposed to climate risk. Whereas it captures complex interactions between climate and macroeconomic variables, our sea-level-augmented Integrated Assessment Model (IAM) is solved instantaneously and offers quasi-analytical pricing formulas for various financial instruments (bonds, stocks, derivatives).[1] In particular, to the best of our knowledge, this paper is the first to propose analytical formulas for long-term interest rates in the context of a stochastic Integrated Assessment Model (IAM).

The model tractability hinges on the properties of affine processes (see, e.g., Duffie, 1996; Duffie et al., 2003; Piazzesi, 2010), that are extensively used in the asset pricing literature. Tractability is also key at the calibration stage. Indeed, the availability of closed-form solutions for first- and second-order moments of state variables (such as temperature and sea levels in 2100) enables us to align the model with the current evaluation of the climate trajectory and its linked economic consequences, both in terms of expectations and uncertainty. Let us take three examples. Firstly, our model takes into account non-industrial emissions of carbon into the atmosphere due to permafrost thaw; we parameterize a dedicated process to match the current expectation (consensus) and variance (uncertainty) regarding these specific emissions, for a given horizon (2100). Second, we make the model consistent with the 2100 expectations of sea level rise (SLR) and damages conditional on different temperature

[1] By "quasi-analytical formula", we mean recursive formula: to get the price of assets of maturity h, you need to have computed it for maturity $h-1$.

anomalies ($+2°$C and $+4°$C). Third, we constrain the model to match a targeted level of uncertainty associated with temperature in 2100.[2,3] This type of calibration approach would be formidably demanding in the context of standard IAMs, whose resolution is not immediate, and where the evaluation of conditional moments is not analytical.

We find that climate risks will exert downward pressure on long-term real yields over the coming decades: in our base calibration, climate risks lead to a decrease in the 10-year rate of around 40 basis points. Slightly less than half of this effect is due to risk premiums; the remainder is due to lower expected growth. If inflation is positively affected by climate-related damage, there will be relatively less downward pressure on nominal interest rates, due to higher inflation expectations (as damage increases) and higher inflation risk premiums. We also look into the effects of climate risks on the valuation of bonds and equities of companies with different exposures to climate risks, and for the valuation of coastal real estate.

We use our model as a laboratory to examine climate risk premiums, which are those price components that would not exist if agents were not risk-averse or if it was possible to diversify climate risks. As a rule, a model recognizes the existence of risk premiums as soon as it entails risk-neutral—or risk-adjusted—distributions that do not coincide with their physical counterparts. Our framework allows for the derivation of the two types of distributions. We find, for instance, that the risk-neutral distributions of temperature are shifted to the right with respect to their physical counterparts. This points to the existence of positive temperature risk premiums. Our results show that this premium would be larger if there was no exogenous technological uncertainty, and lower in the absence of damage or permafrost-related uncertainty. Indeed, two forces push the temperature risk premium in opposite directions: (i) everything else equal, an increase in the uncertainty about exogenous technological progress augments the correlation between temperature and consumption since (ex-damage) consumption positively depends on capital, whose production generates carbon emissions; this tends to generate a negative correlation between temperatures and marginal utility (or

[2]The model resolution and price calculation run several orders of magnitude faster than those based on dynamic programming approaches (Cai and Judd, 2014; Cai and Lontzek, 2019; Barnett et al., 2020). For the latter approaches, solving for the model on a single set of parameters is not fast enough to allow for a calibration approach that necessitates solving the model a large number of times.

[3]No grid-based or tree-based approach—subject to the curse of dimensionality—is needed to solve the present model. By way of comparison, Daniel et al. (2019) employ a tree-based approximated solution method in a context where both the number of dates and the number of states are small (seven dates are considered, from 2015 to 2400; each node is followed by two possible states, leading to 2^7 possible states in 2400, and only 4 in 2100).

the stochastic discount factor, SDF); (ii) higher temperatures imply larger damage intensity, which contributes positively to the covariance between temperature and the SDF. Although the channels are not exactly the same, this is reminiscent of the two opposite forces that are at play in the insurance component of the SCC (Dietz et al., 2018; Lemoine, 2021; Giglio et al., 2021): (i) a scaling effect arises under conventional damage specifications, where climate-induced losses increase in consumption because damages affect consumption multiplicatively; in that context, emission reductions increase future consumption by a larger amount when future marginal is high, generating a negative correlation between consumption benefits associated with lower carbon concentrations and the SDF (hence a negative risk premium); (ii) the damage-reduction effect is more intuitive—reducing damage intensity avoids consumption losses, generating a positive correlation between benefits and the SDF.

A concrete implication of temperature risk premiums is that, according to the model, investors would be willing to pay an extra return—akin to an insurance premium—to enter a swap paying realized temperature at maturity; this excess return would be reflected in the difference between the means of the risk-neutral and the physical distributions. The pricing of climate derivatives—such as this temperature swap—provides natural illustrations of climate risk premiums.[4] Consider for instance a (hypothetical) digital temperature option that yields a unit payoff if future temperatures T_{t+h} reach a certain threshold value T_K, say, and zero otherwise. If T_K is high, this option's price incorporates a risk premium reflecting agents' aversion to extreme climate risks; this specific risk premium can be expressed as the difference between the risk-adjusted probability that $T_{t+h} > T_K$ and its physical counterpart. As an example, the physical and risk-neutral probabilities of having a temperature anomaly larger than 4°C in 2100 are respectively of 12% and 18% in our benchmark calibration. This difference in the thickness of the right-hand tails of the physical distribution and the risk-neutral one can be seen as an extreme-temperature risk premium.

Pricing long-dated assets amounts to computing (risk-adjusted) expectations of functions of the state vector at long horizons. In the vast majority of stochastic IAMs, the analytical computation of such expectations is out of reach and necessitates Monte-Carlo simulations. While the computational time required to calculate one long-term price using simulations is

[4] To date, instruments traded on weather-derivative markets have short maturities (typically a few months) and focus on specific regional areas (Cao and Wei, 2004; Bloch et al., 2010, 2011; Little et al., 2015; Schlenker and Taylor, 2021). In contrast, our analysis pertains to long-dated instruments and to global risks.

not necessarily prohibitive, it can become so if the price needs to be calculated many times, for example as part of a sensitivity analysis, or because one wishes to calibrate the model to match certain prices. Maybe more importantly, relying on simulations to price long-dated assets may be misleading in contexts where these prices may not exist (i.e., are infinite), which may happen in the context of IAM featuring catastrophic events (Weitzman, 2009).[5] Unlike pricing approaches based on simulations, those benefiting from analytical solutions make it possible to directly detect situations characterized by infinite prices. Importantly, this type of issue is not limited to pricing. It may also arise at the solution stage, where the computation of conditional expectations is needed to determine the value function—as is typically the case with Epstein-Zin or other recursive preferences. Related problems may occur if the solution approach is not based on Monte-Carlo simulations but on grid-based techniques: when a model has fat-tailed distributions, grid-based solutions may depend heavily on the choices of grid endpoints (even if the probability of draws beyond these endpoints is extremely low).[6]

The remainder of this paper is organized as follows. Section 2 reviews the literature to which this paper is linked. Section 3 outlines our modeling framework. Section 4 presents analytical pricing formulas and illustrates them in the context of numerical examples. Section 5 concludes. Appendix A describes useful properties of the γ_0 distribution of Monfort et al. (2017), which is intensively used to capture uncertainty in our framework. Appendix B

[5] As an illustration, consider a representative agent featuring time-separable CRRA utility, which implies that the stochastic discount factor between dates t and $t+1$ is given by $\mathcal{M}_{t,t+1} = \exp(-\gamma \Delta c_{t+1})$, where γ is the coefficient of relative risk aversion, and Δc_t denotes log consumption growth. Assume that $\Delta c_t = \mu - D_t$, where $\mu > 0$ and D_t captures disastrous events drawn from a gamma distribution of mean m and of variance v. In this economy, the price of a one-period bond, i.e. $\mathbb{E}_t(\mathcal{M}_{t,t+1})$, does not exist as soon as $\gamma > m/v$. While this is easily seen from the moment generating function of the gamma distribution, it may be overlooked if one uses simulations to price this bond. Indeed, even based on a very large number of draws of $\exp(\gamma D_{t+1})$, it is difficult to detect the nonexistence of the mean of this random variable. Take the following calibration: $\mu = 5\%$, $m = 0.5\%$, $\sqrt{v} = 5\%$, and $\gamma = 2.5$. In that situation, the bond price does not exist because $\gamma > m/v = 2$. Nevertheless, one can draw values of $\mathcal{M}_{t,t+1}$ in its distribution and compute sample means. In this example, 90% of the means of $\mathcal{M}_{t,t+1}$ based on samples of length 100 000 are in between 0.91 and 1.05—a set of non-exuberant values. It is for instance likely that, after 100 000 draws, one obtains a sample mean of 0.96, say, which would point to a one-period interest rate of about 4%, while the model-implied interest rate is of $-\infty$. In other words, in this situation, simulations can potentially misguide the researcher, causing her to overlook that the model in question is subject to the "dismal theorem" of Weitzman (2009).

[6] Papers using numerical methods (grids) to solve for an Epstein-Zin-based IAM include Cai and Lontzek (2019) and Daniel et al. (2019). Van den Bremer and Van der Ploeg (2021) use a perturbation method; they show that this method results in satisfactory approximations when damages are relatively small, typically of a few percentage points of GDP.

provides a comprehensive view of the model's equations. Appendix C contains additional tables and figures. Proofs, details regarding the calibration, and additional results are gathered in the supplemental appendix.

2. LITERATURE REVIEW

Our research relates to the literature investigating the pricing of climate risks. A large share of the theoretical literature is concerned with the computation of the Social Cost of Carbon (SCC), defined as the marginal value of emission reductions (e.g., Weitzman, 2013). Uncertainty and aversion to ambiguity are found to have profound implications on the SCC calculations (e.g., Cai and Lontzek, 2019; Barnett et al., 2020; Van den Bremer and Van der Ploeg, 2021). While the present paper focuses on the pricing of various financial instruments, we also examine the SCC resulting from our model. Our baseline estimate, of \$191 per ton of CO_2, is relatively high compared to average values found in the literature (see Table 2). Such a high value is however consistent with recent studies with a strong focus on uncertainty (e.g., Daniel et al., 2019; Lemoine, 2021; Traeger, 2023).

The empirical literature on the influence of climate risks for asset pricing is rapidly growing. Several articles assess the relative value of green or environmental, social, and governance (ESG) bonds, pointing to small premiums to otherwise similar ordinary bonds (Baker et al., 2018; International Monetary Fund, 2019; Larcker and Watts, 2020; Pástor et al., 2022). Other studies look for market price evidence of climate risk premiums: Huynh and Xia (2020) find that corporate bonds whose value tend to increase when bad news about the climate occur trade at a premium; Painter (2020) shows that long-dated municipal bond yields are higher for counties with large expected losses due to sea level rise. Several studies employ climate projections and simulate the expected effects on asset prices: Klusak et al. (2023) and Zenios (2022) simulate the effect of climate change on sovereign credit ratings; both studies find scenario-based evidence of climate-induced sovereign downgrades in the coming decades, in line with the predictions of Mallucci (2022)'s structural model. Bernstein et al. (2019) and Baldauf et al. (2020) document the negative effect of SLR exposure on residential real estate prices; Goldsmith-Pinkham et al. (2023) highlight the importance of uncertainty in the way future climate risk propagates into current price movements. Since investors

have been considering climate risk for a relatively short period of time, quantitative estimates of climate risk premiums based on (short) historical samples should be taken with caution (Giglio et al., 2020; Pástor et al., 2022). After having constructed a climate-news index, Engle et al. (2020) propose an approach to dynamically hedge the associated risks using stocks-based factor-mimicking portfolios. Andersson, Bolton, and Samama (2019) show that one can closely track leading equity indices with portfolios featuring a carbon footprint 50% smaller than the benchmark.

The present paper is particularly close to those studies that investigate asset pricing in the context of stochastic integrated assessment models (IAMs). In this literature, some studies rely on models whose tractability is obtained by simplifying the climate block of the Dynamic Integrated Climate-Economy model (DICE) of Nordhaus (1992) (e.g. Bansal et al., 2016, 2019; Karydas and Xepapadeas, 2022). Other studies employ standard DICE-related IAMs and look for feasible numerical pricing solutions (e.g., Daniel et al., 2019; Barnett et al., 2020). We manage to combine approximate DICE-type equations and closed-form pricing solutions. This is achieved by making the state variables' dynamics depend on combinations of deterministic and stochastic components. The stochastic components are such that the conditional Laplace transform of the state vector is affine in its past values—in a time-dependent but deterministic fashion. In that sense, the model is affine conditionally on exogenous deterministic processes. This is also the case of the Analytic Climate Economy (ACE) model of Traeger (2023). Our model however differs from the latter along several dimensions; in particular, our model features (a) a feedback loop aimed to capture risks associated with permafrost-related carbon releases, (b) sea level, whose rise generates specific damages, (c) mitigation opportunities.[7] In addition, what we consider the main contribution of this paper is to show how to exploit an affine IAM to analytically derive conditional distributions—and therefore moments—of climate variables, paving the way for rapid pricing and calibration.

3. Model

3.1. **Overview of the model.** Like any integrated assessment model (IAM), our model aims to capture the relationship between the climate and the economy. Figure 1 synthesizes these interactions: a representative agent uses capital to produce a good that she can consume or

[7] In the model, agents cannot dynamically adjust the trajectory of investment in the mitigation technology; instead, they decide on this trajectory, once and for all, at the initial date. See Subsection 3.3 for more details.

invest in the productive capital; the good can also be used by a technology that mitigates the carbon emissions resulting from the production process. Carbon emissions affect temperatures. High temperatures damage productive capital. Subsections 3.2 and 3.3 highlight key features of the climate and economic blocks, respectively.

FIGURE 1. Schematic representation of the model

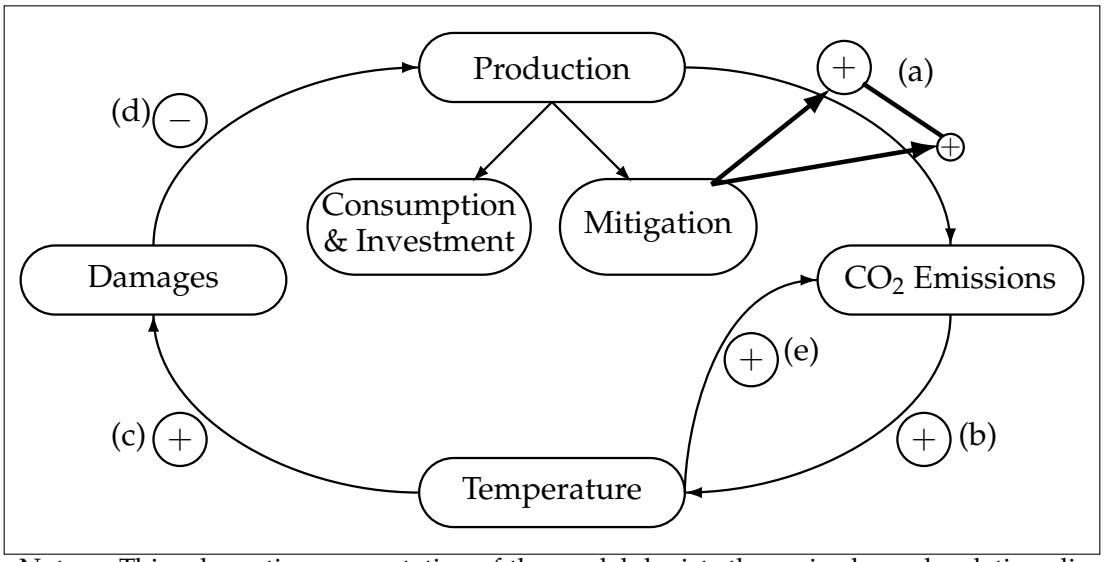

Note — This schematic representation of the model depicts the main channels relating climatic and economic variables. (a): Production increases emissions, but mitigation helps to reduce the positive relationship between the two. (b): Emissions increase temperature anomaly. (c): Larger temperatures increase the probability of agent's being hit by climate-driven damages. (d): Damages negatively impact production through a reduction in the quality of capital. (e): Temperature raises emissions by increasing the probability of triggering a climate change feedback loop (triggered, e.g., by releasing tons of methane trapped in the permafrost).

3.2. **Climate block.** Temperatures are expressed as temperature anomalies from a baseline period.[8] As in the DICE2016 model, we focus on two global temperatures: lower ocean (T_{LO}) and atmosphere (T_{AT}). The dynamics of these two temperatures depends on radiative forcings due to greenhouse gases (F): Earth receives radiant energy from the Sun and emits some energy back into space; at equilibrium, Earth should absorb as much radiant energy as it radiates out of our atmosphere; the difference between the two is radiative forcings. When

[8]Consistently with the formulation of the Paris Agreement's objectives, we use the 1850-1900 baseline period as an approximation of the pre-industrial period.

the latter goes up, absorption increases, and the Earth warms.[9] Specifically, we have:

$$\mathbb{E}_{t-1}(T_{AT,t}) = T_{AT,t-1} + \xi_1 \left(F_{t-1} - \frac{\tau}{\nu} T_{AT,t-1} - \xi_2 \left[T_{AT,t-1} - T_{LO,t-1} \right] \right), \tag{1}$$

where $\mathbb{E}_{t-1}$ denotes the expectation based on the information available on date $t-1$, which we denote by $\mathcal{I}_{t-1}$ (i.e., $\mathbb{E}_{t-1}(T_{AT,t}) = \mathbb{E}(T_{AT,t}|\mathcal{I}_{t-1})$). In standard IAMs, (1) is considered to be deterministic, in the sense that $\mathbb{V}ar_{t-1}(T_{AT,t}) = 0$. By contrast, in order to capture the uncertainty surrounding the temperature's law of motion, we assume that $T_{AT,t}$ is partly random conditional on the past. Specifically:

$$T_{AT,t}|\mathcal{I}_{t-1} \sim \textit{ i.i.d. } \gamma_0 \left(\lambda_{T,t}, \mu_T \right), \quad \text{with} \quad \lambda_{T,t} = \frac{1}{\mu_T} \mathbb{E}_{t-1}(T_{AT,t}), \tag{2}$$

where $\mathbb{E}_{t-1}(T_{AT,t})$ is given in (1), and where γ_0 is the gamma-zero distribution introduced by Monfort et al. (2017). Appendix A outlines the properties of this distribution. Note that (2) is consistent with (1) since the mean of a $\gamma_0(\lambda, \mu)$ distribution is $\lambda\mu$. Another γ_0 property implies that $\mathbb{V}ar_{t-1}(T_{AT,t}) = 2\mu_T \mathbb{E}_{t-1}(T_{AT,t})$. Hence, μ_T characterizes the uncertainty associated with the temperature dynamics. (In particular, we are back to the deterministic case if $\mu_T \approx 0$.)

We could potentially use γ_0 distributions in each of our climate equation, adding one "μ" parameter per equation. This would however complicate the calibration approach since the literature does not provide us with measures of uncertainty characterizing each specific equation of the model. Instead, we rely on four γ_0 distributions to capture four broad uncertainties regarding: (a) the temperature dynamics (eq. 2),[10] (b) damages, (c) permafrost-related carbon release, and (c) sea level rise.

According to (1) and (2), the date-t atmospheric temperature depends on its lagged value ($T_{AT,t-1}$), on the lagged lower-ocean temperature ($T_{LO,t-1}$), and on the lagged radiative forcings (F_{t-1}). In turn, lower-ocean temperature evolves according to:

$$T_{LO,t} = T_{LO,t-1} + \xi_3 \left(T_{AT,t-1} - T_{LO,t-1} \right), \tag{3}$$

[9] See, e.g., Ramaswamy et al. (2001) for a discussion of the relationship between global temperatures and radiative forcings.

[10] This includes, e.g., the uncertainty regarding the so-called climate sensitivity parameter, which characterizes the equilibrium warming response to a doubling of preindustrial CO_2 concentrations (e.g., Macdougall et al., 2017; Barnett et al., 2020). This parameter (τ) only appears in (4); however, substituting for F_{t-1} in (1) (that itself appears in eq. 2) shows that the uncertainty captured by the γ_0 distribution may encompass the one surrounding τ.

and radiative forcings follow:

$$F_t = \underbrace{\tau \log_2(m_0) + \frac{\tau}{\log(2) m_0}\left(\frac{M_{AT,t}}{M_{PI}} - m_0\right)}_{\approx \tau \log_2\left(\frac{M_{AT,t}}{M_{PI}}\right)} + F_{EX,t}, \tag{4}$$

where $F_{EX,t}$ is the (exogenous) part of radiative forcings that is due to non-CO_2 greenhouse gases, $M_{AT,t}$ is the mass of carbon in the atmosphere, and M_{PI} is its preindustrial level. While (4) is not linear in standard IAMs, Supplemental Appendix VI.1 demonstrates that the previous first-order approximation is satisfactory for plausible values of future carbon concentrations. (In eq. 4, m_0 is the value of $M_{AT,t}/M_{PI}$ at which the linearization is performed.)

The atmospheric carbon mass $M_{AT,t}$ appearing in (4) constitutes one of the three reservoirs used to synthesize the carbon cycle. This cycle determines the journey of all carbon atoms on earth:[11] a loop between atmosphere, land, and ocean. We denote by M_t the vector whose components are the carbon masses in atmosphere (AT), upper ocean (UP), and lower ocean (LO). The carbon cycle is modeled as follows:

$$M_t = \begin{bmatrix} M_{AT,t} \\ M_{UP,t} \\ M_{LO,t} \end{bmatrix} = \varphi^{\Delta t} M_{t-1} + \frac{\Delta t}{3.666} \begin{bmatrix} \mathcal{E}_{t-1} \\ 0 \\ 0 \end{bmatrix}, \tag{5}$$

where φ is a square matrix describing yearly transfers of carbon between atmosphere and oceans. (The column components of φ sum to one, see eq. 37 in Appendix B.1.) $\mathcal{E}_t$ is the carbon dioxide (CO_2) emitted into the atmosphere, on average, for each year of period t (one period lasts $\Delta t = 5$ years), converted into carbon masses by applying the conversion rate $1/3.666$. Total emissions are the sum of three components::

$$\mathcal{E}_t = \mathcal{E}_{Land,t} + \mathcal{E}_{Ind,t} + N_t, \tag{6}$$

where $\mathcal{E}_{Ind,t}$ are industrial emissions due to human activity, assumed to grow at the same pace as capital (see Appendix B.2.2), $\mathcal{E}_{Land,t}$ represents an exogenous component including, in particular, emissions due to deforestation, and N_t accounts for carbon releases that are endogenous but do not directly stem from the production process. The latter variable intends to

[11] The main greenhouse gases containing carbon are also the most active in the atmosphere: carbon dioxide (CO_2) and methane (CH_4).

capture feedback effects documented in the literature on tipping points (Lenton et al., 2008). Tipping points stem from the existence of feedback loops in our environment; they underlie arrows (b)↔(e) in Figure 1.[12,13] A positive feedback loop amplifies the positive imbalances in radiative forcings by creating a vicious circle strengthening global warming. Examples of positive feedback loops include the release of hundred of gigatons of methane trapped in the permafrost and in ice lattices in the shallow ocean, the acidification of oceans, the melting of the Greenland ice sheet, or the weakening of the Atlantic thermohaline circulation. If one of these loops is triggered, the probability of triggering the next one jumps, giving rise to tipping point mechanisms (Lemoine and Traeger, 2014, 2016; Steffen et al., 2018; Dietz et al., 2020).

Our framework focuses on feedback loops involving emissions of non-production-based greenhouse gazes (N_t in eq. 6), foremost among which are those linked to permafrost. These emissions are assumed to be drawn from a second γ_0 distribution (as in eq. 2):

$$N_t|\mathcal{I}_{t-1} \sim \gamma_0\left(\lambda_{N,t}, \mu_N\right), \quad \text{with} \quad \lambda_{N,t} = \frac{\kappa_N^{t-1}}{\mu_N}\left(a^{(N)} + b^{(N)} T_{AT,t-1}\right). \tag{7}$$

We impose that $0 \leq \kappa_N < 1$, which ensures that N_t goes to zero in the long run, and that $\lim_{t\to\infty} N_1 + \ldots N_t$ does not diverge, consistently with the fact that the carbon trapped in permafrost is not in infinite supply. As for (2), μ_N characterizes the uncertainty associated with N_t.

We augment the model with global mean sea level, which we denote by H_t. It is assumed to evolve as follows:

$$H_t - H_{t-1}|\mathcal{I}_{t-1} \sim \textit{ i.i.d.}\, \gamma_0\left(\lambda_{H,t}, \mu_H\right), \quad \text{with} \quad \lambda_{H,t} = \frac{1}{\mu_H}\left(a^{(H)} + b^{(H)} T_{AT,t-1}\right). \tag{8}$$

This specification is a stochastic extension of semi-empirical approaches *à la* Rahmstorf (2007), which aim to exploit the link between global sea level and global temperature in past observational data for projecting the future.[14] While the dynamic relationship between sea level

[12]Earth is composed of an unknown number of feedback loops, positive or negative. Negative feedback loops decrease the pressure on global warming by absorbing greenhouse gases from the atmosphere.

[13]While our modeling of feedback loops accommodates sudden and large effects, with highly persistent adverse effects, it does not feature an explicit threshold as in, e.g., Lemoine and Traeger (2014, 2016); Bansal et al. (2016); Taconet et al. (2021).

[14]See Rahmstorf et al. (2012) for an evaluation of semi-empirical approaches. Studies investigating the relationship between temperatures and sea level include, among others, Rahmstorf (2007), Rahmstorf (2010), Kopp et al. (2016), and Mengel et al. (2018).

and temperature is usually expressed in a deterministic fashion, our γ_0-based specification introduces uncertainty in the process. The amount of uncertainty underlying the process is captured by μ_H; if the latter is infinitely small, (8) boils down to the deterministic specification used, e.g., by Rahmstorf (2007), i.e., $H_t = H_{t-1} + a^{(H)} + b^{(H)} T_{AT,t-1}$.

3.3. **Economic block.** We consider a production economy where capital quality can be damaged by climatic disasters. On each period, agents allocate production (Y_t) between consumption (C_t), investment in productive capital (Inv_t), and investment in low carbon emissions technologies (Ψ_t):[15]

$$Y_t = C_t + Inv_t + \Psi_t. \tag{9}$$

Production Y_t results from AK technology:

$$Y_t = A_t K_t, \quad \text{with } A_t = \bar{A} + \sigma_A \eta_{A,t}, \tag{10}$$

where A_t and K_t are productivity and productive capital, respectively. $\bar{A}$ is the average productivity, and $\eta_{A,t} \sim i.i.d. \mathcal{N}(0,1)$ is a productivity shock.[16] The dynamics of productive capital are governed by:

$$K_t^* = (1 - dep) K_{t-1} + Inv_t, \tag{11}$$

$$K_t = \exp(-D_t - b_{SK} \Delta H_t) K_t^*, \tag{12}$$

where dep is the depreciation rate, D_t (≥ 0) represents climatic disasters, and $b_{SK} \Delta H_t$ corresponds to destruction of capital due to sea level rise (SLR).[17] As in Gomes, Grotteria, and Wachter (2019), and Miller, Paron, and Wachter (2020), K_t^* represents "planned capital." Productive capital K_t is smaller than K_t^* when climatic disasters occur ($D_t > 0$) and when sea

[15] We assume that agents perfectly observe the climate state (as described in the previous subsection) on each date t; we don't explicitly model the incentives agents may have to improve their knowledge of the climate system as in, e.g., Aliakbari and McKitrick (2018).

[16] The model we present in the main text features a single i.i.d. Gaussian shock ($\eta_{A,t}$). The supplemental appendix presents a general version of the model where $\eta_{A,t}$ is one component of a vector η_t, that follows a Gaussian vector autoregressive process. Hence, the components of η_t can be persistent and cause each other. These components can be easily introduced in the different equations of the model. Typically, we could have two components in A_t: a volatile one (i.e., serially-uncorrelated, like $\eta_{A,t}$), and a second persistent one (following, e.g., an autoregressive process).

[17] SLR stands as one of the most critical climate change's dangers (e.g., Hauer et al., 2016; Desmet et al., 2021).

level rises ($\Delta H_t > 0$). Under (10) to (12), production is persistently affected following climate-related disasters and SLR. The former are drawn from a γ_0 distribution:

$$D_t|\mathcal{I}_{t-1} \sim \ i.i.d.\ \gamma_0\left(\lambda_{D,t}, \mu_D\right), \quad \text{with} \quad \lambda_{D,t} = \frac{1}{\mu_D}\left(a^{(D)} + b^{(D)} T_{AT,t-1}\right), \tag{13}$$

where $\lambda_{D,t}$ is the disaster intensity. According to the properties of this distribution (eq. 33 in Appendix A), the probability of having $D_t > 0$ is equal to $1 - \exp(-\lambda_{D,t})$. When the disaster intensity is small, this probability is close to $\lambda_{D,t}$.

Hence, increasing industrial emissions pushes temperatures upwards (eqs. 2 to 5), which increases disaster intensity (eq. 13) and, in turn, affects production (eqs. 10 to 12). This adverse mechanism prompts agents to invest in low-carbon technologies. Investing in these technologies reduces the emissions from producing one unit of goods by a factor μ_t, called mitigation rate (with $0 \leq \mu_t \leq 1$). Increasing μ_t is costly. As in the DICE, we posit that associated abatement costs (Ψ_t in eq. 9) are given by:

$$\Psi_t = \Lambda_t Y_t, \quad \text{with } \Lambda_t = \mu_t^{\theta_2} BC_t, \tag{14}$$

where BC_t deterministically decreases through time, reflecting technological progress. The term $\mu_t^{\theta_2}$ captures the fact that, on a given date, the marginal cost of mitigation is increasing (when $\theta_2 > 1$).

Our representative agents face the following trade-off: investing in mitigation reduces long-term risks—making disasters less likely—but comes at the cost of lowering immediate consumption. Their decision regarding how to allocate output between mitigation (Ψ_t), investment in productive capital (Inv_t), and consumption (C_t) depends on their preferences, which we take of the Epstein-Zin-Weil type (see Appendix B.2.3).[18] These preferences allow to dissociate risk aversion and the elasticity of intertemporal substitution (EIS). To facilitate resolution, we set the latter to 1 (Piazzesi and Schneider, 2007).[19]

[18] Epstein-Zin-Weil preferences (Epstein and Zin, 1989; Weil, 1989), or, more generally, recursive preferences, are widely used to capture equity and bond risk premiums (Bansal and Yaron, 2004). These preferences have been used in numerous recent IAMs (Cai and Lontzek, 2019; Jensen and Traeger, 2014; Lemoine and Traeger, 2014).

[19] In an IAM context, Hambel, Kraft, and Schwartz (2021) also work under the assumption of a unit EIS. This value is however slightly below the lower bound of the 90% confidence interval found by Schorfheide et al. (2018). Daniel, Litterman, and Wagner (2019) take an EIS of 0.9.

To get instant results, we simplify the agents' optimization problem. While, on each date, agents optimally determine how to allocate output after mitigation ($(1-\Lambda_t)Y_t$) between consumption C_t and investment Inv_t (see eq. 9), they decide the mitigation rate path (μ_t) only once and for all on the initial date, and further commit to that parametric path. More precisely, on date $t=0$, agents consider the following parametric form:

$$\mu_t = \min\left[\exp\left(-\left|\theta_{a,opt}\right| + \left|\theta_{b,opt}\right| \times t\right); 1\right], \quad t > 0, \tag{15}$$

and select $\{\theta_{a,opt}, \theta_{b,opt}\}$ so as to maximize their date-0 utility.[20] The choice of this parametric time function is based on the usual shapes of emission control rates obtained in standard IAMs.[21] Supplemental Appendix VI.2 presents exercises suggesting that the optimal mitigation rate trajectory is only moderately sensitive to our simplification approach based on (i) the use of a parametric form of the mitigation rate trajectory and (ii) the assumption according to which agent do not dynamically optimize.

3.4. **The resulting affine state dynamics.** Solving the model essentially amounts to determining the law of motion of consumption. Supplemental Appendix I.1 shows that the resulting optimal consumption growth path, for any date $t > 0$, is of the form:

$$\Delta c_t = \mu_{c,t} + \sigma_{c,t}\eta_{A,t} - D_t - b_{SK}\Delta H_t, \tag{16}$$

where $\mu_{c,t}$ and $\sigma_{c,t}$ are deterministic functions of the model parameters:

$$\begin{cases} \mu_{c,t} &= \log\delta + \log\Big((1-\Lambda_t)\bar{A} + (1-dep)\Big) \\ \sigma_{c,t} &= \frac{(1-\Lambda_t)}{(1-\Lambda_t)\bar{A}+(1-dep)}\sigma_A, \end{cases} \tag{17}$$

Tractability hinges on the fact that the resulting state vector X_t—which gathers all economic and climatic variables introduced above—is an affine process. Formally, the conditional

[20] In practice, for a given model parameterization, we numerically look for the values of $\theta_{a,opt}$ and $\theta_{b,opt}$ leading to the highest utility on date 0. This numerical optimization has to be performed for each considered set of parameters in the context of the calibration approach (see Subsection 3.5); but it is extremely fast thanks to the existence of an analytical solution to the utility function (Proposition 8 in Supplemental Appendix III.1).

[21] See, e.g., Cai and Lontzek (2019), Figure 2.C. Our resulting path is given in Supplemental Appendix VI.2, where it is compared to the path underlying the 2016 version of the DICE model (Nordhaus, 2017).

Laplace transform of X_t, which characterizes the state vector's dynamics, is of the form:

$$\mathbb{E}_t[\exp(u'X_{t+1})] = \exp[\underbrace{\alpha_t(u) + \beta_t(u)'X_t}_{=\psi_t(u)}], \tag{18}$$

where functions α_t and β_t deterministically depend on the model parameters (see Proposition 2 in Supplemental Appendix II.3). Once functions α_t and β_t are known, simple recursive formulas can be used to deduce the conditional multi-horizon Laplace transform of X_t (Corollary 1). The latter is also exponential affine in X_t, that is:

$$\mathbb{E}_t[\exp(u'X_{t+h})] = \exp[a_{t,h}(u) + b_{t,h}(u)'X_t]. \tag{19}$$

As illustrated by Duffie et al. (2000), the knowledge of the conditional Laplace transform (19) is equivalent to that of the distribution of X_{t+h} conditional on X_t. To the best of our awareness, the present article is the first to propose analytical formulas for evaluating conditional moments and distributions of macroeconomic and climate variables in a stochastic IAM framework. Section 4 shows how this can be exploited to price assets; it is also key at the calibration stage. The latter is outlined in the next subsection; we refer to Supplemental Appendix IV for computational details.

3.5. **Calibration.** Whereas numerous parameters of the model are directly taken from existing literature (in particular from Barrage and Nordhaus, 2023, and Folini et al., 2023, see Table 6), others have not direct equivalent in previous studies; this is notably the case of the parameters governing the positive feedback loops (N_t, eq. 7), economic damages (D_t, eq. 13), or sea level rise (H_t, eq. 8). We calibrate these parameters so as to match "targets" (or conditional moments) for which our framework offers analytical formulas:

(N). The four parameters characterizing N_t's dynamics (μ_N, a_N, b_N, and κ_N) are calibrated to match the following conditional moments: (a) the expectation of the 2100 permafrost-related carbon release ($N_1 + \cdots + N_h$, period h corresponding to 2100) conditional on $T_{AT,h} = 2°\text{C}$, (b) its expectation, but conditional on $T_{AT,h} = 4°\text{C}$, (c) its standard deviation conditional on $T_{AT,h} = 4°\text{C}$, and (d) the expectation of total permafrost-related carbon release conditional on a long-run temperature value ($\widetilde{T}_{AT}$).

(D). The damage specification involves three parameters (μ_D, a_D, and b_D), that are calibrated to match (a) the expectation of 2100 cumulated damages conditional on $T_{AT,h} = 2°\text{C}$,

(b) their expectation conditional on $T_{AT,h} = 4°C$, and (c) their standard deviation conditional on $T_{AT,h} = 4°C$.

(H). The three parameters of the SLR specification (μ_H, a_H, and b_H) are calibrated to match (a) the expectation of the 2100 sea level conditional on $T_{AT,h} = 2°C$, (b) its expectation conditional on $T_{AT,h} = 4°C$, and (c) its standard deviation conditional on $T_{AT,h} = 4°C$.

Table 1 shows the numerical values of the targeted moments and the associated parameters (target sources are given in the caption of the table). Figure 2 proposes a graphical representation of the previous three steps of the calibration.

Moreover, we calibrate $\bar{A}$ and σ_A appearing in (10) so that the average and the standard deviation of pre-damage growth match those computed on per capita real GDP growth over the last 40 years. Another parameter to calibrate is b_{SK}, that determines SLR-related damages (in eq. 12). We set it to 0.1, based on Diaz (2016).[22]

The last step of our calibration approach pertains to μ_T, which characterizes the uncertainty in temperature dynamics (see eq. 2). Once all the other parameters have been calibrated, we determine the value of this parameter so as to obtain a conditional standard deviation of atmospheric temperature in 2100, which we set equal to 0.75°C, which broadly reflects the temperature uncertainty reported in the IPCC AR6 report.[23]

Figures 3 and 4 display, in blue, the resulting model-implied trajectories of atmospheric temperature and global mean sea level, respectively. The plots additionally present confidence intervals for the two variables extending to the year 2100. These intervals have been established analytically, utilizing inverse Fourier transforms that are readily available given the multi-horizon Laplace transfrom of X_t.[24]

[22] More precisely, Diaz (2016) estimates that under optimal adaptation strategies (respectively under the no-adaptation strategy), annual damage and adaptation costs would amount to 0.2% of GDP (respectively 1.5%) in 2100 under RCP8.5, for which global mean SLR would reach about 0.8 meters (see Subsection 3.5 and Figure 2 in Diaz (2016)). Assuming a linear sea-level increase over time, this gives a ΔH of about 0.05 meters for one model period (5 years). That is, for 2100, we would have $0.2\% = b_{SK}\Delta H$ (i.e., $b_{SK} = 0.002/0.05 = 0.04$) in the optimal case and $b_{SK} = 0.015/0.05 = 0.3$ in the no-adaptation case. Our choice of $b_{SK} = 0.1$ puts us closer to the optimal adaption case.

[23] Figure 4.2 of the IPCC AR6 shows that the 90% confidence interval for the 2100 temperature anomaly is of 1.5°C under SSP1-2.6 and of 3.0°C under SSP3-7.0. Using that the width of a 90% confidence interval is equal to 3.3 standard deviations (under Gaussianity), we obtain a standard deviation of about 0.5°C under SSP1-2.6 and of 1°C under SSP3-7.0. We take the average of these two numbers.

[24] $\mathbb{E}_t(\mathbb{1}_{\{a'X_{t+h}\}})$, i.e., the c.d.f. of $a'X_{t+h}$ evaluated at b, and conditional on the information available on date t, can be computed using an expression of the form of that given in (24) (option pricing formula), with $\omega = 0$, and replacing the risk-neutral Laplace transform $\varphi_t^{(h)}$ with its physical counterpart, given in (19).

FIGURE 2. Model calibration

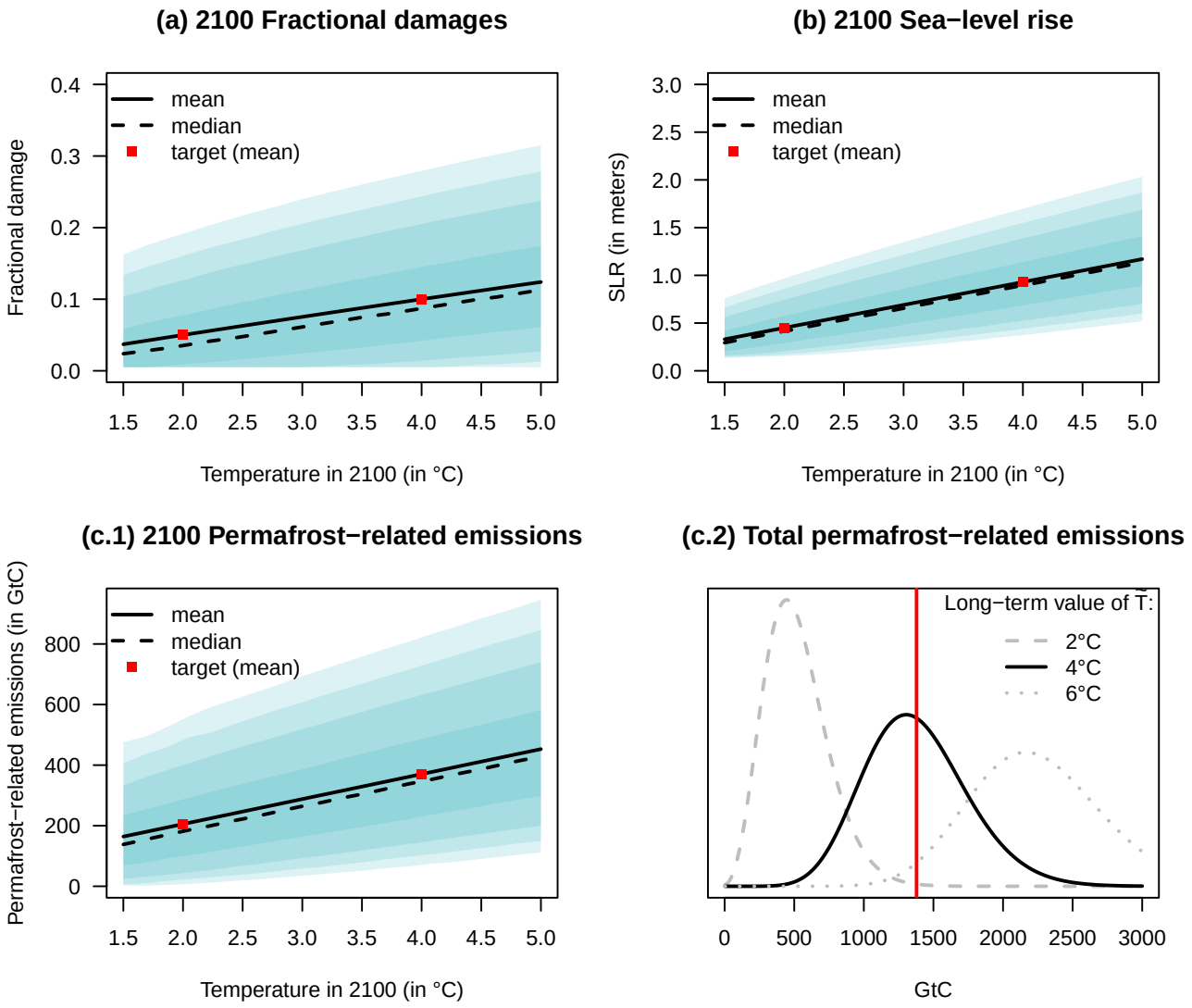

Notes: This figure illustrates the calibration approach by showing the fit of some moments pertaining to economic damages (D_t, eq. 13), sea level rise (H_t, eq. 8), and permafrost-related carbon releases (N_t, eq. 7). The damage specification involves 3 parameters (μ_D, a_D, and b_D), that are calibrated to match (D.i) the expectation of 2100 damages conditional on $T_{AT,h} = 2°C$, (D.ii) the expectation of 2100 damages conditional on $T_{AT,h} = 4°C$, and (D.iii) the 2100 standard deviation of damages conditional on $T_{AT,h} = 4°C$. The two red dots in Panel (a) correspond to (D.i) and (D.ii). The SLR specification involves 3 parameters (μ_H, a_H, and b_H), that are calibrated to match (SLR.i) the expectation of the 2100 sea level conditional on $T_{AT,h} = 2°C$, (SLR.ii) the expectation of the 2100 sea level conditional on $T_{AT,h} = 4°C$, and (SLR.iii) the 2100 standard deviation of sea level on $T_{AT,h} = 4°C$. The two red dots in Panel (b) correspond to (SLR.i) and (SLR.ii). The 4 parameters characterizing N_t's dynamics (μ_N, a_N, b_N, and κ_N) are calibrated to match the following conditional moments: (N.i) the expectation of the 2100 permafrost-related carbon release ($N_1 + \cdots + N_h$, period h corresponding to 2100) conditional on $T_{AT,h} = 2°C$, (N.ii) the same expectation, but conditional on $T_{AT,h} = 4°C$, (N.iii) the standard deviation of the 2100 permafrost-related carbon release conditional on $T_{AT,h} = 4°C$, and (N.iv) the expectation of total permafrost-related carbon release conditional on a long-run temperature value ($\widetilde{T}_{AT}$). The two red dots in Panel (c.1) correspond to (N.i) and (N.ii). The red vertical line in Panel (c.2) correspond to (N.iv).

TABLE 1. Estimated parameters

Parameter	Notation	Equation	Value	Unit/Note
Production function				
Target: avg mean growth in the absence of climate risks			8.0	%/period (5yrs)
Target: Std dev. of growth in the absence of climate risks			3.0	%/period (5yrs)
Average TFP	$\bar{A}$	(10)	0.44	
Standard deviation of TFP shock	σ_A	(10)	3.50	%
Damage specification				
Target: Expected 2100 fractional damage conditional on $T_{AT} = 2°C$			5.0	%
Target: Expected 2100 fractional damage conditional on $T_{AT} = 4°C$			10.0	%
Target: Std dev. of 2100 fractional damage conditional on $T_{AT} = 4°C$			7.5	%
Uncertainty parameter	μ_D	(13)	0.0352	
Constant term in damage specification	$a^{(D)}$	(13)	-0.0024	
Slope coefficient in damage specification	$b^{(D)}$	(13)	0.0037	
Permafrost-related emissions				
Target: Expected 2100 release conditional on $T_{AT} = 2°C$			205.4	$GtCO_2$
Target: Expected 2100 release conditional on $T_{AT} = 4°C$			370.4	$GtCO_2$
Target: Std dev. of 2100 release conditional on $T_{AT} = 4°C$			191.7	$GtCO_2$
Target: Expected release conditional on $\widetilde{T}_{AT} = 4°C$			1378.8	$GtCO_2$
Uncertainty parameter	μ_N	(7)	49.6	
Constant term in carbon-release specification	$a^{(N)}$	(7)	-77.4	
Slope coefficient in carbon-release specification	$b^{(N)}$	(7)	98.0	
Decay rate of releases	κ_N	(7)	0.77	
Sea-level rise (SLR)				
Target: Expected 2100 SLR conditional on $T_{AT} = 2°C$			0.45	m
Target: Expected 2100 SLR conditional on $T_{AT} = 4°C$			0.93	m
Target: Std dev. of 2100 SLR conditional on $T_{AT} = 4°C$			0.36	m
Uncertainty parameter in SLR specif.	μ_H	(8)	0.0715	
Constant in SLR specif.	$a^{(H)}$	(8)	-0.0287	m/period
Coefficient on T_{AT} in SLR specif.	$b^{(H)}$	(8)	0.0320	m/period/°C
Uncertainty about temperature process				
Target: Std dev. of 2100 atmospheric temperature			0.75	°C
Uncertainty parameter in T_{AT} specification	μ_T	(2)	0.0583	
Mitigation process				
Based on agents' optimization on initial date				
Coef. on imposed function form of μ_t	$\theta_{a,opt}$	(15)	-1.333	
Coef. on imposed function form of μ_t	$\theta_{b,opt}$	(15)	0.068	

Notes: Production-function targets are based on the annual time series of World GDP per capita (in 2010 U.S. Dollars) extracted from the FRED database (Ticker: NYGDPPCAPKDWLD), period 1980-2022. The first two damage targets are consistent with Kahn et al. (2021) and Howard and Sterner (2017); the relatively large standard deviation of damages is aimed at capturing the significant uncertainty surrounding the damage-function estimates, and to allow for estimates such as those of Burke et al. (2015) (about -25% at 4°C, see their Figure 5.d) to remain in the plausible model-implied range; it can also be seen as a way to recognize the underestimation of non-market damages (Sterner and Persson, 2008). Permafrost-related targets are based on MacDougall and Knutti (2016) (Table 1), assuming that RCP2.6 (respectively RCP8.5) corresponds to a 2100 temperature anomaly of 2°C (resp. 4°C); our 4th target is based on their 2300 result (RCP8.5). Global-mean-sea-level targets are based on Horton et al. (2020) (Table 1). The standard deviation of 2100 atmospheric temperature reflects the uncertainty shown in Figure 4.2 of the IPCC AR6. Coefficients $\theta_{a,opt}$ and $\theta_{b,opt}$ are determined so as to maximizes utility at time $t = 0$.

FIGURE 3. Conditional distribution of future temperatures (swaps versus physical)

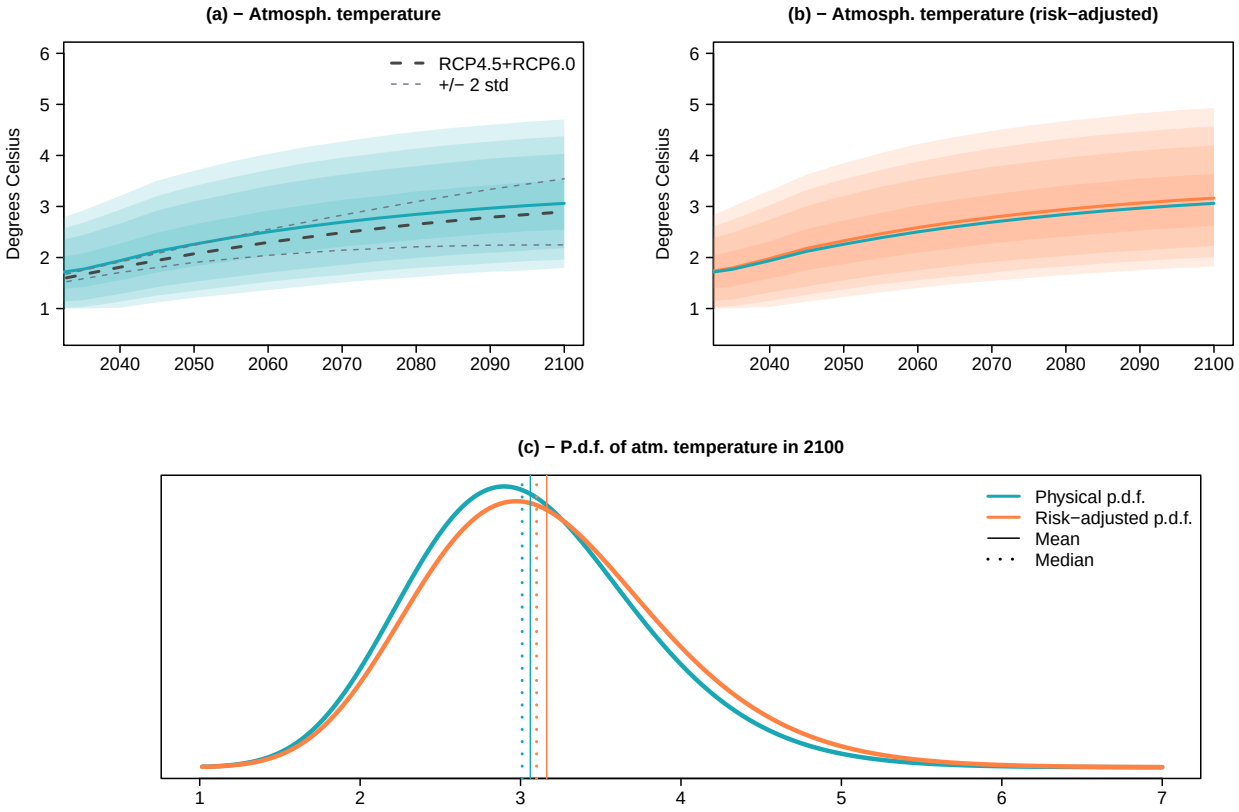

Notes: Panel (a) displays the conditional distribution of future atmospheric temperatures. The shaded areas are 50%, 80%, 90%, and 95% confidence intervals. The central blue line shows the means of the distributions. The dashed lines indicates two IPCC's Representative Concentration Pathway (RCP) scenarios, namely RCP4.5 and RCP6.0. Panel (b) shows the risk-adjusted (or risk-neutral) distribution of temperatures (see Subsection 4.2.2 for the interpretation of this distribution). The orange solid line of Panel (b) is the term structure of conditional expectations under the latter distribution; it therefore corresponds to the term structure of temperature swap prices ($T^S_{0,h}$). (If agents were not risk-averse, the orange line would coincide with the blue one in Panel (b); in other words, the deviation between the two lines reflects climate risk premiums.) Panel (c) shows conditional temperature distributions under the physical (blue) and risk-adjusted (orange) measures, for the 2100 horizon.

3.6. **Social Cost of Carbon.** Because the social cost of carbon (SCC) occupies a central place in the IAM literature, it is interesting to evaluate it in our calibrated framework—where it is given in closed form (see Supplemental Appendix III.3).[25]

With our baseline calibration, we obtain an SCC of \$191 per ton of CO_2, which is rather at the upper end of the range of values presented in the literature (see Table 2). This large SCC reflects the significant and uncertain damage underlying our baseline parameterization, as well as the inclusion of positive feedback effects through permafrost-related emissions

[25]Following the literature, we define the SCC as the marginal rate of substitution between atmospheric carbon concentration and consumption, that is: $SCC_t = -\frac{\partial U_t}{\partial M_{AT,t}} \Big/ \frac{\partial U_t}{\partial C_t}$.

FIGURE 4. Conditional distribution of future global sea level (swaps versus physical)

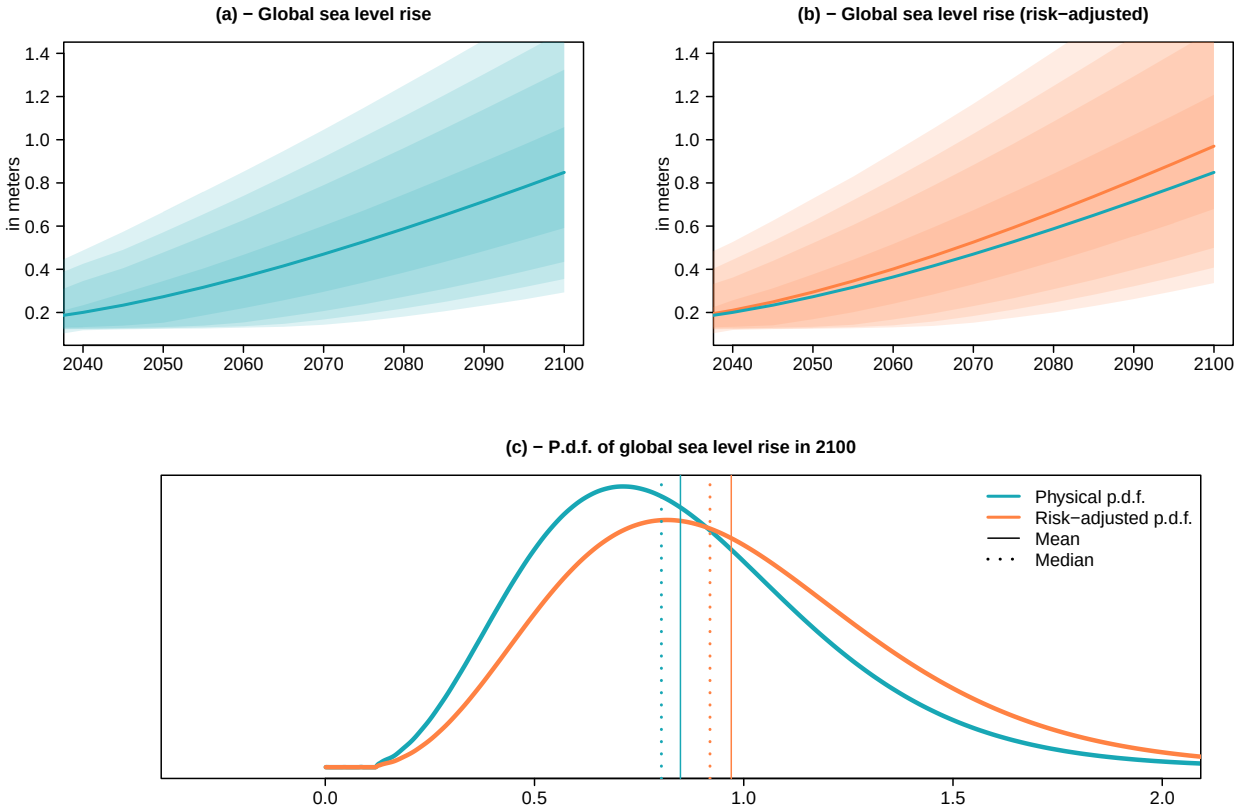

Notes: Panel (a) displays the conditional distribution of future global sea level rise (relative to 1951-1980 sea level). The shaded areas are 50%, 80%, 90%, and 95% confidence intervals. The central blue line shows the means of the distributions. Panel (b) shows the risk-adjusted (or risk-neutral) distribution of sea level (see Subsection 4.2.2 for the interpretation of this distribution). The orange solid line of Panel (b) is the term structure of conditional expectations under the latter distribution; it therefore corresponds to the term structure of sea-level swap prices. (If agents were not risk-averse, the orange line would coincide with the blue one in Panel (b); in other words, the deviation between the two lines reflects climate risk premiums.) Panel (c) shows conditional sea level distributions under the physical (blue) and risk-adjusted (orange) measures, for the 2100 horizon.

(N_t). This value is however broadly in line with recent contributions with a strong focus on uncertainty (e.g., Daniel et al., 2019; Lemoine, 2021; Traeger, 2023).

Table 3 reports SCC obtained under different model calibrations. It shows for instance that the SCC is reduced by about 20% when we remove the risk from the model ($\mu_T = \mu_N = \mu_H = \mu_D = \sigma_A = 0$). The results highlight the importance of permafrost-related carbon release: the SCC is reduced by 27% when these emissions are removed from the model ($a^{(N)} = b^{(N)} = 0$). Table 3 also illustrates the key effect of expected damages on this price: the SCC is divided by slightly more than two (to \$83) when expected damages are halved ("Small damages" row).

TABLE 2. SCC comparison

Study	SCC (U.S. $ per tCO_2)	Tipping points	Stochastic IAM	Discount Rate
Stern (2007)	85			0%
Jensen and Traeger (2014)	[10 ; 23]		✓	1.5%
Lemoine and Traeger (2014)	[10 ; 14]	✓	✓	1.5%
Bansal et al. (2016)	[1 ; 28]	✓	✓	1%
Nordhaus (2017)	31			1.5%
Cai and Lontzek (2019)	[10 ; 27]	✓	✓	1.5%
Daniel et al. (2019)	[106 ; 142]	✓	✓	0.5%
Pindyck (2019)	[22 ; 82]			3%
Barnett et al. (2020)	[65 ; 112]		✓	1%
Hambel et al. (2021)	[18 ; 43]		✓	1.5%
Lemoine (2021)	710		✓	1.5%
Van den Bremer and Van der Ploeg (2021)	[40 ; 66]		✓	1.5%
Bauer and Rudebusch (2023)	[101 ; 963]			3%↘1%
Traeger (2023)	[75 ; 547]		✓	[0.5%]
This paper	**191**	✓	✓	1.5%

Note: This table reports different SCC estimates. The SCC is expressed in 2020 USD per ton of CO_2 (i.e., 3.667 times smaller than the SCC expressed in USD per ton of Carbon). Cited studies differ along many dimensions, the last three columns highlight particularly important ones. Figures in square brackets indicate the range of values found in the studies. The estimates of Jensen and Traeger (2014) are those they report on p.111. Barnett et al. (2020): see their Table 4. Cai and Lontzek (2019): see their Table 6. Bansal et al. (2016): see their Table III. Lemoine and Traeger (2014): see their Section IV. Van den Bremer and Van der Ploeg (2021): see their Table 4 ("risk-adjusted ethics-based calibration"). Daniel et al. (2019): see their Figure 3.A ("EZ" results). Lemoine (2021): see his Table 1 (600 years). Traeger (2023): see his Table 1. Pindyck (2019)'s estimates are based on surveys of experts (numbers on page 142). Bauer and Rudebusch (2023) use horizon-varying real rates (of about 3% for shorter horizons, to 1% for longer ones) to discount DICE-based CO_2-reduction benefits; see their Table 2.

4. PRICING

Our framework offers quasi-explicit pricing formulas for various financial instruments whose payoffs are directly or indirectly exposed to the climate. Subsection 4.1 introduces generic pricing formulas. Subsection 4.2 discusses the pricing of specific assets, including bonds, equity, and climate derivatives. (Real estate prices are also discussed the supplemental appendix.)

4.1. **Stochastic discount factor.**

Proposition 9 states that our model involves an exponential affine stochastic discount factor (SDF):

$$\mathcal{M}_{t,t+1} = \exp[-(\mu_{r,0,t+1} + \mu'_{r,1,t+1}X_t) + \Pi'_{t+1}X_{t+1} \underbrace{-\alpha_t(\Pi_{t+1}) - \beta_t(\Pi_{t+1})'X_t}_{=-\psi_t(\Pi_{t+1}),\text{ see eq. (18)}}], \tag{20}$$

where Π_{t+1}, $\mu_{r,0,t+1}$, and $\mu_{r,1,t+1}$ are detailed in the supplemental appendix (in Proposition 9).

TABLE 3. Social Cost of Carbon and other model outputs

A. Social Cost of Carbon (in U.S. $ per ton of CO_2)						
Specification	$\gamma = 7$		$\gamma = 2$		$\gamma = 10$	
Baseline	**191**		**164**		**213**	
Deterministic model	157	*−18%*	157	*−4%*	157	*−26%*
No exog. techno. uncertainty ($\sigma_A = 0$)	191	*+0%*	164	*+0%*	213	*+0%*
No damage uncertainty ($\mu_D = 0$)	164	*−14%*	158	*−4%*	167	*−22%*
Small damages (twice lower)	83	*−56%*	78	*−52%*	87	*−59%*
No permafrost uncertainty ($\mu_N = 0$)	187	*−2%*	164	*−0%*	206	*−3%*
No permaf. releases ($a^{(N)} = b^{(N)} = 0$)	139	*−27%*	122	*−26%*	153	*−28%*
No sea-level uncertainty ($\mu_H = 0$)	187	*−2%*	164	*−0%*	208	*−3%*
No sea-level risks ($a^{(H)} = b^{(H)} = 0$)	111	*−42%*	89	*−46%*	129	*−39%*
B. Temperature risk premium (in °C)						
Specification	$\gamma = 7$		$\gamma = 2$		$\gamma = 10$	
Baseline	**0.102**		**0.018**		**0.190**	
Deterministic model	0.000	*−0.102°C*	0.000	*−0.018°C*	0.000	*−0.190°C*
No exog. techno. uncertainty ($\sigma_A = 0$)	0.131	*+0.029°C*	0.026	*+0.009°C*	0.227	*+0.037°C*
No damage uncertainty ($\mu_D = 0$)	0.077	*−0.026°C*	0.016	*−0.002°C*	0.122	*−0.068°C*
Small damages (twice lower)	0.010	*−0.093°C*	-0.000	*−0.018°C*	0.020	*−0.169°C*
No permafrost uncertainty ($\mu_N = 0$)	-0.004	*−0.106°C*	-0.004	*−0.022°C*	0.002	*−0.188°C*
No permaf. releases ($a^{(N)} = b^{(N)} = 0$)	-0.016	*−0.119°C*	-0.007	*−0.025°C*	-0.018	*−0.208°C*
No sea-level uncertainty ($\mu_H = 0$)	0.099	*−0.003°C*	0.018	*−0.000°C*	0.182	*−0.008°C*
No sea-level risks ($a^{(H)} = b^{(H)} = 0$)	0.035	*−0.067°C*	0.002	*−0.015°C*	0.079	*−0.111°C*
C. SLR risk premium (in meters)						
Specification	$\gamma = 7$		$\gamma = 2$		$\gamma = 10$	
Baseline	**0.121**		**0.030**		**0.194**	
Deterministic model	0.000	*−0.121 m*	0.000	*−0.030 m*	0.000	*−0.194 m*
No exog. techno. uncertainty ($\sigma_A = 0$)	0.127	*+0.006 m*	0.031	*+0.001 m*	0.201	*+0.007 m*
No damage uncertainty ($\mu_D = 0$)	0.114	*−0.008 m*	0.029	*−0.001 m*	0.173	*−0.021 m*
Small damages (twice lower)	0.023	*−0.098 m*	0.006	*−0.024 m*	0.034	*−0.160 m*
No permafrost uncertainty ($\mu_N = 0$)	0.085	*−0.036 m*	0.023	*−0.007 m*	0.127	*−0.068 m*
No permaf. releases ($a^{(N)} = b^{(N)} = 0$)	0.061	*−0.061 m*	0.016	*−0.014 m*	0.091	*−0.104 m*
No sea-level uncertainty ($\mu_H = 0$)	0.038	*−0.083 m*	0.008	*−0.022 m*	0.067	*−0.127 m*
No sea-level risks ($a^{(H)} = b^{(H)} = 0$)	0.130	*+0.009 m*	0.130	*+0.100 m*	0.130	*−0.064 m*
D. Long-term rate (in percent; maturity: 2100)						
Specification	$\gamma = 7$		$\gamma = 2$		$\gamma = 10$	
Baseline	**2.64**		**2.82**		**2.49**	
Deterministic model	2.87	*+23 bps*	2.87	*+5 bps*	2.87	*+38 bps*
No exog. techno. uncertainty ($\sigma_A = 0$)	2.75	*+11 bps*	2.84	*+3 bps*	2.65	*+16 bps*
No damage uncertainty ($\mu_D = 0$)	2.74	*+10 bps*	2.84	*+2 bps*	2.67	*+18 bps*
Small damages (twice lower)	2.86	*+23 bps*	2.97	*+15 bps*	2.80	*+31 bps*
No permafrost uncertainty ($\mu_N = 0$)	2.65	*+1 bps*	2.82	*+0 bps*	2.52	*+3 bps*
No permaf. releases ($a^{(N)} = b^{(N)} = 0$)	2.72	*+8 bps*	2.87	*+5 bps*	2.60	*+11 bps*
No sea-level uncertainty ($\mu_H = 0$)	2.65	*+1 bps*	2.82	*+0 bps*	2.51	*+2 bps*
No sea-level risks ($a^{(H)} = b^{(H)} = 0$)	2.76	*+12 bps*	2.92	*+11 bps*	2.62	*+13 bps*

Notes: This table illustrates the sensitivity of the SCC and of other model outputs. The SCC is expressed in U.S. $ per ton of carbon dioxide. The temperature and SLR risk premiums (Panels B and C) correspond to the difference between the risk-adjusted and physical expectations of temperature and SLR in 2100 (see Subsection 4.2.2). The long-term rate (Panel D) is the model-implied 2020 real rate of maturity 2100. The deterministic model is a model where we remove all sources of uncertainty ($\mu_D = \mu_N = \mu_T = \mu_H = \sigma_A = 0$). Values in italics indicate changes from the baseline case. In the "Small damages" scenario, both $\lambda_{D,t}$ (eq. 13) and $\lambda_{H,t}$ (eq. 8) are divided by 2. "bps" stands for basis points.

This notably implies that the short-term risk-free rate is affine in the state vector X_t. Indeed, by (18), we have $\psi_t(\Pi_{t+1}) = \mathbb{E}_t(\Pi'_{t+1}X_{t+1})$ and, therefore:

$$r_t = -\log \mathbb{E}_t(\mathcal{M}_{t,t+1}) = \mu_{r,0,t+1} + \mu'_{r,1,t+1}X_t. \tag{21}$$

The fact that the SDF is exponential affine in the state vector, that itself follows an affine process, ensures the fast pricing of various generic assets. To start with, consider an asset whose only payoff is $\exp(\omega' X_{t+h})$, settled on date $t+h$. On date t, the price of this asset is exponential affine in the state vector X_t, that is:

$$\varphi_t^{(h)}(\omega) := \mathbb{E}_t[\mathcal{M}_{t,t+h}\exp(\omega' X_{t+h})] = \exp\left(\varphi_{0,t}^{(h)}(\omega) + \varphi_{1,t}^{(h)}(\omega)'X_t\right), \tag{22}$$

where functions $\varphi_{0,t}^{(h)}$ and $\varphi_{1,t}^{(h)}$ are deterministic functions that can be evaluated recursively (see Proposition 10). This further opens the door to the pricing of payoffs that are linear in X_t, i.e. of the form $\omega' X_{t+h}$ (see Corollary 2):

$$\widetilde{\varphi}_t^{(h)}(\omega) := \mathbb{E}_t[\mathcal{M}_{t,t+h} \times (\omega' X_{t+h})] = \lim_{\varepsilon \to 0} \frac{\varphi_t^{(h)}(\varepsilon\omega) - \varphi_t^{(h)}(0)}{\varepsilon}. \tag{23}$$

Moreover, using the Fourier-transform approach of Duffie et al. (2000), one can price instruments providing option-like payoffs, of the form $\exp(\omega' X_{t+h})\mathbb{1}_{\{a'X_{t+h}<b\}}$ (Proposition 11):[26]

$$\begin{aligned}\hat{\varphi}_t^{(h)}(\omega, a, b) &:= \mathbb{E}_t\left(\mathcal{M}_{t,t+h}\exp\left(\omega' X_{t+h}\right)\mathbb{1}_{\{a'X_{t+h}<b\}}\right) \\ &= \frac{\varphi_t^{(h)}(\omega)}{2} - \frac{1}{\pi}\int_0^\infty \frac{\mathrm{Im}[\varphi_t^{(h)}(\omega + iax)\exp(-ibx)]}{x}dx,\end{aligned} \tag{24}$$

where $\mathrm{Im}(x)$ denotes the imaginary part of x and where function $\varphi_t^{(h)}$ is defined in (22). It is important to note that the integral appearing in (24) is one-dimensional, irrespective of the dimension of X_t. As a result, Monte-Carlo simulations are not required to evaluate this integral, as it is easily evaluated using Riemann sums.

Finally, the date-t price of an asset providing $(\omega' X_{t+h})\mathbb{1}_{\{a'X_{t+h}<b\}}$ on date $t+h$ is:

$$\bar{\varphi}_t^{(h)}(\omega, a, b) := \mathbb{E}_t\left(\mathcal{M}_{t,t+h}(\omega' X_{t+h})\mathbb{1}_{\{a'X_{t+h}<b\}}\right) = \lim_{\varepsilon \to 0} \frac{\hat{\varphi}_t^{(h)}(\varepsilon\omega, a, b) - \hat{\varphi}_t^{(h)}(0, a, b)}{\varepsilon}, \tag{25}$$

[26] Duffie et al. (2000) expose their approach in the context of time-invariant Laplace transforms; it is straightforward to check that the same machinery applies to the present case, with $\varphi_t^{(h)}$ functions that deterministically depend on time.

where $\hat{\varphi}_t^{(h)}(\omega, a, b)$ is given by (24) (see Corollary 3).

4.2. **Examples.** This subsection shows how the previous formulas can be used to price different types of assets, directly exposed to climate risks (e.g., climate derivatives), or indirectly (e.g., equity, housing).[27] The latter category includes for instance treasury bonds that are risk-free in a credit-risk sense, but that are affected by climate risks through economic growth, to which the SDF is linked. We start with this asset class.

4.2.1. *Real and nominal bonds.* As long as the model is not augmented with an inflation process (which will be done below), we can only price real, or inflation-linked, bonds. The SDF given in (20) is indeed real—it allows to price payoffs expressed in units of goods. In particular, $\mathbb{E}_t(\mathcal{M}_{t,t+h})$ is the price of a bond providing a payoff of one unit of good on date $t+h$. (Note that $\mathcal{M}_{t,t+h} = \mathcal{M}_{t,t+1} \times \cdots \times \mathcal{M}_{t+h-1,t+h}$.) In other words, $\mathbb{E}_t(\mathcal{M}_{t,t+h})$ is the price of a zero-coupon inflation-linked bond of maturity h. Equation (22) gives:

$$\mathcal{B}_{t,h} := \mathbb{E}_t(\mathcal{M}_{t,t+h}) = \varphi_t^{(h)}(0).$$

Hence, denoting by $r_{t,h}$ the associated yield-to-maturity ($r_{t,1}$ being equal to r_t, given in eq. 21), we have:

$$r_{t,h} = -\frac{1}{h}\varphi_{0,t}^{(h)}(0) - \frac{1}{h}\varphi_{1,t}^{(h)}(0)' X_t. \tag{26}$$

This expression is reminiscent of the solutions of the so-called market models (Brace et al., 1997; Miltersen et al., 1997), in the sense that the resulting interest rates linearly depend on the state vector, but in a way that deterministically depends on time (since functions $\varphi_{0,t}^{(h)}$ and $\varphi_{1,t}^{(h)}$ are time-varying, but deterministic).

Panel (a) of Figure 5 shows, in black, the model-implied term structure of real rates. It is downward-sloping, starts at less than 3% and settles below 2.5% for ultra-long maturities. These properties of the risk-free term structure of real rates are broadly in line with Gollier and Hammitt (2014) or, more recently, Bauer and Rudebusch (2023). As explained for instance in Gollier and Weitzman (2010), downward-sloping term structure of real interest rates are mechanically obtained in structural frameworks when growth shocks are persistent; this is typically the case in IAMs, as temperature increases have persistent adverse effects on growth. For ultra-long maturities (1000 years), we obtain real rates of 2.5%, a level that

[27] The case of housing is presented in the supplemental appendix (VI.5).

is consistent with the upper bound of 2.6% determined by Giglio et al. (2021) to price very-long-term payoffs.

FIGURE 5. Term structures of interest rates

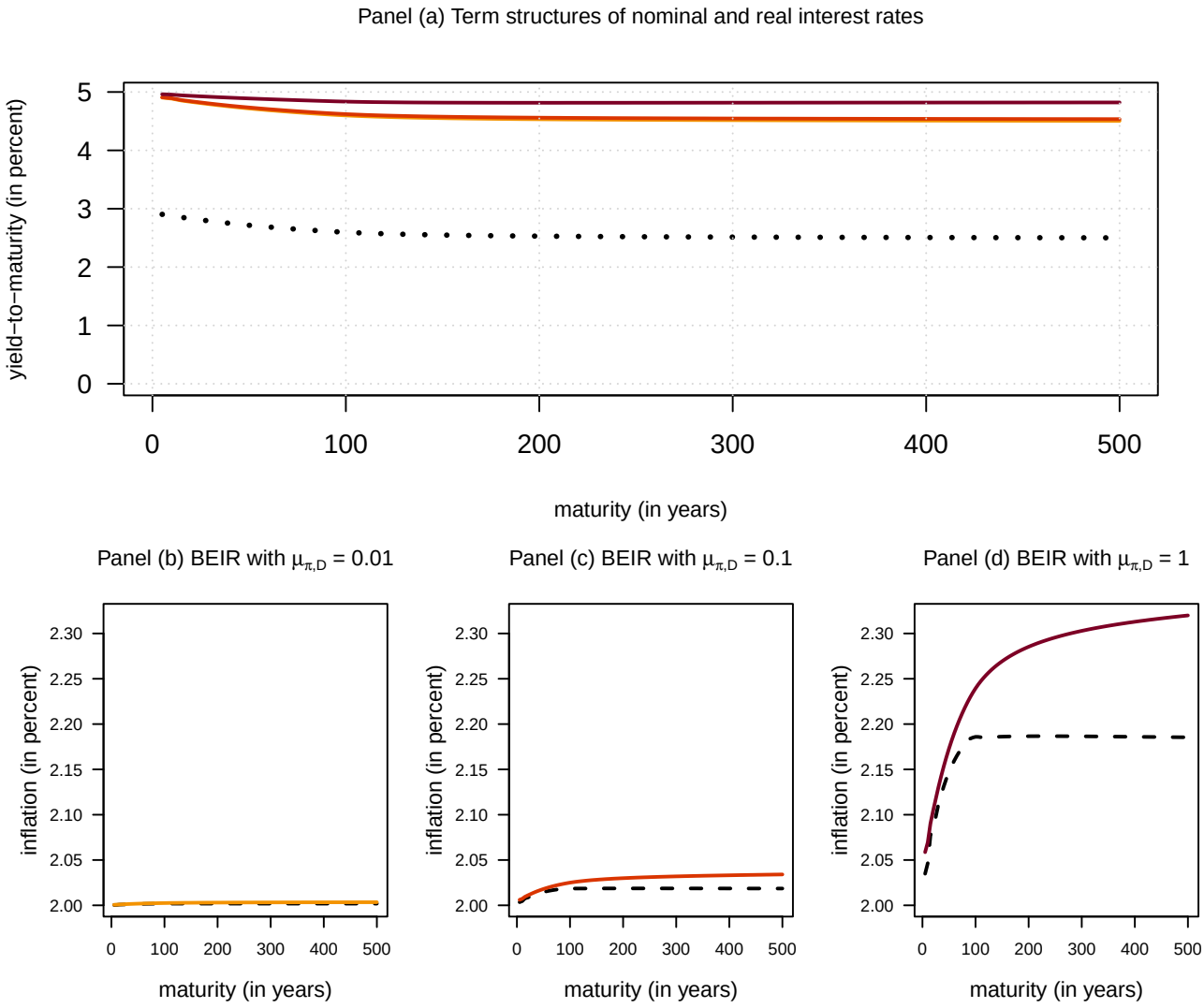

Notes: This figure shows real and nominal term structure of interest rates (Panel (a)), and inflation compensations—that is the difference between nominal and real rates (Panels (b) to (d)) associated with three different inflation specifications. These term structures are computed as of the initial date. Real rates are given by (26); nominal rates are given by (28). Inflation can be affected by climate-related damages; it is given by $\pi_t = 2\% + \mu_{\pi,D} D_t$. On Panels (b) to (d), the dashed line indicates the term structure of inflation expectations, i.e., $\frac{1}{h}\mathbb{E}_0(\log(PI_h/PI_0))$, where PI_t the is the price index. On these panels, the spread between the solid and the dashed line is therefore an inflation risk premium.

While the term structures shown in Figure 5 are those associated with the initial period ($t = 0$), equation (26) can be used to determine the model-implied yields for any value of the state vector X, at any date t, and for any maturity h. Exploiting that, Figure 6 shows the

FIGURE 6. Expected influence of climate risk on long term rates

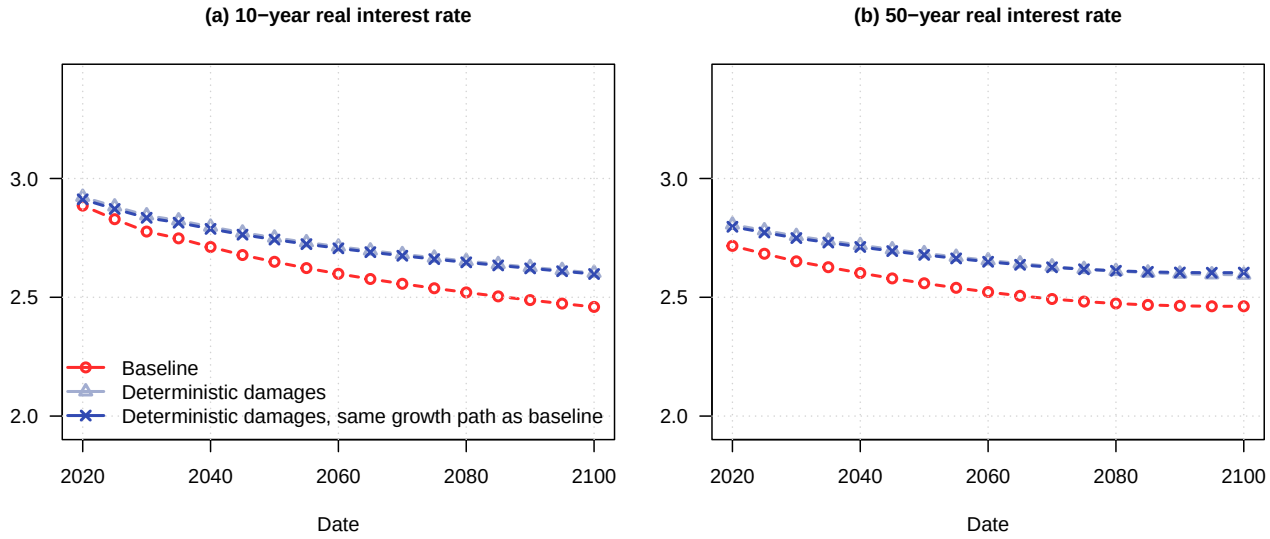

Notes: This figure displays the expected trajectories of the 10-year (Panel (a)) and the 50-year (Panel (b)) real rates. Specifically, the plots show $\mathbb{E}_0(r_{t,h})$, for dates t going from the initial date to 2100, for $h = 2$ periods (10 years) and $h = 10$ periods (50 years). The two blue lines (triangles and crosses) are obtained with a counterfactual model where we remove climate-related risks ($\mu_D = \mu_H = \mu_N = \mu_T = 0$). The lines with crosses are based on a model where we have adjusted $\mu_{c,t}$ (see eq. 16) such that expected growth is the same as under the baseline model (with stochastic climate-change damages).

expected trajectories of the 10-year and of the 50-year yields until the end of the century.[28] The red line shows that long-term rates are expected to decrease through time (red line). The 10-year yield, in particular, would decrease by 40 basis points (bps) by 2100. Two mechanisms contribute to this: first, consumption growth is expected to decrease over time, under the effect of rising temperatures and associated damages (expected growth channel); second, growth uncertainty will increase over time, accentuating precautionary effect (growth risk channel). In order to get a sense of the relative importance of these two effects, we compute the same interest rates under a version of the model where we remove climate-related risks (setting $\mu_D = \mu_H = \mu_N = \mu_T = 0$). The resulting term structures are displayed in blue in Figure 6 (triangles). The decrease in long-term rates, of 25 bps over the next 80 years,

[28] Specifically, the plots show the trajectories of $\mathbb{E}_0(r_{t,h})$, for dates t going from the initial date to 2100, for $h = 2$ (10 years) and $h = 10$ (50 years).

is smaller than in the baseline base (40 bps).[29] The difference can be attributed to climate-induced growth risk channel.

Panel D of Table 3 illustrates the sensitivity of the 2100 real interest rate to various modeling ingredients. In a deterministic model, this rate would be 23 bps higher than in our baseline specification. If we remove damage uncertainty alone (setting μ_D to 0), the interest rate increases by 10 bps, an increase that is about the same as that obtained when we only remove exogenous growth volatility ($\sigma_A = 0$).

Let us now turn to nominal bonds. For that purpose, we need to introduce a price index. We can add such a variable among the state variables of X_t, allowing for effects of the other state variables on inflation, defined as the change in the log price index. Formally, if inflation (π_t) can be expressed as an affine deterministic function of X_t, that is if

$$\pi_t = \mu_{\pi,0,t} + \mu'_{\pi,1} X_t,$$

then we can augment X_t with the log price index ($\log PI_t$). The latter then satisfies:

$$\log PI_t = \log PI_{t-1} + \pi_t = \log PI_{t-1} + \mu_{\pi,0,t} + \mu'_{\pi,1} X_t. \tag{27}$$

The price-index-augmented X_t remains an affine process.

Consider the payoff of a nominal zero-coupon bond of maturity h, issued on date t. At maturity, its real payoff is $PI_t/PI_{t+h} = \exp(\mu'_{PI}(X_t - X_{t+h}))$, where μ_{PI} is a selection vector that is such that $\log(PI_t) = \mu'_{PI} X_t$. Using (22), the date-$t$ price of a zero-coupon nominal bond of maturity h is:

$$\mathcal{B}^{\$}_{t,h} := \exp\left(\varphi^{(h)}_{0,t}(-\mu_{PI}) + \left[\mu_{PI} + \varphi^{(h)}_{1,t}(-\mu_{PI})\right]' X_t\right).$$

Denoting by $i_{t,h}$ the yield-to-maturity of a maturity-h nominal zero-coupon bond, we get:

$$i_{t,h} = -\frac{1}{h}\varphi^{(h)}_{0,t}(-\mu_{PI}) - \frac{1}{h}\left[\mu_{PI} + \varphi^{(h)}_{1,t}(-\mu_{PI})\right]' X_t. \tag{28}$$

[29] This reduction may potentially hide a second expected-growth effect: in the deterministic model, agents tend to invest less in the mitigation technology; as a result, average growth is higher. To assess this, we have designed a third counterfactual model where climate change risks are still deterministic, but where we adjust the deterministic component of consumption growth (namely, $\mu_{c,t}$ in eq. 16) such that expected growth is the same as under the baseline model (with stochastic climate-change damages). The resulting trajectory (dark blue line in Figure 6) is very close to the one with deterministic damages and no adjustment, which shows that this additional growth effect is a second-order one.

To fix ideas, we can for instance have $\pi_t = \mu_{\pi,0,t} + \mu_{\pi,D} D_t$, where parameter $\mu_{\pi,D} \geq 0$ determines the influence of climate-related damages (D_t) on inflation. Such a specification, in which damages have opposing effects on inflation and production, aligns with the interpretation of climate-related damages as supply shocks (see, e.g., Batten, 2018; Andersson et al., 2020).[30]

Panel (a) of Figure 5 shows nominal yield curves (solid lines) obtained for for $\mu_{\pi,0,t} = 2\%$ and for different values of $\mu_{\pi,D}$: 0.01, 0.1, and 1. (The intermediate value corresponds to a situation where a climate-related damages decreasing output by 1% induce a 0.1% increase in inflation.) As is the case for the real yield curve, the nominal yield curves displayed on Figure 5 are also sloping downwards, albeit to a lesser extent. This is because the inflation compensation, or break-even inflation rates (BEIR)—the difference between nominal and real yields, shown in the lower panels—are sloping upwards. The positive slope of the BEIR has two sources: (a) since damages are expected to increase through time, that is also the case for inflation as soon as $\mu_{\pi,D} > 0$ (expectation effect), and (b) inflation risk premiums increase through maturities (risk-adjustment effect). The fact that supply shocks imply upward-sloping inflation risk premiums is a well-known result of the macro-finance literature (see, e.g., Rudebusch and Swanson, 2012; Gurkaynak and Wright, 2012, Subsection 4.5): supply shocks generate a negative correlation between consumption and inflation, which implies that nominal bonds tend to depreciate during recessions; as a result, risk-averse investors are willing to hold these bonds only if, on average, they provide an excess return with respect to risk-free (i.e., real) bonds. In Panels (b) to (d) of Figure 5, the term structures of inflation risk premiums correspond to the spread between the solid line (BEIR) and the dashed line (expected inflation). For the intermediate inflation sensitivity ($\mu_{\pi,D} = 0.1$), expectation and risk effects each account for about half of the climate-related part of the inflation compensation (i.e., the difference between the solid line and $\mu_{\pi,0,t} = 2\%$). For the large sensitivity ($\mu_{\pi,D} = 1$), expectation and risk-adjustment effects have similar magnitudes.

4.2.2. *Climate derivatives and risk premiums.* A straightforward application of our framework is the pricing of climate derivatives, or climate linkers. Because of their nature, the valuation

[30] Available evidence regarding the inflationary effects of climate shocks is scarce and show mixed results. While Mukherjee and Ouattara (2021) find that temperature shocks lead to inflationary pressure, Parker (2018) finds only muted effect in advanced countries. Focusing on the euro area, Beirne et al. (2021) obtain significant positive effects of natural disasters on overall headline inflation, with diverging results at the sub-index level.

of these instruments provides a natural illustration of the notion of climate risk premium and, more generally, of the risk-adjusted—or risk-neutral—distributions of climate variables.

Start with the definition of a temperature-indexed swap. A swap is a basic derivative product that materializes the agreement between two counterparties to exchange cash flows at predetermined dates. The first type of the cash flows—the fixed leg of the swap—is determined at the time the swap is negotiated (t, say) and paid by the protection buyer to the protection seller. In the context of a temperature-indexed swap, this cash flow would be $T^S_{AT,t,h}N$, where N denotes the notional amount, $T^S_{AT,t,h}$ is the negotiated swap temperature, h being the swap maturity. The second type of cash flow—the floating leg of the swap—depends on an index that is observed at maturity, the temperature $T_{AT,t+h}$ in the present case. This second cash flow, namely $T_{AT,t+h}N$, is paid by the protection seller to the protection buyer on date $t+h$.

As for any swap, the swap temperature negotiated by the the two counterparties on date t (namely $T^S_{AT,t,h}$) has to be such that the values of the two legs are equal on date t. Formally, we have $\mathbb{E}_t(\mathcal{M}_{t,t+h}T_{AT,t+h}) = \mathbb{E}_t(\mathcal{M}_{t,t+h})\mathbb{E}_t(\mathcal{M}_{t,t+h}T^S_{AT,t,h})$, or:

$$T^S_{AT,t,h} = \mathbb{E}_t\left(\frac{\mathcal{M}_{t,t+h}}{\mathbb{E}_t(\mathcal{M}_{t,t+h})}T_{AT,t+h}\right) = \varphi_t^{(h)}(\mu_{TAT})/\varphi_t^{(h)}(0), \tag{29}$$

where μ_{TAT} is the selection vector that is such that $T_{AT,t} = \mu'_{TAT}X_t$. Equation (29) shows that $T^S_{AT,t,h}$ can be seen as a risk-adjusted expectation of $T_{AT,t+h}$. Formally, (29) rewrites $T^S_{AT,t,h} = \mathbb{E}_t^{\mathbb{Q}^h}(T_{AT,t+h})$, where $\mathbb{E}_t^{\mathbb{Q}^h}$ denotes the expectation under the h-forward risk-neutral measure.[31] A third way to rewrite (29) is:

$$T^S_{AT,t,h} = \mathbb{E}_t\left[T_{AT,t+h}\right] + prem_{t,h}, \quad \text{with} \quad prem_{t,h} = \frac{\mathbb{C}ov_t\left[T_{AT,t+h}, \mathcal{M}_{t,t+h}\right]}{\mathbb{E}_t\left[\mathcal{M}_{t,t+h}\right]}, \tag{30}$$

which shows that $prem_{t,h}$—the difference between the swap-implied temperature ($T^S_{AT,t,h}$) and the expected temperature ($\mathbb{E}_t\left[T_{AT,t+h}\right]$)—depends on the covariance between temperatures and the SDF. In economic terms, if states of higher temperature are perceived as "bad states of the world" (states of high marginal utility, or high SDF) then the the covariance

[31] In other words, $\mathcal{M}_{t,t+h}/\mathbb{E}_t\left[\mathcal{M}_{t,t+h}\right]$ is the Radon-Nikodym derivative linking the physical and risk-neutral measures. The h-forward risk-neutral measure $\mathbb{Q}^h$ is equivalent (in the measure sense) to the physical one. Under $\mathbb{Q}^h$, the numeraire is a zero-coupon bond of maturity h (see e.g. Jamshidian, 1989). That is, conditional on the information available on date t, the risk-adjusted probability of an event Ω_{t+h} (say) is equal to $\mathbb{E}_t(\mathcal{M}_{t,t+h}\mathbb{1}_{\{\Omega_{t+h}\}})/\mathbb{E}_t(\mathcal{M}_{t,t+h})$.

term is positive, and the swap-implied temperature is above its expectation. In that case, the protection buyer is willing to lose money, on average, to be hedged against temperature risk—which is akin to paying an insurance premium.

Figure 3 displays the term structure of temperature swaps (orange solid line of Panel b). Specifically, it shows $T^S_{AT,t,h} = \mathbb{E}_t^{\mathbb{Q}^h}[T_{AT,t+h}]$ for different maturities h, as of the initial date ($t = 0$). The blue line displays expected atmospheric temperatures, i.e., $\mathbb{E}_t(T_{AT,t+h})$. The deviation between the blue and the orange lines therefore reflects temperature risk premiums ($prem_{t,h}$ in eq. 30). For the baseline calibration, we find a 2100 temperature risk premium of about 0.10°C; this value corresponds to the deviation between the means of the physical and risk-neutral distributions plotted on Panel (c) of Figure 3 (these means are indicated by vertical solid lines). Panel B of Table 2 documents the sensitivity of the temperature risk premium to various model ingredients. We find, in particular, that this premium would be larger if there was no exogenous technological uncertainty ($\sigma_A = 0$), and lower in the absence of damage uncertainty ($\mu_D = 0$) or of permafrost-related uncertainty ($\mu_N = 0$). This is suggestive of two forces that push the temperature risk premium in opposite directions. The first is the *capital accumulation channel*: everything else equal, an increase in σ_A augments the correlation between temperature and consumption since (ex-damage) consumption positively depends on capital, whose production generates carbon emissions; this tends to generate a negative correlation between temperatures and the SDF. The second is the *damage channel*: higher temperatures imply larger damage intensity, which works oppositely. As explained in the introduction, this is reminiscent of the two opposite forces that are at play to account for the insurance component of the SCC, namely the *scaling* and the *damage-reduction* channels (see Lemoine, 2021).

This is further illustrated by Figure VI.4, that shows how the SCC risk premiums and the 2100 temperature risk premiums jointly depend on the volatility of exogenous technological progress (σ_A, black line) or the scale of damages (in grey). Panel (a) corresponds to our baseline framework, with Epstein-Zin preferences; Panels (b) and (c) correspond to CRRA versions of the model, with two different risk aversion parameters.[32] The SCC risk premium is measured as the difference between the SCC and the sum of discounted expected benefits

[32]Supplemental Appendix VI.3 complements these results by computing the same objects for alternative IAMs based on Lemoine (2021) (using different damage specifications) and focusing on the influence of σ_A. The results are qualitatively similar to those presented here.

associated with the removal of one ton of CO_2 from the atmosphere, expressed as a fraction of the SCC. Start with the effect of σ_A, the volatility of exogenous technological progress (black line). Both the SCC risk premium and the temperature risk premium decrease when σ_A increases, under the effects of the *scaling channel* and of the *capital accumulation channel*, respectively. Consistently with Dietz et al. (2018) and Lemoine (2021), in the CRRA case (Panels b and c), the SCC risk premium is positive for $\sigma_A = 0$, and it turns negative for higher values of σ_A.[33] Turn to the effect of the scale of damages on the two types of risk premiums (grey lines). The relative importance of risk premiums in the SCC maintains the same order of magnitude when the scale of damages varies; but since the SCC positively depends on the scale of damages, the SCC risk premium also increases in absolute value. The temperature risk premium also positively depends on the scale of damages, consistently with the *damage channel* defined above.

We have observed that temperature risk premiums, defined as the variance between a temperature swap and the physical expectation of temperature, align with the difference in the first-order moments of the risk-neutral and physical conditional distributions of temperature (eq. 30). Higher-order moments have an impact on different temperature risk premiums related to assets with payoffs not linearly dependent on climate variables. Consider for instance a digital option that provides a payoff of 1 if temperature, at maturity, is larger than a given strike (T_K, say), and zero otherwise. The price of this option embeds a risk premium that depends on the difference between the right tails of the two distributions. Formally, the date-t price of this option is $\mathbb{E}_t(\mathcal{M}_{t,t+h}\mathbb{1}_{\{T_{AT,t+h}>T_K\}})$. Supposing that the option payment is deferred until maturity, the option price is:[34]

$$\frac{\mathbb{E}_t\left(\mathcal{M}_{t,t+h}\mathbb{1}_{\{T_{AT,t+h}>T_K\}}\right)}{\mathbb{E}_t(\mathcal{M}_{t,t+h})} = \mathbb{E}_t\left(\frac{\mathcal{M}_{t,t+h}}{\mathbb{E}_t(\mathcal{M}_{t,t+h})}\mathbb{1}_{\{T_{AT,t+h}>T_K\}}\right) = \mathbb{P}_t^{\mathbb{Q}_h}(T_{AT,t+h} > T_K). \quad (31)$$

[33] We do not have a positive SCC for $\sigma_A = 0$ in the Epstein-Zin context. Note however that, in the general context of recursive preferences, the interpretation of (our measure of) SCC risk premium is less straightforward because the difference between the SCC and the net present value of expected benefits cannot be expressed as a sum of covariances between the SDF and the benefits as is the case with CRRA preferences (see Supplemental Appendix V.3). See Appendix A.5 in Bansal et al. (2019) for the Epstein-Zin case. The difficulty to define an SCC risk premium in the Epstein-Zon case is also mentioned in Jensen and Traeger (2021) (p.27, and Footnote 18).

[34] Supposing that the option payment is deferred until maturity is without loss of generality; it facilitates the exposition, as the price of the option can then be directly interpreted as a probability, as shown by (31).

FIGURE 7. Social Cost of Carbon and temperature risk premiums

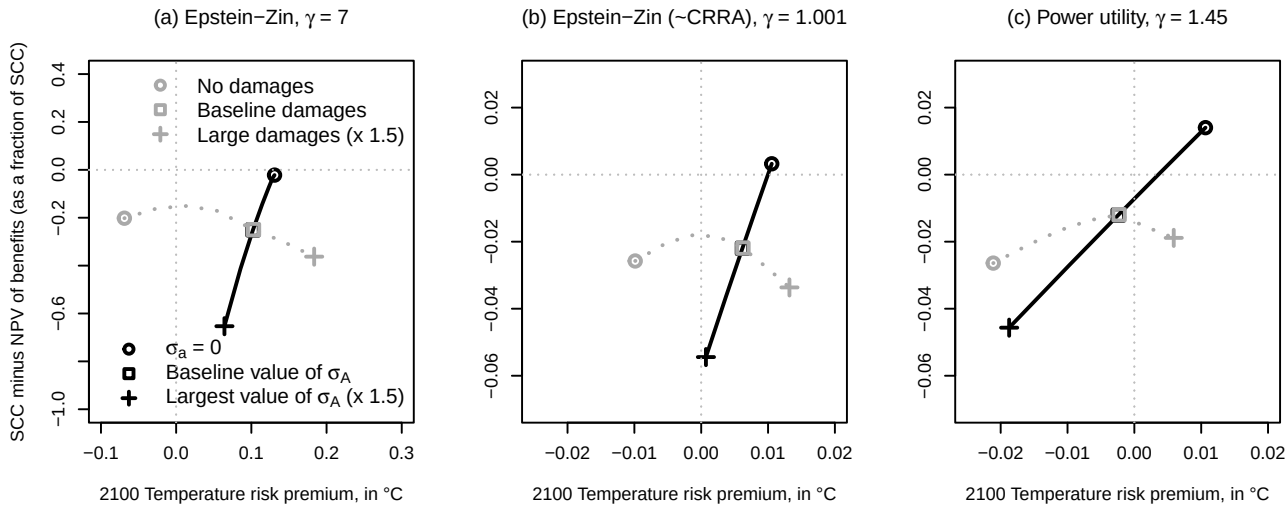

Notes: This figure shows the relationship between SCC and temperature risk premiums when varying the volatility of exogenous technological progress (black line) or the scale of damages (in grey). The x-axis coordinates are 2100 temperature risk premiums—the difference between the risk-adjusted and the physical expectation of temperature. The y-axis coordinate is the difference between the SCC and the sum discounted expected benefits associated with the removal of one ton of CO_2 from the atmosphere, expressed as a fraction of the SCC. Since we consider a unit intertemporal elasticity of substitution in the Epstein-Zin context, Panel (B), where $\gamma \approx 1$, corresponds to a situation where the Epstein-Zin and CRRA-based preferences coincide. The values of σ_A (see eq. 10) go from 0 to 1.5 times its baseline value (see Table 1). For damages, we jointly rescale $a^{(D)}$, $b^{(D)}$, μ_D, and b_{SK}.

TABLE 4. Climate options: types, payoffs, and pricing formulas

Type	Payoff (maturity, date $t+h$)	Price (date t)
Digital	$\mathbb{1}_{\{T_{t+h}>T_K\}}$	$\hat{\varphi}_t^{(h)}(0,-\mu_T,-T_k)$
Call	$(T_{t+h}-T_K)^+ = \mathbb{1}_{\{T_{t+h}>T_K\}}(T_{t+h}-T_K)$	$\bar{\varphi}_t^{(h)}(\mu_T,-\mu_T,-T_k) - T_K\bar{\varphi}_t^{(h)}(0,-\mu_T,-T_k)$
Put	$(T_{t+h}-T_K)^- = \mathbb{1}_{\{T_{t+h}<T_K\}}(T_K-T_{t+h})$	$T_K\bar{\varphi}_t^{(h)}(0,\mu_T,T_k) - \bar{\varphi}_t^{(h)}(\mu_T,\mu_T,T_k)$

Notes: This table reports the payoffs and prices of three types of temperature options (digital, call, and put). Functions $\hat{\varphi}_t^{(h)}$ and $\bar{\varphi}_t^{(h)}$ are defined in (24) and (25), respectively.

The previous expression shows that the option price is the size of the right-hand tail of the risk-neutral distribution. It can be decomposed as:

$$\mathbb{P}_t(T_{AT,t+h} > T_K) + \underbrace{\mathbb{P}_t^{\mathbb{Q}_h}(T_{AT,t+h} > T_K) - \mathbb{P}_t(T_{AT,t+h} > T_K)}_{\text{risk premium}}.$$

The risk premium is positive if the risk-adjusted tail is larger than its physical counterpart, which, according to (31), corresponds to situations where there is a positive conditional correlation between high temperatures and the SDF.

Our framework offers for analytical formulas to price such digital options, as well as calls and puts. Table 4 reports the payoffs and pricing formulas for the three types of options. For expository purposes, our numerical experiment focuses on digital options, whose prices can be interpreted as risk-adjusted probabilities of high temperatures (eq. 31). Figure 8 plots the prices of such digital options for T_K =2°C, 3°C and 4°C, and maturities up to 2100. Consistently with what precedes, we observe that risk-adjusted probabilities are higher than their physical counterparts. For $T_K = 4$°C, and for the maturity year 2100, the risk-adjusted probability is of 18%, 6 percentage points higher than the model-implied physical probability of exceeding this threshold. We also find that ratios between risk-adjusted and physical probabilities increase with the temperature strike. That type of result is reminiscent of a finding of the disaster-risk pricing literature: risk premiums can represent the bulk of the prices of those financial instruments providing larger payoffs in disastrous situations (financial meltdowns, defaults of large corporate or sovereign entities, e.g., Elton et al., 2001; Coval et al., 2009; Monfort et al., 2021; Gouriéroux et al., 2021).

FIGURE 8. Price of digital options, with contributions of risk premiums

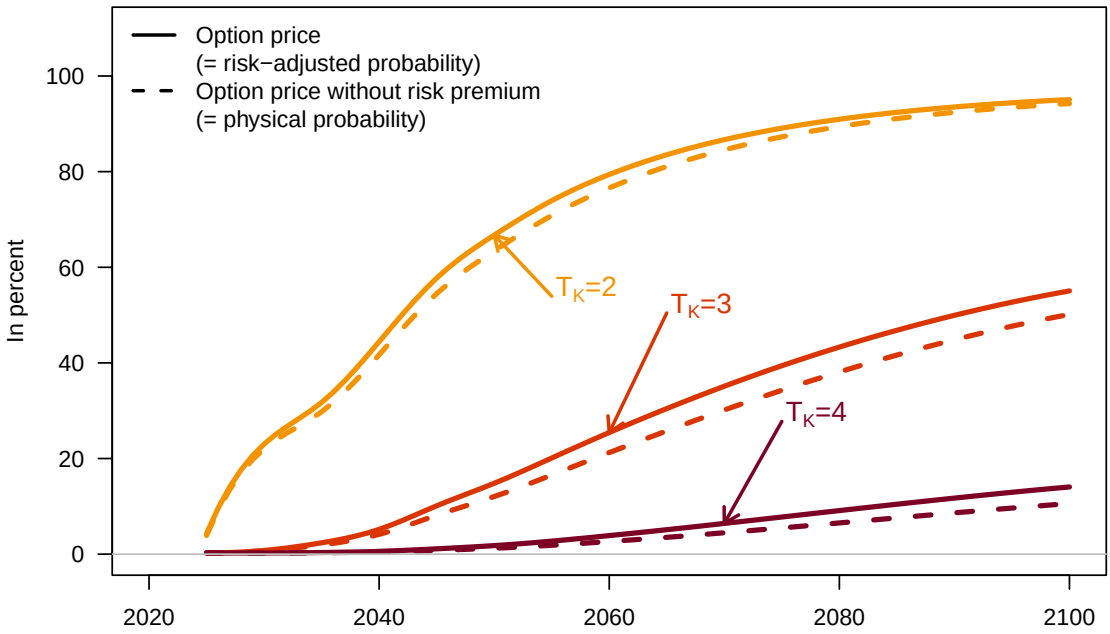

Notes: This figure shows the prices of digital options for different strikes (T_K) and maturities (x axis). More specifically, the solid lines display, for different maturities (h), $Dig_{t,h}(T_K)/B_{t,h}$, where $Dig_{t,h}$ is the date-t price of an option providing the payoff $\mathbb{1}_{\{T_{AT,t+h}>T_K\}}$ on date $t+h$ and $B_{t,h} = \mathbb{E}_t(\mathcal{M}_{t,t+h})$ is the date-t price of a zero-coupon bond of maturity h. The dashed lines show the probabilities that $T_{AT,t+h} > T_K$. If agents were not risk-averse, then solid lines would coincide with dashed lines; in other words, the deviations between solid and dashed lines reflect climate risk premiums.

4.2.3. *Equity and bonds whose issuer is exposed to climate risk.* The affine nature of our state vector paves the way for a wide range of equity and bond pricing methodologies built upon the properties of such processes. One can for instance price equity by employing the Bansal and Yaron (2004) approach, which consists in specifying a process for the dividend growth rate and deduce an approximate expression for the stock return using Campbell and Shiller (1988)'s linearization. One can also price defaultable bonds by specifying default intensities that linearly depends on the state vector (Duffie and Singleton, 1999; Duffie, 2005).

In this subsection, we consider a more structural approach, based on the Black-Scholes-Merton framework (Black and Scholes, 1973; Merton, 1974).[35] This type of approach allows for the joint pricing of equity and defaultable bonds. At the heart of the model stands the specification of the process followed by the value of a firm's asset ($\mathcal{A}_t$). The firm issues two types of financial instruments: equity and debt. Equity shares do not entitle the holders to receive dividends. Debt, on the other hand, takes the form of a zero-coupon bond that promises a payment of $\overline{\mathcal{A}}$ at a specified time ($t+h$, say). If the firm's asset value at time $t+h$ is greater than $\overline{\mathcal{A}}$, bondholders receive this amount, and the remaining asset value goes to shareholders. However, if the asset value falls short of the promised payment, the firm defaults, resulting in the lenders receiving a payment equal to the asset value, while shareholders receive no payment. Hence, in this model, the equity of the firm is modeled as a call option on its assets.

We assume that:

$$\log \mathcal{A}_t = \log \mathcal{A}_{t-1} + r_{A,t}, \quad \text{with} \quad r_{A,t} = \mu_{A,0,t} + \mu'_{A,1} X_t, \tag{32}$$

where $\mu_{A,0,t}$ is deterministic. Note that $\mu_{A,0,t}$ cannot be chosen independently from $\mu_{A,1}$ because the firm's value has to satisfy the Euler equation.[36]

This specification allows, for example, temperature and sea level to have an effect on the growth rate of $\mathcal{A}_t$; this is done by setting the appropriate entries of vector $\mu_{A,1}$ to non-zero

[35] Goldsmith-Pinkham et al. (2023) also use the Merton model to estimate the effect of SLR on exposed US municipalities' credit spreads. As the standard Black-Scholes-Merton framework, their model features a single source of shock (a Brownian process), that is not explicitly linked to climate dynamics.

[36] We must have, for any $h > 0$: $\mathbb{E}_t(\mathcal{M}_{t,t+h} \exp(r_{A,t+1} + \cdots + r_{A,t+h})) = 1$. In other words, once we specify $\mu_{A,1}$, the sequence of $\mu_{A,0,t}$ is given. Take a given $\mu_{A,1}$. Define $\widetilde{A}_t$ such that $\log \widetilde{A}_t = \log \widetilde{A}_{t-1} + \mu'_{A,1} X_t$, and determine $\widetilde{\mu}_A$ such that $\log(\widetilde{A}_t) = \widetilde{\mu}'_A X_t$. Assume you have already computed $\{\mu_{A,0,t+1}, \ldots, \mu_{A,0,t+h-1}\}$. Since $\mathbb{E}_t(\mathcal{M}_{t,t+h}\widetilde{A}_{t+h}) = \varphi_t^{(h)}(\widetilde{\mu}_A)$, and since the Euler equation rewrites $\exp(\mu_{A,0,t+1} + \cdots + \mu_{A,0,t+h})\mathbb{E}_t(\mathcal{M}_{t,t+h}\widetilde{A}_{t+h}) = 1$, it comes that $\mu_{A,0,t+h} = -\log(\varphi_t^{(h)}(\widetilde{\mu}_A)) - \mu_{A,0,t+h-1} - \cdots - \mu_{A,0,t+1}$.

values. As in the case of the price index (eq. 27), $\log \mathcal{A}_t$ can be included among the state vector's components, such that $\log \mathcal{A}_t = \mu_A' X_t$ (which defines the selection vector μ_A).

The date-t price of a zero-coupon bond of residual maturity h then is:

$$\begin{aligned}\mathcal{B}^*_{t,h} &:= \mathbb{E}_t\left(\mathcal{M}_{t,t+h}\left\{\mathbb{1}_{\{\mathcal{A}_{t+h}>\overline{\mathcal{A}}\}} + \frac{\mathcal{A}_{t+h}}{\overline{\mathcal{A}}}\mathbb{1}_{\{\log(\mathcal{A}_{t+h})\leq\log(\overline{\mathcal{A}})\}}\right\}\right)\\ &= \hat{\varphi}_t^{(h)}\left(0,-\mu_A,-\log(\overline{\mathcal{A}})\right) + \frac{1}{\overline{\mathcal{A}}}\bar{\varphi}_t^{(h)}\left(\mu_A,\mu_A,\log(\overline{\mathcal{A}})\right),\end{aligned}$$

where functions $\hat{\varphi}_t^{(h)}$ and $\bar{\varphi}_t^{(h)}$ are defined through (24) and (25), respectively.

The value of the firm's equity can then be expressed as the value of a call option on the firm's assets:

$$\begin{aligned}Equity_t &:= \mathbb{E}_t\left(\mathcal{M}_{t,t+h}\left\{(\mathcal{A}_{t+h}-\overline{\mathcal{A}})\mathbb{1}_{\{\mathcal{A}_{t+h}>\overline{\mathcal{A}}\}}\right\}\right)\\ &= \bar{\varphi}_t^{(h)}\left(\mu_A,-\mu_A,-\log(\overline{\mathcal{A}})\right) - \overline{\mathcal{A}}\hat{\varphi}_t^{(h)}\left(0,-\mu_A,-\log(\overline{\mathcal{A}})\right).\end{aligned}$$

Note that the present modeling framework is richer than the original Black-Scholes-Merton framework as it features stochastic interest rates—the risk-free bond price formula of Subsection 4.2.1 are still valid—and the firm value may be affected by various sources of uncertainty.

In our numerical example, we consider two firms: a benchmark firm and a "coastal" one, that is particularly exposed to SLR risk. The growth rate of the assets value of the latter is characterized by $\mu_{A,1}' X_t = \chi \Delta c_t$, where χ is sometimes referred to as the leverage parameter in the literature.[37] The second firm exhibits a heightened vulnerability to sea level changes; it is such that $\mu_{A,1}' X_t = \chi \Delta c_t - 0.1 H_t$. In other words, an unexpected 0.1 meter rise in sea level means that the company's value growth rate is reduced by one percentage point. Figure 9 depicts the expected trajectories of the asset values of both types of firms in the coming decades. The asset value of the second firm is likely to grow faster as investors demand a higher return to compensate for their greater risk-taking.

Figure 9 focuses on the firms' values ($\mathcal{A}_t$); let us turn to equity and debt. (On each date, we have $\mathcal{A}_t = Equity_t + \overline{\mathcal{A}} \times B^*_{t,h}$.) In our example, we consider a single maturity, of 20 years. Panel (a) of Figure 10 shows the expected annual equity returns as a function of indebtedness. In the absence of debt ($\overline{\mathcal{A}} = 0$), equity and asset values coincide, and the expected

[37] We set this parameter to 2.5, in line with the values found in Abel (1999), Collin-Dufresne et al. (2016) and Seo and Wachter (2018) (2.74, 2.5 and 2.6, respectively).

equity return is the same as that of $\mathcal{A}_t$. When firms become indebted, expected equity returns increase, as equity gets riskier than the asset value. Panel (b) displays the yields-to-maturity of the bonds issued by the two types of firms. The "coastal" firm faces higher funding costs, reflecting higher probabilities of default (PDs); these PDs are plotted in Panel (c). This plot distinguishes risk-neutral and physical PDs. As is usual in credit-risk models, risk-neutral PDs are higher than physical ones, which stems from the fact that defaults tend to take place in bad states of the world (see, e.g., D'Amato and Remolona, 2003). This is also shown by Panel (d), which displays the ratio between the two types of PDs. For high levels of indebtedness, the ratios decrease and converge towards one for both types of firms: as $\overline{\mathcal{A}}$ becomes high, corporate defaults become more frequent and do not only occur in the bad states of the world. As a result, the relative importance of risk premium diminishes.

FIGURE 9. Merton model (1/2)

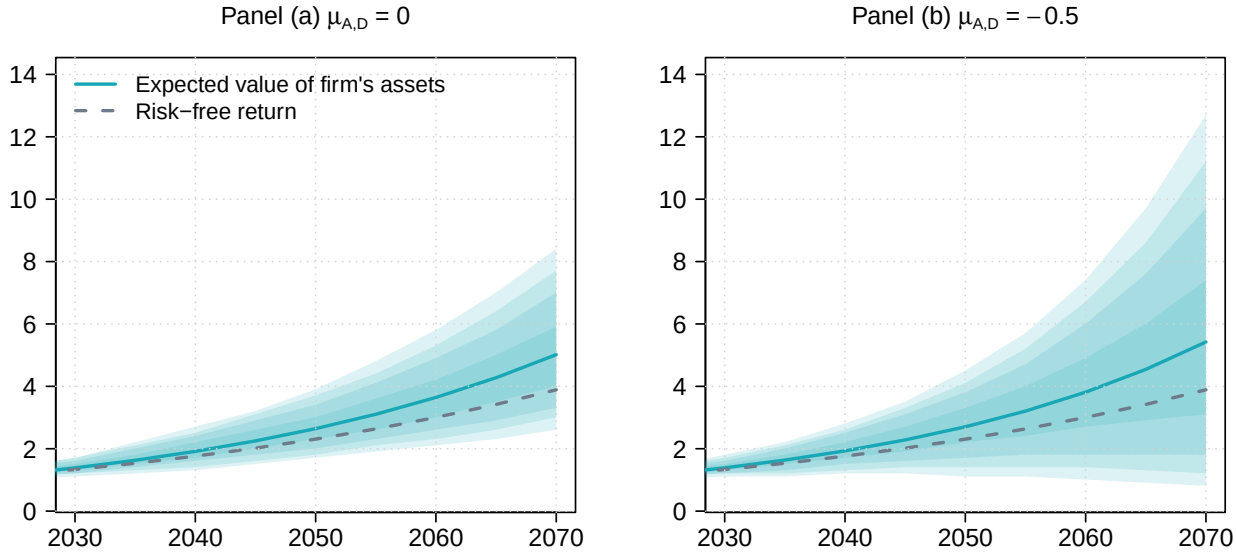

Notes: This figure represents the conditional distributions of the firm's asset in the context of the Black-Scholes-Merton model described in Subsection 4.2.3. The two panels correspond to two different specifications of the growth rate of the firm's assets (see eq. 32). In the first case (Panel a), the exposure of the asset process is characterized by $\mu'_{A,1}X_t = \chi\Delta c_t$, with $\chi = 2.5$. The second firm (Panel b) is more exposed to sea-level rise: $\mu'_{A,1}X_t = \chi\Delta c_t - 0.1H_t$. The value of the second firm's assets is expected to grow more rapidly since investors require a larger return to compensate for their larger riskiness. The dashed line shows the return on a risk-free investment (that yields a return $r_{t,h}$, see eq. 26).

FIGURE 10. Merton model (2/2)

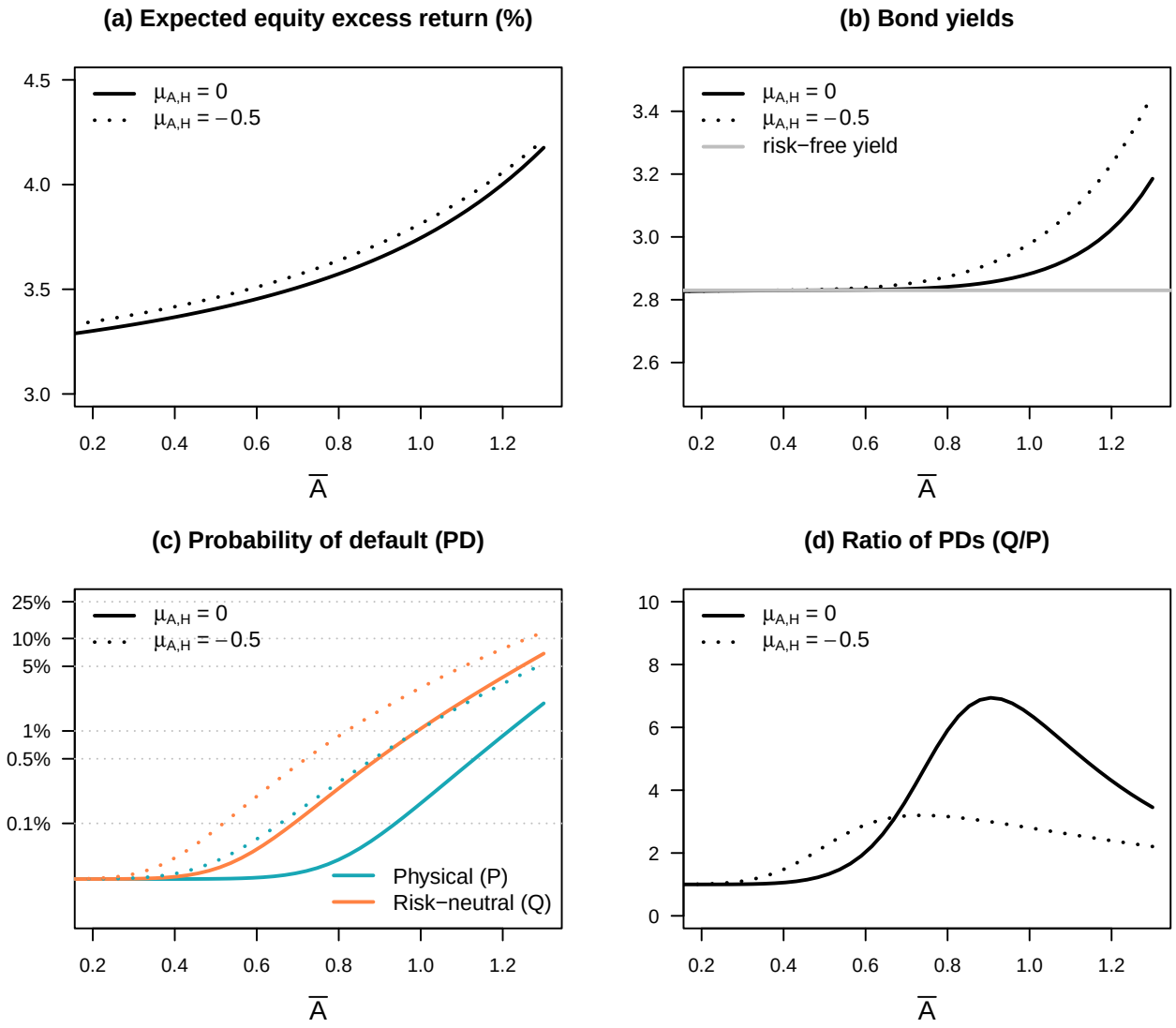

Notes: This figure shows outputs of the Black-Scholes-Merton model described in Subsection 4.2.3. The x-axes correspond to varying values of $\overline{\mathcal{A}}$, that measures the firm's indebtedness. We consider two types of firms, represented by solid lines and dotted lines; the second type is more exposed to climate-related damages (see caption of Figure 9). Panel (a) displays the expected returns of equity (as of the initial date); Panel (b) presents bond yields; Panel (c) shows the risk-neutral and physical probabilities of defaults (PDs); Panel (d) shows the ratio between risk-neutral and physical PDs.

5. CONCLUDING REMARKS

This paper proposes an analytical framework aiming to investigate the effects of climate risks on the pricing of long-dated assets. Our integrated assessment model (IAM) is solved instantaneously and offers quasi-analytical pricing formulas for various assets (bonds, equity, climate derivatives, real estate). Tractability results from the fact that, conditional on the

path of some deterministic exogenous variables, the state vector follows an affine process. The model accommodates climate-related capital destruction as well as adverse feedback loops reflecting, e.g., permafrost-related carbon releases. An additional original feature of the model is that it includes an endogenous sea-level process.

The model's tractability is exploited at the calibration stage. While many parameters are borrowed from the literature, we determine several others—typically those that have no direct equivalent in previous studies—by matching targeted moments. For instance, we look for a model parameterization that is consistent with available estimations of temperature on permafrost-related carbon releases.

Equipped with this model, we examine climate risk premiums. These premiums arise from differences between the physical and risk-neutral distributions, which we can determine analytically in our framework. We define, in particular, the temperature risk premium as the deviation between the mean of the risk-neutral and physical distributions of the atmospheric temperature for a given horizon. This premium would stand as the difference between the price of a swap indexed to the future temperature and the physical expectation of this temperature. We argue that the sign of the temperature risk-premium is ambiguous, as it would depend on the relative importance of two forces driving it in opposite directions: (i) everything else equal, temperature is higher in scenarios where exogenous productivity shocks have led a rapid accumulation of capital, whose production implies carbon emissions; this *capital accumulation channel* contributes to the positiveness of the correlation between consumption and temperatures, and therefore to the negativeness of the temperature risk premium; but (ii) higher temperatures increase the intensity of climate-related damages; this *damage channel* has opposite effects. (These two opposite forces are reminiscent, but not equivalent, to those shaping the sign of the climate beta discussed, e.g., in Dietz et al., 2018, and Lemoine, 2021.) The second effect dominates in our baseline calibration, where the temperature risk premium is of 0.10°C at horizon 2100. Our results however underscore the significant sensitivity of climate risk premiums to assumptions about damages, positive feedback effects, and associated uncertainties.

The current framework is flexible and could be enriched in several dimensions, without necessarily complicating model resolution or asset valuation. For instance, one may substitute additional deterministic relationships with specifications based on γ_0 (or other affine)

distributions. Moreover, as shown in the supplemental appendix, one can incorporate additional persistent Gaussian exogenous processes.[38] Such extensions may be applied, for example, to introduce exogenous long-term risks into the exogenous productivity growth process (as in, e.g., Bansal and Yaron, 2004; Bansal and Shaliastovich, 2013), or to incorporate additional sources of uncertainty into the system (in the spirit of the temperature shocks of Jensen and Traeger, 2021, or of the Brownian process used in Barnett et al., 2020). These possibilities remain open for further research.

REFERENCES

Abel, A. B. (1999). Risk Premia and Term Premia in General Equilibrium. *Journal of Monetary Economics 43*(1), 3–33.

Aliakbari, E. and R. McKitrick (2018). Information Aggregation in a Prediction Market for Climate Outcomes. *Energy Economics 74*(C), 97–106.

Andersson, M., C. Baccianti, and J. Morgan (2020). Climate Change and the Macro-Economy. Occasional Paper Series 243, European Central Bank.

Andersson, M., P. Bolton, and F. Samama (2019). Hedging Climate Risk. *Financial Analysts Journal 72*, 13–32.

Baker, M., D. Bergstresser, G. Serafeim, and J. Wurgler (2018). Financing the Response to Climate Change: The Pricing and Ownership of U.S. Green Bonds. NBER Working Papers 25194, National Bureau of Economic Research, Inc.

Baldauf, M., L. Garlappi, and C. Yannelis (2020). Does Climate Change Affect Real Estate Prices? Only If You Believe In It. *The Review of Financial Studies 33*(3), 1256–1295.

Bansal, R., D. Kiku, and M. Ochoa (2019). Climate Change Risk. Technical report, Federal Reserve Bank of San Francisco Working Paper.

Bansal, R., M. Ochoa, and D. Kiku (2016). Climate Change and Growth Risks. Working Paper 23009, National Bureau of Economic Research.

Bansal, R. and I. Shaliastovich (2013). A Long-Run Risks Explanation of Predictability Puzzles in Bond and Currency Markets. *Review of Financial Studies 26*(1), 1–33.

Bansal, R. and A. Yaron (2004). Risks for the Long Run: A Potential Resolution of Asset Pricing Puzzles. *Journal of Finance 59*, 1481–1509.

Barnett, M., W. Brock, and L. P. Hansen (2020, 02). Pricing Uncertainty Induced by Climate Change. *The Review of Financial Studies 33*(3), 1024–1066.

[38] Specifically, while the model presented in the main text features a single i.i.d. Gaussian shock, the version presented in the supplemental appendix includes a vector η_t that follows an auto-regressive process. The components of this vector could be added to the different equations of the model without altering its tractability.

Barnett, M., W. Brock, L. P. Hansen, and H. Hong (2020). Pricing Uncertainty Induced by Climate Change. *Review of Financial Studies 33*(3), 1024–1066.

Barrage, L. and W. D. Nordhaus (2023). Policies, Projections, and the Social Cost of Carbon: Results from the DICE-2023 Model. Working Paper 31112, National Bureau of Economic Research.

Batten, S. (2018). Climate Change and the Macro-Economy: a Critical Review. Bank of England working papers 706, Bank of England.

Bauer, M. D. and G. D. Rudebusch (2023). The Rising Cost of Climate Change: Evidence from the Bond Market. *The Review of Economics and Statistics 105*(5), 1255–1270.

Beirne, J., Y. Dafermos, A. Kriwoluzky, N. Renzhi, U. Volz, and J. Wittich (2021). The Effects of Natural Disasters on Price Stability in the Euro Area. Working Papers 244, Department of Economics, SOAS University of London, UK.

Bernstein, A., M. T. Gustafson, and R. Lewis (2019). Disaster on the Horizon: The Price Effect of Sea Level Rise. *Journal of Financial Economics 134*(2), 253–272.

Black, F. and M. S. Scholes (1973). The Pricing of Options and Corporate Liabilities. *Journal of Political Economy 81*(3), 637–54.

Bloch, D., J. Annan, and J. Bowles (2010). Cracking the Climate Change Conundrum with Derivatives. *Wilmott Journal 2*(5), 271–287.

Bloch, D., J. Annan, and J. Bowles (2011). Applying Climate Derivatives to Flood Risk Management. *Wilmott 2011*(56), 88–103.

Brace, A., D. Gatarek, and M. Musiela (1997). The Market Model of Interest Rate Dynamics. *Mathematical Finance 7*(2), 127–155.

Burke, M., S. Hsiang, and E. Miguel (2015). Global Non-Linear Effect of Temperature on Economic Production. *Nature 527*(7577), 235–239.

Cai, Y. and K. L. Judd (2014). Advances in Numerical Dynamic Programming and New Applications. In K. Schmedders and K. L. Judd (Eds.), *Handbook of Computational Economics Vol. 3*, Volume 3 of *Handbook of Computational Economics*, Chapter 8, pp. 479 – 516. Elsevier.

Cai, Y. and T. S. Lontzek (2019). The Social Cost of Carbon with Economic and Climate Risks. *Journal of Political Economy 127*(6), 2684–2734.

Campbell, J. Y. and R. J. Shiller (1988). Stock Prices, Earnings, and Expected Dividends. *Journal of Finance 43*(3), 661–676.

Cao, M. and J. Wei (2004). Weather Derivatives Valuation and Market Price of Weather Risk. *Journal of Futures Markets 24*(11), 1065–1089.

Clayton, J. (1996). Rational Expectations, Market Fundamentals and Housing Price Volatility. *Real Estate Economics 24*(4), 441–470.

Collin-Dufresne, P., M. Johannes, and L. A. Lochstoer (2016). Parameter Learning in General Equilibrium: The Asset Pricing Implications. *The American Economic Review 106*(3), 664–698.

Coval, J. D., J. W. Jurek, and E. Stafford (2009). Economic Catastrophe Bonds. *American Economic Review 99*(3), 628–666.

D'Amato, J. and E. M. Remolona (2003). The Credit Spread Puzzle. *BIS Quarterly Review*.

Daniel, K. D., R. B. Litterman, and G. Wagner (2019). Declining CO_2 Price Paths. *Proceedings of the National Academy of Sciences 116*(42), 20886–20891.

Dell, M., B. F. Jones, and B. A. Olken (2009). Temperature and Income: Reconciling New Cross-Sectional and Panel Estimates. *The American Economic Review 99*(2), 198–204.

Desmet, K., R. E. Kopp, S. A. Kulp, D. K. Nagy, M. Oppenheimer, E. Rossi-Hansberg, and B. H. Strauss (2021). Evaluating the Economic Cost of Coastal Flooding. *American Economic Journal: Macroeconomics 13*(2), 444–486.

Diaz, D. B. (2016). Estimating Global Damages from Sea Level Rise with the Coastal Impact and Adaptation Model (CIAM). *Climatic Change 137*(1), 143–156.

Dietz, S., R. V. der Ploeg, A. Rezai, and F. Venmans (2020). Are Economists Getting Climate Dynamics Right and Does It Matter? CESifo Working Paper Series 8122, CESifo.

Dietz, S., C. Gollier, and L. Kessler (2018). The Climate Beta. *Journal of Environmental Economics and Management 87*(C), 258–274.

Duffie, D. (1996). *Dynamic Asset Pricing Theory* (second ed.). Princeton, New Jersey: Princeton University Press.

Duffie, D. (2005). Credit Risk Modeling with Affine Processes. *Journal of Banking & Finance 29*(11), 2751–2802.

Duffie, D., D. Filipovic, and W. Schachermayer (2003). Affine Processes and Applications in Finance. *Annals of Applied Probability 13*(3), 984–1053.

Duffie, D., J. Pan, and K. Singleton (2000). Transform Analysis and Asset Pricing for Affine Jump-Diffusions. *Econometrica 68*(6), 1343–1376.

Duffie, D. and K. J. Singleton (1999). Modeling Term Structures of Defaultable Bonds. *Review of Financial Studies 12*(4), 687–720.

Elton, E. J., M. J. Gruber, D. Agrawal, and C. Mann (2001). Explaining the Rate Spread on Corporate Bonds. *Journal of Finance 56*(1), 247–277.

Engle, R. F., S. Giglio, B. Kelly, H. Lee, J. Stroebel, and A. Karolyi (2020). Hedging Climate Change News. *Review of Financial Studies 33*(3), 1184–1216.

Epstein, L. G. and S. E. Zin (1989). Substitution, Risk Aversion, and the Temporal Behavior of Consumption and Asset Returns: A Theoretical Framework. *Econometrica 57*(4), 937–69.

Folini, D., F. KÃ¼bler, A. Malova, and S. Scheidegger (2023). The Climate in Climate Economics. *Review of Economic Studies , forthcoming*.

Garner, A. J., M. E. Mann, K. A. Emanuel, R. E. Kopp, N. Lin, R. B. Alley, B. P. Horton, R. M. DeConto, J. P. Donnelly, and D. Pollard (2017). Impact of Climate Change on New York City's Coastal Flood Hazard: Increasing Flood Heights from the Preindustrial to 2300 CE. *Proceedings of the National Academy of Sciences 114*(45), 11861–11866.

Giglio, S., B. Kelly, and J. Stroebel (2021). Climate Finance. *Annual Review of Financial Economics 13*(1), 15–36.

Giglio, S., B. T. Kelly, and J. Stroebel (2020). Climate Finance. NBER Working Papers 28226, National Bureau of Economic Research, Inc.

Giglio, S., M. Maggiori, K. Rao, J. Stroebel, A. Weber, and S. V. Nieuwerburgh (2021). Climate Change and Long-Run Discount Rates: Evidence from Real Estate. *Review of Financial Studies 34*(8), 3527–3571.

Giovannini, A. and P. Weil (1989). Risk Aversion and Intertemporal Substitution in the Capital Asset Pricing Model. NBER Working Papers 2824, National Bureau of Economic Research, Inc.

Goldsmith-Pinkham, P., M. T. Gustafson, R. C. Lewis, and M. Schwert (2023). Sea-Level Rise Exposure and Municipal Bond Yields. *The Review of Financial Studies*.

Gollier, C. and J. K. Hammitt (2014). The Long-Run Discount Rate Controversy. *Annual Review of Resource Economics 6*(1), 273–295.

Gollier, C. and M. L. Weitzman (2010). How Should the Distant Future be Discounted when Discount Rates are Uncertain? *Economics Letters 107*(3), 350–353.

Gomes, J. F., M. Grotteria, and J. A. Wachter (2019). Cyclical Dispersion in Expected Defaults. *Review of Financial Studies 32*(4), 1275–1308.

Gordon, M. J. (1962). The Savings Investment and Valuation of a Corporation. *The Review of Economics and Statistics 44*(1), 37–51.

Gouriéroux, C., A. Monfort, S. Mouabbi, and J.-P. Renne (2021). Disastrous Defaults. *Review of Finance 25*(6), 1727–1772.

Gurkaynak, R. S. and J. H. Wright (2012, June). Macroeconomics and the Term Structure. *Journal of Economic Literature 50*(2), 331–67.

Hambel, C., H. Kraft, and E. Schwartz (2021). Optimal Carbon Abatement in a Stochastic Equilibrium Model with Climate Change. *European Economic Review 132*(C).

Hauer, M., J. Evans, and D. Mishra (2016). Millions Projected to Be at Risk from Sea-level Rise in the Continental United States. *Nature Climate Change 6*, 691–695.

Horton, B. P., N. S. Khan, N. Cahill, J. S. Lee, T. A. Shaw, A. J. Garner, A. C. Kemp, S. E. Engelhart, and S. Rahmstorf (2020). Estimating Global Mean Sea-Level Rise and its Uncertainties by 2100 and 2300 from an Expert Survey. *npj Climate and Atmospheric Science 3*(1), 1–8.

Howard, P. H. and T. Sterner (2017). Few and Not So Far Between: A Meta-analysis of Climate Damage Estimates. *Environmental & Resource Economics 68*(1), 197–225.

Huynh, T. D. and Y. Xia (2020). Climate Change News Risk and Corporate Bond Returns. *Journal of Financial and Quantitative Analysis*, 1–25.

International Monetary Fund (2019). Sustainable Finance: Looking Farther. Global Financial Stability Report, Chapter 6 October 2019, IMF.

Jamshidian, F. (1989). An Exact Bond Option Formula. *The Journal of Finance 44*(1), 205–209.

Jensen, S. and C. P. Traeger (2014). Optimal Climate Change Mitigation under Long-Term Growth Uncertainty: Stochastic Integrated Assessment and Analytic Findings. *European Economic Review 69*, 104–125.

Jensen, S. and C. P. Traeger (2021). Pricing Climate Risk. CESifo Working Paper Series 9196, CESifo.

Kahn, M. E., K. Mohaddes, R. N. Ng, M. H. Pesaran, M. Raissi, and J.-C. Yang (2021). Long-Term Macroeconomic Effects of Climate Change: A Cross-Country Analysis. *Energy Economics 104*(C).

Karydas, C. and A. Xepapadeas (2022). Climate Change Financial Risks: Implications for Asset Pricing and Interest Rates. *Journal of Financial Stability 63*, 101061.

Keys, B. J. and P. Mulder (2020). Neglected No More: Housing Markets, Mortgage Lending, and Sea Level Rise. NBER Working Papers 27930, National Bureau of Economic Research, Inc.

Klusak, P., M. Agarwala, M. Burke, M. Kraemer, and K. Mohaddes (2023). Rising Temperatures, Falling Ratings: The Effect of Climate Change on Sovereign Creditworthiness. *Management Science 0*(0), null.

Kopp, R. E., A. C. Kemp, K. Bittermann, B. P. Horton, J. P. Donnelly, et al. (2016). Temperature-Driven Global Sea-Level Variability in the Common Era. *Proceedings of the National Academy of Sciences 113*(11), E1434–E1441.

Larcker, D. F. and E. M. Watts (2020). Where's the Greenium? *Journal of Accounting and Economics 69*(2).

Lemoine, D. (2021). The Climate Risk Premium: How Uncertainty Affects the Social Cost of Carbon. *Journal of the Association of Environmental and Resource Economists 8*(1), 27–57.

Lemoine, D. and C. Traeger (2014). Watch your Step: Optimal Policy in a Tipping Climate. *American Economic Journal: Economic Policy 6*(1), 137–66.

Lemoine, D. and C. Traeger (2016). Economics of Tipping the Climate Dominoes. *Nature Climate Change 6*, 514–519.

Lenton, T. M., H. Held, E. Kriegler, J. W. Hall, W. Lucht, S. Rahmstorf, and H. J. Schellnhuber (2008). Tipping Elements in the Earth's Climate System. *Proceedings of the National Academy of Sciences 105*(6), 1786–1793.

Little, L. R., A. J. Hobday, J. Parslow, C. R. Davies, and R. Q. Grafton (2015). Funding Climate Adaptation Strategies with Climate Derivatives. *Climate Risk Management 8*, 9–15.

MacDougall, A. H. and R. Knutti (2016). Projecting the Release of Carbon from Permafrost Soils using a Perturbed Parameter Ensemble Modelling Approach. *Biogeosciences 13*(7), 2123–2136.

Macdougall, A. H., N. C. Swart, and R. Knutti (2017). The Uncertainty in the Transient Climate Response to Cumulative CO2 Emissions Arising from the Uncertainty in Physical Climate Parameters. *Journal of Climate 30*, 813–827.

Mallucci, E. (2022). Natural Disasters, Climate Change, and Sovereign Risk. *Journal of International Economics 139*, 103672.

Meese, R. and N. Wallace (1994). Testing the Present Value Relation for Housing Prices: Should I Leave My House in San Francisco? *Journal of Urban Economics 35*(3), 245–266.

Mengel, M., A. Nauels, J. Rogelj, et al. (2018). Committed Sea-Level Rise Under the Paris Agreement and the Legacy of Delayed Mitigation Action. *Nature Communication 9*, 1–10.

Merton, R. C. (1974). On the Pricing of Corporate Debt: The Risk Structure of Interest Rates. *Journal of Finance 29*(2), 449–70.

Miller, M., J. D. Paron, and J. A. Wachter (2020). Sovereign Default and the Decline in Interest Rates. Technical report.

Miltersen, K. R., K. Sandmann, and D. Sondermann (1997). Closed Form Solutions for Term Structure Derivatives with Log-Normal Interest Rates. *Journal of Finance 52*(1), 409–430.

Monfort, A., F. Pegoraro, J.-P. Renne, and G. Roussellet (2017). Staying at Zero with Affine Processes: An Application to Term Structure Modelling. *Journal of Econometrics 201*(2), 348–366.

Monfort, A., F. Pegoraro, J.-P. Renne, and G. Roussellet (2021). Affine Modeling of Credit Risk, Pricing of Credit Events, and Contagion. *Management Science 67*(6), 3674–3693.

Mukherjee, K. and B. Ouattara (2021). Climate and Monetary Policy: Do Temperature Shocks Lead to Inflationary Pressures? *Climatic Change 167*(3), 1–21.

Murfin, J. and M. Spiegel (2020). Is the Risk of Sea Level Rise Capitalized in Residential Real Estate? *The Review of Financial Studies 33*(3), 1217–1255.

Nordhaus, W. D. (1992). An Optimal Transition Path for Slowing Climate Change. *Science 20*, 1315–1319.

Nordhaus, W. D. (2017). Revisiting the Social Cost of Carbon. *Proceedings of the National Academy of Sciences 114*(7), 1518–1523.

Nordhaus, W. D. and P. Sztorc (2013). DICE 2013R: Introduction and User's Manual, Second Edition.

Painter, M. (2020). An Inconvenient Cost: The Effects of Climate Change on Municipal Bonds. *Journal of Financial Economics 135*(2), 468–482.

Parker, M. (2018). The Impact of Disasters on Inflation. *Economics of Disasters and Climate Change 2*(1), 21–48.

Pástor, L., R. F. Stambaugh, and L. A. Taylor (2022). Dissecting Green Returns. *Journal of Financial Economics 146*(2), 403–424.

Piazzesi, M. (2010). Affine Term Structure Models. In *Handbook of Financial Econometrics, Volume 1* (Yacine Aït-Sahalia and Lars Peter Hansen North Holland ed.)., Chapter 12, pp. 389–472. Elsevier.

Piazzesi, M. and M. Schneider (2007). Equilibrium Yield Curves. In *NBER Macroeconomics Annual 2006, Volume 21*, NBER Chapters, pp. 389–472. National Bureau of Economic Research, Inc.

Pindyck, R. S. (2019). The Social Cost of Carbon Revisited. *Journal of Environmental Economics and Management 94*, 140–160.

Rahmstorf, S. (2007). A Semi-Empirical Approach to Projecting Future Sea-Level Rise. *Science 315*(5810), 368–370.

Rahmstorf, S. (2010). A New View on Sea Level Rise. *Nature Climate Change 1*, 44–45.

Rahmstorf, S., M. Perrette, and M. Vermeer (2012). Testing the Robustness of Semi-Empirical Sea Level Projections. *Climate Dynamics 39*, 861–875.

Ramaswamy, V., O. Boucher, J. Haigh, D. Hauglustaine, J. Haywood, et al. (2001). *Radiative Forcing of Climate Change*, Chapter Chapter 6, pp. 19–28. Cambridge, UK and New-York, NY, USA: Cambridge University Press.

Rudebusch, G. D. and E. T. Swanson (2012). The Bond Premium in a DSGE Model with Long-Run Real and Nominal Risks. *American Economic Journal: Macroeconomics 4*(1), 105–143.

Schlenker, W. and C. A. Taylor (2021). Market Expectations of a Warming Climate. *Journal of Financial Economics 142*(2), 627–640.

Schorfheide, F., D. Song, and A. Yaron (2018). Identifying Long-Run Risks: A Bayesian Mixed-Frequency Approach. *Econometrica 86*(2), 617–654.

Seo, S. B. and J. A. Wachter (2018). Do Rare Events Explain CDX Tranche Spreads? *Journal of Finance 73*, 2343–2383.

Steffen, W., J. Rockström, K. Richardson, T. M. Lenton, C. Folke, et al. (2018). Trajectories of the Earth System in the Anthropocene. *Proceedings of the National Academy of Sciences 115*(33), 8252–8259.

Stern, N. (2007). *The Economics of Climate Change: The Stern Review*. Cambridge University Press.

Sterner, T. and U. M. Persson (2008). An Even Sterner Review: Introducing Relative Prices into the Discounting Debate. *Review of Environmental Economics and Policy 2*(1), 61–76.

Taconet, N., C. Guivarch, and A. Pottier (2021). Social Cost of Carbon under Stochastic Tipping Points. *Environmental and Resource Economics 78*(4), 709–737.

Traeger, C. P. (2023). ACE-Analytic Climate Economy. *American Economic Journal: Economic Policy 15*(3), 372–406.

Van den Bremer, T. S. and F. Van der Ploeg (2021). The Risk-Adjusted Carbon Price. *American Economic Review 111*(9), 2782–2810.

Vermeer, M. and S. Rahmstorf (2009). Global Sea Level Linked to Global Temperature. *Proceedings of the National Academy of Sciences 106*(51), 21527–21532.

Weil, P. (1989). The Equity Premium Puzzle and the Risk-Free Rate Puzzle. *Journal of Monetary Economics 24*(3), 401–421.

Weitzman, M. L. (2009). On Modeling and Interpreting the Economics of Catastrophic Climate Change. *The Review of Economics and Statistics 91*(1), 1–19.

Weitzman, M. L. (2012). GHG Targets as Insurance Against Catastrophic Climate Damages. *Journal of Public Economic Theory 14*(2), 221–244.

Weitzman, M. L. (2013). Tail-Hedge Discounting and the Social Cost of Carbon. *Journal of Economic Literature 51*(3), 873–882.

Zenios, S. A. (2022). The Risks from Climate Change to Sovereign Debt. *Climatic Change 172*(3), 1–19.

APPENDIX A. THE γ_0 DISTRIBUTION

In several of the model equations, randomness is introduced by means of the γ_0 distribution, proposed by Monfort et al. (2017). We have $X \sim \gamma_0(\lambda, \mu)$ if and only if there exists a Poisson variable $Z \sim \mathcal{P}(\lambda)$ such that the conditional distribution of X given Z is a Dirac mass at zero if $Z = 0$, and a gamma distribution featuring a shape parameter Z and a scale parameter μ otherwise (i.e., if $Z > 0$). In words, this distribution arises as a Poisson mixture of gamma distributions.

It is easily seen that $X = 0$ if and only if $Z = 0$. As a consequence:

$$\mathbb{P}(X = 0) = \exp(-\lambda). \tag{33}$$

As noted by Monfort et al. (2017), the γ_0 distribution admits a particularly simple Laplace transform:

$$\mathbb{E}(\exp[uX]) = \exp\left(\frac{u\mu}{1-u\mu}\lambda\right). \tag{34}$$

Importantly, the fact that this Laplace tansform is exponential affine in λ implies that it can be used as a basic block to construct affine processes. (These processes can be multivariate, as is the case in the present paper.) For the same reason, all the cumulants of X are affine in λ. In particular, we extensively exploit the analytical expressions of the first two (mean and variance) in the present paper:

$$\mathbb{E}(X) = \mu\lambda, \quad \text{and} \quad \mathbb{V}ar(X) = 2\mu\mathbb{E}(X) = 2\mu^2\lambda. \tag{35}$$

Appendix B. Model

B.1. **Climate block.** The atmospheric temperature ($T_{AT,t}$) depends on radiative forcings (F_t) and on the lower-ocean temperature ($T_{LO,t-1}$) (this is eq. 2):

$$T_{AT,t}|\mathcal{I}_{t-1} \sim i.i.d.\, \gamma_0\left(\frac{1}{\mu_t}\left[T_{AT,t-1} + \xi_1\left\{F_{t-1} - \frac{\tau}{\nu}T_{AT,t-1} - \xi_2\left(T_{AT,t-1} - T_{LO,t-1}\right)\right\}\right], \mu_T\right).$$

The lower-ocean temperature moves according to (3): $T_{LO,t} = T_{LO,t-1} + \xi_3\left(T_{AT,t-1} - T_{LO,t-1}\right)$.

We employ a linearized version of the relationship between radiative forcings and atmospheric carbon concentration (see Supplemental Appendix VI.1):

$$F_t = \tau\log_2(m_0) + \frac{\tau}{\log(2)m_0}\left(\frac{M_{AT,t}}{M_{PI}} - m_0\right) + F_{EX,t},$$

(this is eq. 4), where exogenous radiative forcings ($F_{EX,t}$) are given by:

$$F_{EX,t} = \begin{cases} \phi_0 + \frac{1}{16}(\phi_1 - \phi_0)(t-1) & \text{if } t \leq 16 \quad (t = 16 \text{ corresponds to } 2100) \\ \phi_1 & \text{if } t > 16. \end{cases} \tag{36}$$

The carbon cycle dynamics takes the following matrix form (this is eq. 5):

$$\begin{bmatrix} M_{AT,t} \\ M_{UP,t} \\ M_{LO,t} \end{bmatrix} = \begin{bmatrix} 1-\varphi_{12} & \varphi_{12}\frac{mateq}{mueq} & 0 \\ \varphi_{12} & 1-\varphi_{12}\frac{mateq}{mueq} - \varphi_{23} & \varphi_{23}\frac{mueq}{mleq} \\ 0 & \varphi_{23} & 1-\varphi_{23}\frac{mueq}{mleq} \end{bmatrix}^{\Delta t} \begin{bmatrix} M_{AT,t-1} \\ M_{UP,t-1} \\ M_{LO,t-1} \end{bmatrix} + \frac{\Delta t}{3.666}\begin{bmatrix} \mathcal{E}_{t-1} \\ 0 \\ 0 \end{bmatrix}. \tag{37}$$

The dynamics of sea level reads (this is eq. 8):

$$H_t - H_{t-1}|\mathcal{I}_{t-1} \sim i.i.d.\, \gamma_0\left(\lambda_{H,t}, \mu_H\right), \quad \text{with} \quad \lambda_{H,t} = \frac{1}{\mu_H}\left(a^{(H)} + b^{(H)}T_{AT,t-1}\right).$$

B.2. **Economic block.**

B.2.1. *Goods: production and use.* On date t, production is (this is eq. 10):

$$Y_t = A_t K_t, \quad \text{with } A_t = \bar{A} + \sigma_A \eta_{A,t},$$

where A_t and K_t are productivity and productive capital, respectively, and where $\eta_{A,t} \sim i.i.d. \mathcal{N}(0,1)$ is a productivity shock. Productive capital evolves according to (11) and (12):

$$K_t^* = (1 - dep)K_{t-1} + Inv_t \quad \text{and} \quad K_t = \exp(-D_t - b_{SK}\Delta H_t)K_t^*,$$

where dep is the depreciation rate, D_t (≥ 0) represents climate-related disasters, and $b_{SK}\Delta H_t$ is the destruction of capital due to sea level rise. Climate-related disasters follow (eq. 13):

$$D_t | \mathcal{I}_{t-1} \sim i.i.d. \, \gamma_0 \left(\lambda_{D,t}, \mu_D\right), \quad \text{with} \quad \lambda_{D,t} = \frac{1}{\mu_D}\left(a^{(D)} + b^{(D)} T_{AT,t-1}\right).$$

The production of date t, namely Y_t, can be used for consumption (C_t), to increase the stock of capital (investment Inv_t, see eq. 11), or to invest in the mitigation technology (Ψ_t):

$$Y_t = C_t + Inv_t + \Psi_t.$$

B.2.2. *Industrial emissions and mitigation technology.* Without mitigation ($\mu_t = 0$), and up to deterministic decrease in the carbon intensity of production σ_t (see eq. 39), industrial carbon emissions are supposed to grow as planned capital. The supplemental appendix shows that this leads to

$$\mathcal{E}_{Ind,t} = \sigma_t(1 - \mu_t) q_0 \exp\left(\sum_{i=1}^{t-1} [\mu_{c,i} + \sigma_{c,i}\eta_{A,i}]\right),$$

where $\mu_{c,i} + \sigma_{c,i}\eta_{A,i}$ is the growth rate of pre-damage consumption for date t (see eq. 17).

To preserve the conditional affine property of the model dynamics, industrial emissions have to linearly depend on shocks $\eta_{A,t}$. Using (a) that $\exp(\mu + \sigma\varepsilon) \approx \exp(\mu + \frac{\sigma^2}{2})(1 + \sigma\varepsilon)$ when $\varepsilon \sim \mathcal{N}(0,1)$ and for a small σ, and (b) that the $\eta_{A,t}$ are i.i.d., we obtain the following expression for industrial emissions:

$$\mathcal{E}_{Ind,t} = \lambda_t \left(1 + \tilde{y}_{t-1}\right), \tag{38}$$

with $\tilde{y}_t = \sum_{i=1}^{t} \sigma_{c,i}\eta_{A,i}$ and $\lambda_t = \sigma_t(1 - \mu_t) q_0 \exp\left(\sum_{i=1}^{t-1}\left(\mu_{c,i} + \frac{\sigma_{c,i}^2}{2}\right)\right)$, where the carbon intensity σ_t—the emission resulting from the production of one unit of good in the absence of mitigation—follows:

$$\sigma_t = \sigma_{t-1}(1 + g_{\sigma,t}), \text{ with } g_{\sigma,t} = g_{\sigma,t-1}(1 + \delta_\sigma)^{\Delta t}. \tag{39}$$

Increasing the mitigation rate μ_t is costly. As in the DICE framework, we posit that one needs to invest an amount $\Psi_t(\mu_t)$ to achieve a mitigation rate μ_t:

$$\Psi_t = \Lambda_t Y_t, \quad \text{with } \Lambda_t = \mu_t^{\theta_2} BC_t,$$

where:

$$BC_t = \frac{BP_t \sigma_t}{1000 \times \theta_2}, \quad \text{with} \quad BP_t = pback(1 - gback)^{t-1}. \tag{40}$$

In our framework, agents do not dynamically optimize with respect to the mitigation rate. They decide, on the initial date, a trajectory that they commit to later on. Formally, on date 0, they consider trajectories of the following form (this is eq. 15; see Subsection 3.3):

$$\mu_t = \min\left(\exp\left(-\theta_{a,opt} + \theta_{b,opt} \times t\right); 1\right).$$

Hence, on date $t = 0$, they look for the pair $\{\theta_{a,opt}, \theta_{b,opt}\}$, with $\theta_{a,opt} \geq 0$ and $\theta_{b,opt} \geq 0$ that optimizes their date-0 utility.

B.2.3. *Agents' preferences, and resulting consumption process.* Agents feature Epstein and Zin (1989) preferences, with a unit elasticity of intertemporal substitution (EIS). Specifically, the time-t utility of a consumption stream (C_t) is recursively defined by:

$$u_t \quad = \quad (1-\delta)c_t + \frac{\delta}{1-\gamma} \log\left(\mathbb{E}_t \exp\left[(1-\gamma)u_{t+1}\right]\right), \tag{41}$$

where c_t denotes the logarithm of the agent's consumption level C_t, δ the time discount factor and γ the risk aversion parameter.[39]

At each date, agents optimally determine how to allocate output after mitigation ($(1 - \Lambda_t)Y_t$) between consumption and investment in productive capital. As shown in Supplemental Appendix I.1, under (41), when the capital accumulation is described by (11) and (12), this optimization results in the following consumption growth (this is eq. 16):

$$\Delta c_t = \log(C_t/C_{t-1}) = \mu_{c,t} + \sigma_{c,t}\eta_{A,t} - D_t - b_{SK}\Delta H_t,$$

where $\mu_{c,t}$ and $\sigma_{c,t}$ are given by (17) and where Λ_t is given by (14).

B.3. **Total carbon emissions.** We consider three sources of emissions: economic activities, lands, and permafrost melting (this is eq. 6):

$$\mathcal{E}_t = \mathcal{E}_{Land,t} + \mathcal{E}_{Ind,t} + N_t.$$

[39] eq. (41) results from a first-order Taylor expansion around $\rho = 1$ of the general Epstein and Zin (1989) recursive utility defined by: $u_t = \frac{1}{1-\rho} \log\left((1-\delta)C_t^{1-\rho} + \delta\left(\mathbb{E}_t\left[\exp\{(1-\gamma)u_{t+1}\}\right]\right)^{\frac{1-\rho}{1-\gamma}}\right)$, where ρ is the inverse of the EIS.

As in the DICE model, exogenous land emissions are given by:

$$\mathcal{E}_{Land,t} = \varepsilon_0(1-\rho)^{t-1}, \tag{42}$$

with $0 < \rho < 1$.

N_t corresponds to sudden releases of carbon in the atmosphere, e.g., due to permafrost erosion (see Subsection 3.2). Specifically, we posit:

$$N_t|\mathcal{I}_{t-1} \sim \textit{i.i.d.}\, \gamma_0\left(\lambda_{N,t}, \mu_N\right), \quad \text{with} \quad \lambda_{N,t} = \frac{\kappa_N^{t-1}}{\mu_N}\left(a^{(N)} + b^{(N)} T_{AT,t-1}\right). \tag{43}$$

APPENDIX C. ADDITIONAL TABLES ANF FIGURES

TABLE 5. Initial values of the state vector, X_0

Variable	Notation	Eq.	Value	Unit	Reference
Initial emissions	$\mathcal{E}_0$	(6)	43.50	$GtCO_2$	DICE2023
Initial industrial emissions	$\mathcal{E}_{ind,0}$	(38)	37.60	$GtCO_2$	DICE2023
Initial radiative forcings	F_0	(4)+(2)	2.00	W/m^2	CDICE
Initial carbon concent. (atmos.)	$M_{AT,0}$	(5)	851	GtC	CDICE
Initial carbon concent. (upper ocean)	$M_{UP,0}$	(5)	628	GtC	CDICE
Initial carbon concent. (lower ocean)	$M_{LO,0}$	(5)	1323	GtC	CDICE
Initial temp. anomaly (atmos.)	$T_{AT,0}$	(2)	1.10	°C	CDICE
Initial temp. anomaly (lower ocean)	$T_{LO,0}$	(3)	0.27	°C	CDICE
Initial sea level	H_0	(8)	0.13	m	Vermeer and Rahmstorf (2009)

Notes: This table presents the initial values of our state vector $X_{t=0}$, where date $t = 0$ corresponds to 2020. CDICE corresponds to Folini et al. (2023).

TABLE 6. Calibrated parameters

Parameter	Notation	Equation	Value	Unit/Note	Reference
Time step	Δt		5	years	
Risk aversion	γ	(41)	7.0		
Discount factor (annual)	$1-\delta^{\frac{1}{\Delta t}}$	(41)	1.50	percent per year	
Capital depreciation rate	dep	(12)	6	percent per year	
Avg ratio M_{AT}/M_{PI} over 2020-2100	m_0	(4)	1.92		CDICE+RCP
Decline rate of decarbonization	δ_σ	(39)	-4.00	percent per period	DICE2023
Industrial emissions in 2020	e_0	(σ_0)	37.60	$GtCO_2$ per year	DICE2023
Initial world gross output in 2020	q_0	(38)	135.70	trillions of 2019 USD	DICE2023
Emission control rate in 2020	μ_0	(38)	5.00	percent	DICE2023
Carbon intensity in 2020	σ_0	(39)	$\frac{e_0}{q_0(1-\mu_0)}=0.29$	$kgCO_2$ per one thousand USD of 2020 production	DICE2023
Initial growth of carbon intensity σ_1	$g_{\sigma,1}$	(39)	-1.50	percent per period	DICE2023
Backstop price	$pback$	(40)	695	2019 USD	DICE2023
Initial cost decline backstop cost	$gback$	(40)	5.00	percent per period	DICE2023
Exponent control cost function	θ_2	(14)+(40)	2.60		DICE2023
Carbon emissions from land in 2020	ε_0	(42)	5.90	$GtCO_2$ per year	DICE2023
Decline rate in land emissions	ρ	(42)	10.00	percent per period	DICE2023
2020 forcings of non-CO_2 GHG	ϕ_0	(36)	0.52	W/m^2	DICE2023
2100 forcings of non-CO_2 GHG	ϕ_1	(36)	0.80	W/m^2	DICE2023
Equilibrium concentration in atmosphere	$mateq$	(37)	607	GtC	CDICE
Equilibrium concentration in upper strata	$mueq$	(37)	489	GtC	CDICE
Equilibrium concentration in lower strata	$mleq$	(37)	1281	GtC	CDICE
Transfer coef. from atm. to up. ocean	φ_{12}	(37)	0.05300		CDICE
Transfer coef. from up. to lo. ocean	φ_{23}	(37)	0.00820		CDICE
Climate eq. coefficient for upper level	ξ_1	(2)	0.68500	per period	CDICE
Transfer coef. upper to lower stratum	ξ_2	(2)	0.73000	per period	CDICE
Transfer coef. for lower stratum	ξ_3	(3)	0.03445	per period	CDICE
Forcings of equilibrium CO_2 doubling	τ	(4)+(2)	3.45	W/m^2	CDICE
Equilibrium temperature impact	ν	(2)	3.25	°C per doubling CO_2	CDICE
Destruction of capital due to rising SL	b_{SK}	(16)	0.10		Diaz (2016)

Notes: This table presents the parameters used in our baseline model. DICE2023 refers to Barrage and Nordhaus (2023). CDICE refers to Folini, KÃ¼bler, Malova, and Scheidegger (2023). See Footnote 22 for explanations regarding the calibration of b_{SK}.

—Supplemental Appendix—

An Analytical Framework to Price Long-Dated Climate-Exposed Assets

Pauline CHIKHANI and Jean-Paul RENNE

This supplemental appendix is organized as follows:

- Section I is about the consumption process and the emission growth rates in the production economy. More precisely, Subsection I.1 solves for the optimal consumption process in the economy depicted in Section 3 of the paper, and Subsection I.2 determines the industrial emission process.
- Section II provides various analytical results: In particular, Subsection II.1 gives the matrix representation of the state vector's dynamics. Subsections II.2 and II.3 give the Laplace transforms of the state vector. Subsections II.4 and II.5 derive the conditional mean and variance of the state vector.
- Section III provides various asset-pricing results. The Stochastic Discount Factor (SDF) is given in Subsection III.1. The asset-pricing formulas introduced in Section 4 of the paper are detailed in Subsection III.2. The computation of the social cost of carbon (SCC) is presented in Subsection III.3.
- Section IV details the calibration approach.
- Section V develops a version of the model where Epstein-Zin preferences are replaced with time-separable power utility.
- Section VI reports additional results. Subsection VI.1 discusses the linearization of the radiative forcing specification. Subsection VI.2 reports the resulting mitigation path and discusses the assumption according to which agents do not dynamically re-optimize mitigation. Subsection VI.3 compares the SCC risk premium and the temperature risk premium in the context of alternative modeling approaches. Subsection VI.4 presents the result of a sensitivity analysis.

APPENDIX I. CONSUMPTION AND EMISSION GROWTH RATES IN THE PRODUCTION ECONOMY

I.1. **Solving for the consumption process.** In this appendix, we derive the consumption growth process in our production economy. Let us denote agents' wealth by $\mathcal{W}_t$. In the context of Epstein-Zin-Weil preferences, and with a unit Elasticity of Intertemporal Substitution, it can be shown that:[40]

$$C_t = (1-\delta)\mathcal{W}_t. \tag{I.1}$$

Since agents' wealth at time t is $\mathcal{W}_t = C_t + K^*_{t+1}$, where K^*_{t+1} is planned capital (see eq. 11), it comes, using (I.1), that:

$$\delta \mathcal{W}_t = K^*_{t+1}, \tag{I.2}$$

eq. (I.1) then gives:

$$C_t = \frac{1-\delta}{\delta} K^*_{t+1}. \tag{I.3}$$

We have:

$$Y_t = C_t + Inv_t + \Psi_t, \tag{I.4}$$

where, Ψ_t, the investment in low-carbon technologies, is given by $\Psi_t = \Lambda_t Y_t$.

On date $t+1$, we have $Y_{t+1} = A_{t+1}K_{t+1}$, which implies that (I.4) rewrites (for date $t+1$):

$$C_{t+1} = (1-\Lambda_{t+1})A_{t+1}K_{t+1} - Inv_{t+1} \tag{I.5}$$

Using (I.3) in $K^*_{t+1} = (1-dep)K_t + Inv_t$ gives:

$$Inv_t = \frac{\delta}{1-\delta} C_t - (1-dep)K_t. \tag{I.6}$$

Using the previous expression in (I.5) yields

$$C_{t+1} = (1-\Lambda_{t+1})A_{t+1}K_{t+1} - \frac{\delta}{1-\delta} C_{t+1} + (1-dep)K_{t+1},$$

that is, using $K_{t+1} = \exp(-D_{t+1} - b_{SK}\Delta H_{t+1})K^*_{t+1}$, and (I.3):

$$\frac{1}{1-\delta} C_{t+1} = \Big((1-\Lambda_{t+1})A_{t+1} + (1-dep)\Big)\exp(-D_{t+1} - b_{SK}\Delta H_{t+1})\frac{\delta}{1-\delta} C_t.$$

Finally:

$$\frac{C_{t+1}}{C_t} = \delta\Big((1-\Lambda_{t+1})A_{t+1} + (1-dep)\Big)\exp(-D_{t+1} - b_{SK}\Delta H_{t+1}).$$

Assuming that $A_t = \bar{A} + \sigma_A \eta_{A,t}$, we get:

$$\frac{C_{t+1}}{C_t} = \delta\Big((1-\Lambda_{t+1})(\bar{A} + \sigma_A \eta_{A,t+1}) + (1-dep)\Big)\exp(-D_{t+1} - b_{SK}\Delta H_{t+1}).$$

[40] See, e.g., Appendix B in Giovannini and Weil (1989).

The resulting log growth rate of consumption is:

$$\begin{aligned}\Delta c_{t+1} &= \log\delta + \log\Big((1-\Lambda_{t+1})(\bar{A}+\sigma_A\eta_{A,t+1}) + (1-dep)\Big) - \\ &\quad D_{t+1} - b_{SK}\Delta H_{t+1} \\ &\approx \mu_{c,t+1} + \sigma_{c,t+1}\eta_{A,t+1} - D_{t+1} - b_{SK}\Delta H_{t+1}, \end{aligned} \tag{I.7}$$

where $\mu_{c,t}$ and $\sigma_{c,t}$ are given by (17). This is (16).

I.2. **Emission growth rate.** This subsection derives the specification of industrial emissions, namely (38).

Up to potential mitigation (μ_t, see Section 3) and to deterministic decrease in the carbon intensity of production σ_t (see eq. 39), industrial carbon emissions are supposed to grow as (planned) capital. More precisely, as in the DICE framework, industrial carbon emissions of date t are of the form $\sigma_t(1-\mu_t)q_t$, where q_t follows:

$$\frac{q_{t+1}}{q_t} = \frac{K^*_{t+1}}{K_t}.$$

Using $K^*_{t+1} = \frac{1-\delta}{\delta}C_t$ (eq. I.3) and $K_t = \exp(-D_t - b_{SK}\Delta H_t)K^*_t$, we obtain:

$$\frac{q_{t+1}}{q_t} = \frac{C_t}{C_{t-1}}\exp(D_t + b_{SK}\Delta H_t).$$

Using (I.7), it comes that the log growth rate of q_t is approximately equal to $\mu_{c,t} + \sigma_{c,t}\eta_{A,t}$ (with a one-period lag). This would lead to the following expression for industrial emissions:

$$\mathcal{E}_{Ind,t} = \sigma_t(1-\mu_t)q_0\exp\left(\sum_{i=1}^{t-1}[\mu_{c,i} + \sigma_{c,i}\eta_{A,i}]\right).$$

However, to preserve the conditional affine property of the model dynamics, industrial emissions have to linearly depend on the shocks $\eta_{A,t}$. Using (a) that $\exp(\mu+\sigma\varepsilon) \approx \exp(\mu + \frac{\sigma^2}{2})(1+\sigma\varepsilon)$ when $\varepsilon \sim \mathcal{N}(0,1)$ and for a small σ, and (b) that the $\eta_{A,t}$s are i.i.d., we get the following expression for industrial emissions:

$$\mathcal{E}_{Ind,t} = \sigma_t(1-\mu_t)q_0\exp\left(\sum_{i=1}^{t-1}\left(\mu_{c,i} + \frac{\sigma^2_{c,i}}{2}\right)\right)(1+\tilde{y}_{t-1}), \tag{I.8}$$

with $\tilde{y}_t = \sum_{i=1}^{t}\sigma_{c,i}\eta_{A,i}$. Equation (I.8) can also be written as $\mathcal{E}_{Ind,t} = \lambda_t\,(1+\tilde{y}_{t-1})$, with:

$$\lambda_t = \sigma_t(1-\mu_t)q_0\exp\left(\sum_{i=1}^{t-1}\left(\mu_{c,i} + \frac{\sigma^2_{c,i}}{2}\right)\right).$$

APPENDIX II. STATE VECTOR'S CONDITIONAL MOMENTS AND LAPLACE TRANSFORM

II.1. **Rewriting the model in matrix form.** We decompose the state variable, denoted by X_t, as follows:

$$X_t = \begin{bmatrix} Z_t \\ W_t \end{bmatrix}, \quad \text{where} \quad Z_t = \begin{bmatrix} \Delta c_t \\ \tilde{y}_t \\ \mathcal{E}_t \\ \mathcal{E}_{Ind,t} \\ F_t \\ M_{AT,t} \\ M_{UP,t} \\ M_{LO,t} \\ T_{AT,t} \\ T_{LO,t} \\ Cum_{D,t} \\ Cum_{\mathcal{E},t} \\ Cum_{\Delta c,t} \\ H_t \end{bmatrix}, \quad \text{and} \quad W_t = \begin{bmatrix} \eta_{t[n_\eta \times 1]} \\ D_t \\ N_t \\ T_{AT,t} \\ \Delta H_t \end{bmatrix}, \tag{II.1}$$

where $Cum_{D,t} = -\sum_{i=1}^{t} D_i$, $Cum_{\mathcal{E},t} = \sum_{i=1}^{t} \mathcal{E}_i$, and $c_t - c_0 = Cum_{\Delta c,t} = \sum_{i=1}^{t} \Delta c_i$. Although the paper considers a single Gaussian shock (namely $\eta_{A,t}$ in eq. 10), the present appendices allow for a vector of Gaussian variables (η_t, of dimension $n_\eta \times 1$). Moreover, the components of η_t are not necessarily serially and mutually uncorrelated; specifically, η_t follows a vector auto-regressive process:

$$\eta_t = \Phi \eta_{t-1} + \varepsilon_{\eta,t}, \quad \varepsilon_{\eta,t} \sim i.i.d. \mathcal{N}(0, \mathbf{Id}_{n_\eta \times n_\eta}). \tag{II.2}$$

Except for η_t, the dynamics of the components of Z_t is presented in Appendix B. The resulting dynamics of Z_t can be concisely written in matrix form:

$$A_0^* Z_t = A_{1,t}^* Z_{t-1} + \omega_{0,t}^* + \omega_t^* W_t, \tag{II.3}$$

where:

$$A_0^* = \begin{bmatrix} 1 & 0 & \dots & & & & & & & & \dots & 0 & b_{SK} \\ 0 & 1 & 0 & \dots & & & & & & & & & \\ 0 & 0 & 1 & -1 & 0 & \dots & & & & & & & \\ 0 & 0 & 0 & 1 & 0 & \dots & & & & & & & \\ & & \dots & 0 & 1 & -\frac{\tau}{\log(2) M_{PI}(m_0)} & \dots & & & & & & \\ & & & \dots & 0 & 1 & 0 & \dots & & & & & \\ & & & & \dots & 0 & 1 & 0 & \dots & & & & \\ & & & & & \dots & 0 & 1 & 0 & \dots & & & \\ & & & & & & \dots & 0 & 1 & 0 & \dots & & \\ & & & & & & & \dots & 0 & 1 & 0 & \dots & \\ & & & & & & & & \dots & 0 & 1 & 0 & 0 \\ 0 & 0 & -1 & 0 & \dots & & & & & \dots & 0 & 1 & 0 \\ -1 & 0 & \dots & & & & & & & & \dots & 0 & 1 \\ & & & & & & & & & & \dots & 0 & 0 \end{bmatrix},$$

$$A_{1,t}^* = \begin{bmatrix} 0 & \dots & & & & & & & & & & \dots & 0 & b_{SK} \\ 0 & 1 & 0 & \dots & & & & & & & & & & \\ 0 & 0 & 0 & \dots & & & & & & & & & & \\ 0 & \lambda_t & 0 & \dots & & & & & & & & & & \\ 0 & \dots & & & & & & & & & & & & \\ 0 & 0 & \frac{\Delta t}{3.666} & 0 & 0 & \begin{bmatrix} \varphi_{11} & \varphi_{21} & 0 \\ \varphi_{12} & \varphi_{22} & \varphi_{32} \\ 0 & \varphi_{23} & \varphi_{33} \end{bmatrix}^{\Delta t} & 0 & \dots & & & & & \\ 0 & 0 & 0 & 0 & 0 & & 0 & \dots & & & & & & \\ 0 & 0 & 0 & 0 & 0 & & 0 & \dots & & & & & & \\ 0 & \dots & & & & & & & & & & & & \\ & & & & & \dots & \xi_3 & 1-\xi_3 & 0 & \dots & & & \\ & & & & & & \dots & 0 & 1 & 0 & \dots & & \\ & & & & & & & \dots & 0 & 1 & 0 & 0 & \\ & & & & & & & & \dots & 0 & 1 & 0 & \\ 0 & \dots & & & & & & & & & \dots & 0 & 1 \end{bmatrix},$$

and

$$\omega_{0,t}^* = \begin{bmatrix} \mu_{c,t} \\ 0 \\ \mathcal{E}_{Land,t} \\ \lambda_t \\ \frac{\tau}{\log(2)}\left(\log(m_0)-1\right)+F_{EX,t} \\ 0 \\ 0 \\ 0 \\ 0 \\ 0 \\ 0 \\ 0 \\ 0 \\ 0 \end{bmatrix}, \quad \omega_t^* = \begin{bmatrix} \sigma_{c,t} & -1 & 0 & 0 & 0 \\ \sigma_{c,t} & 0 & 0 & 0 & 0 \\ 0 & 0 & 1 & 0 & 0 \\ 0 & 0 & 0 & 0 & 0 \\ 0 & 0 & 0 & 0 & 0 \\ 0 & 0 & 0 & 0 & 0 \\ 0 & 0 & 0 & 0 & 0 \\ 0 & 0 & 0 & 0 & 0 \\ 0 & 0 & 0 & 1 & 0 \\ 0 & 0 & 0 & 0 & 0 \\ 0 & -1 & 0 & 0 & 0 \\ 0 & 0 & 0 & 0 & 0 \\ 0 & 0 & 0 & 0 & 0 \\ 0 & 0 & 0 & 0 & 1 \end{bmatrix}.$$

Note that ω_t^* here has 5 columns because η_t is a scalar in our setting. In general (if η_t is of dimension $n_\eta \times 1$), the number of columns of ω_t^* is $n_\eta + 4$.

Pre-multiplying both sides of (II.3) by $(A_0^*)^{-1}$, we obtain:

$$Z_t = A_{1,t} Z_{t-1} + \omega_{0,t} + \omega_t W_t, \tag{II.4}$$

with

$$A_{1,t} = (A_0^*)^{-1} A_{1,t}^*, \quad \omega_{0,t} = (A_0^*)^{-1}\omega_{0,t}^*, \quad \omega_t = (A_0^*)^{-1}\omega_t^*.$$

II.2. **Laplace transform of W_t.**

Proposition 1. *The Laplace transform of W_t, considering $u_W = [u_\eta', u_D, u_N, u_T, u_H]'$, is given by:*

$$\psi_W(u_W) := \mathbb{E}_t(\exp[u_W' W_{t+1}]) = \exp(\alpha_W(u_W) + \beta_W(u_W)' X_t) \quad \forall t, \tag{II.5}$$

with

$$\begin{cases} \alpha_{W,t}(u_W) &= \frac{u_\eta u_\eta'}{2} + \frac{u_D\mu_D}{1-u_D\mu_D}\ell_0^{(D)} + \frac{u_N\mu_N}{1-u_N\mu_N}\kappa_N^{t+1}\ell_0^{(N)} + \frac{u_T\mu_T}{1-u_T\mu_T}\ell_0^{(T)} + \frac{u_H\mu_H}{1-u_H\mu_H}\ell_0^{(H)} \\ \beta_{W,t}(u_W) &= \begin{bmatrix} 0_{n_Z\times 1} \\ \Phi' u_\eta \\ 0_{(n_W-n_\eta)\times 1} \end{bmatrix} + \\ & \qquad \frac{u_D\mu_D}{1-u_D\mu_D}\ell_1^{(D)} + \frac{u_N\mu_N}{1-u_N\mu_N}\kappa_N^{t+1}\ell_1^{(N)} + \frac{u_T\mu_T}{1-u_T\mu_T}\ell_1^{(T)} + \frac{u_H\mu_H}{1-u_H\mu_H}\ell_1^{(H)}, \end{cases} \tag{II.6}$$

where the $\ell_0^{(w)}$ and $\ell_0^{(w)}$ ($w \in \{D, N, T, H\}$) are such that variable w_t is $\gamma_0(\ell_0^{(w)} + \ell_1^{(w)\prime} X_t, \mu_w)$. For instance, according to (8), $\ell_0^{(H)} = a^{(H)}/\mu_H$, and $\ell_1^{(H)}$ is the vector that is such that $\ell_1^{(H)\prime} X_t = a^{(H)} T_{AT,t}/\mu_H$. (That is, it has only one non-zero entry.)

Proof. The shocks being conditionally independent, and using the Laplace transform of the gamma-zero distribution (Appendix A) used to model D_t and N_t (see eqs. 13 and 7), we have:

$$\begin{aligned}
&\mathbb{E}_t\left(\exp\left(u_W' W_{t+1}\right)\right) = \mathbb{E}_t\left[\exp\left(u_\eta' \eta_{t+1} + u_D D_{t+1} + u_N N_{t+1}\right)\right] \\
= \;& \exp\left(u_\eta' \Phi \eta_t\right) \mathbb{E}_t\left(\exp\left(u_\eta' \varepsilon_{\eta,t+1}\right)\right) \times \\
& \mathbb{E}_t\left(\exp\left(u_D D_{t+1}\right)\right) \mathbb{E}_t\left(\exp\left(u_N N_{t+1}\right)\right) \mathbb{E}_t\left(\exp\left(u_T T_{AT,t+1}\right)\right) \mathbb{E}_t\left(\exp\left(u_H H_{t+1}\right)\right) \\
= \;& \exp\left[u_\eta' \Phi \eta_t + \frac{u_\eta u_\eta'}{2} + \frac{u_D \mu_D}{1 - u_D \mu_D}\left(\ell_0^{(D)} + \ell_1^{(D)\prime} X_t\right) + \right. \\
& \left. \frac{u_N \mu_N \kappa_N^t}{1 - u_N \mu_N}\left(\ell_0^{(N)} + \ell_1^{(N)\prime} X_t\right) + \frac{u_T \mu_T}{1 - u_T \mu_T}\left(\ell_0^{(T)} + \ell_1^{(T)\prime} X_t\right) + \frac{u_H \mu_H}{1 - u_H \mu_H}\left(\ell_0^{(H)} + \ell_1^{(H)\prime} X_t\right)\right],
\end{aligned}$$

which gives the result. □

II.3. **Simple and multi-horizon Laplace transforms of $X_t = [Z_t', W_t']'$.** In Proposition 2 and Corollary 1, we consider a linear combination of the components of X_{t+1}, namely $u' X_{t+1} = u_Z' Z_{t+1} + u_W' W_{t+1}$ (i.e. $u = [u_Z', u_W']'$).

Proposition 2. One-period-ahead Laplace transform of $X_t = [Z_t', W_t']'$. *We have:*

$$\exp(\psi_t(u)) := \mathbb{E}_t(\exp(u' X_{t+1})) = \exp(\alpha_t(u) + \beta_t(u)' X_t),$$

with

$$\left\{\begin{array}{rcl} \alpha_t(u) & = & u_Z' \omega_{0,t+1} + \alpha_{W,t}(u_W + \omega_{t+1}' u_Z) \\ \beta_t(u) & = & \left[\begin{array}{c} A_{1,t+1}' u_Z \\ 0_{n_W \times 1} \end{array}\right] + \beta_{W,t}(u_W + \omega_{t+1}' u_Z), \end{array}\right. \tag{II.7}$$

where functions $\alpha_{W,t}$ and $\beta_{W,t}$ are defined by (II.6).

Proof. We have:

$$\begin{aligned}
&\mathbb{E}_t(\exp(u' X_{t+1})) = \mathbb{E}_t[\exp(u_Z' Z_{t+1} + u_W' W_{t+1})] \\
= \;& \mathbb{E}_t(\exp(u_Z'(A_{1,t+1} Z_t + \omega_{0,t+1} + \omega_{t+1} W_{t+1}) + u_W W_{t+1})) \\
= \;& \exp\left[u_Z'(A_{1,t+1} Z_t + \omega_{0,t+1})\right] \mathbb{E}_t\left[\exp\left(\{u_W' + u_Z' \omega_{t+1}\} W_{t+1}\right)\right] \\
= \;& \exp\left[u_Z'(A_{1,t+1} Z_t + \omega_{0,t+1}) + \alpha_{W,t}\left(u_W + \omega_{t+1}' u_Z\right) + \beta_{W,t}\left(u_W + \omega_{t+1}' u_Z\right)' X_t\right],
\end{aligned}$$

which gives the result. □

Proposition 3. Multi-horizon Laplace transform of $X_t = [Z_t', W_t']'$. *We have:*

$$\begin{aligned}\psi_t^{(h)}(u_1,\dots,u_h) &:= \mathbb{E}_t(\exp[u_1'X_{t+1}+\cdots+u_h'X_{t+h}) \\ &= \exp\left[\psi_{0,t}^{(h)}(u_1,\dots,u_h)+\psi_{1,t}^{(h)}(u_1,\dots,u_h)'X_t\right], \end{aligned} \tag{II.8}$$

where, for all t and for $h>1$:

$$\left\{\begin{array}{rcl}\psi_{0,t}^{(h)}(u_1,\dots,u_h) &=& \psi_{0,t+1}^{(h-1)}(u_2,\dots,u_h)+\alpha_t\left(u_1+\psi_{1,t+1}^{(h-1)}(u_2,\dots,u_h)\right)\\ \psi_{1,t}^{(h)}(u_1,\dots,u_h) &=& \beta_t\left(u_1+\psi_{1,t+1}^{(h-1)}(u_2,\dots,u_h)\right),\end{array}\right. \tag{II.9}$$

and with, for all s, $\psi_{0,s}^{(1)}(u)=\alpha_s(u)$ and $\psi_{1,s}^{(1)}(u)=\beta_s(u)$, functions α_s and β_s being defined in (II.7).

In practice: *Using the notation $U_k = \psi_{1,t+h-k}^{(k)}(u_{h-k+1},\dots,u_h)$ [with, in particular, $U_h = \psi_{1,t}^{(h)}(u_1,\dots,u_h)$], the second equation of (II.9) implies that, for $k\geq 2$:*

$$U_k = \beta_{t+h-k}(u_{h-k+1}+U_{k-1}),$$

which allows to compute the U_k ($k=1,\dots,h$) by backward recursions, starting from $U_1=\beta_{t+h-1}(u_h)$. Once the U_k ($k=1,\dots,h$) are computed, the first equation of (II.9) gives $\psi_{0,t}^{(h)}(u_1,\dots,u_h)$. Specifically, for $h\geq 1$, we have:

$$\psi_{0,t}^{(h)}(u_1,\dots,u_h)=\alpha_t(u_1+U_{h-1})+\alpha_{t+1}(u_2+U_{h-2})+\cdots+\alpha_{t+h-2}(u_{h-1}+U_1)+\alpha_{t+h-1}(u_h).$$

Proof. We have:

$$\begin{aligned}&\mathbb{E}_t(\exp[u_1'X_{t+1}+\cdots+u_h'X_{t+h}]) \\ =\ &\mathbb{E}_t\left(\mathbb{E}_{t+1}(\exp[u_1'X_{t+1}+\cdots+u_h'X_{t+h}])\right) \\ =\ &\mathbb{E}_t\left(\exp\left[u_1'X_{t+1}+\psi_{0,t+1}^{(h-1)}(u_2,\dots,u_h)+\psi_{1,t+1}^{(h-1)}(u_2,\dots,u_h)'X_{t+1}\right]\right) \\ =\ &\exp\left[\psi_{0,t+1}^{(h-1)}(u_2,\dots,u_h)+\alpha_t\left(u_1+\psi_{1,t+1}^{(h-1)}(u_2,\dots,u_h)\right)+\beta_t\left(u_1+\psi_{1,t+1}^{(h-1)}(u_2,\dots,u_h)\right)'X_t\right],\end{aligned}$$

which leads to the result by induction. □

Corollary 1. (Simple) multi-horizon Laplace transform of $X_t = [Z_t', W_t']'$. *Using the ψ notation introduced in Proposition 3 (via equation II.8), we have:*

$$\psi_t^{(h)}(0,\dots,0,u)=\mathbb{E}_t(\exp(u'X_{t+h}))=\exp\left[a_{t,h}(u)+b_{t,h}(u)'X_t\right],$$

where $b_{t,k}(u) = \beta_t \circ \cdots \circ \beta_{t+k-1}(u)$, *and*

$$a_{t,h} = \alpha_{t+h-1}(u) + \alpha_{t+h-2}(b_{t+h-1,1}(u)) + \cdots + \alpha_{t+1}(b_{t+2,h-2}(u)) + \alpha_t(b_{t+1,h-1}(u)),$$

where functions α_s *and* β_s *are defined in (II.7).*

In practice: *Using the notation* $U_k = \psi^{(k)}_{1,t+h-k}(0,\ldots,0,u)$ *[with, in particular,* $U_h = \psi^{(h)}_{1,t}(0,\ldots,0,u) = b_{t,h}(u)$*], the second equation of (II.9) implies that, for* $k \geq 2$*:*

$$U_k = \beta_{t+h-k}(U_{k-1}),$$

which allows to compute the U_k $(k = 1,\ldots,h)$ *by backward recursions, starting from* $U_1 = \beta_{t+h-1}(u)$*. Once the* U_k $(k = 1,\ldots,h)$ *are computed, the first equation of (II.9) gives* $a_{t,h}(u) = \psi^{(h)}_{0,t}(u_1,\ldots,u_h)$*. Specifically, for* $h \geq 1$*, we have:*

$$a_{t,h}(u) = \alpha_t(U_{h-1}) + \alpha_{t+1}(U_{h-2}) + \cdots + \alpha_{t+h-2}(U_1) + \alpha_{t+h-1}(u).$$

II.4. **Conditional mean and variance of** W_t**.**

Proposition 4. *The conditional mean of* W_{t+1}*, given the information available at* t*, is given by:*

$$\mathbb{E}_t\left(W_{t+1}\right) = \alpha^{(1)}_{W,t} + \beta^{(1)}_{W,t} X_t, \tag{II.10}$$

where

$$\left\{\begin{array}{rcl}
\alpha^{(1)}_{W,t} & = & \begin{bmatrix} \mathbf{0}_{(n_Z+n_\eta)\times 1} \\ \mu_D \ell_0^{(D)} \\ \kappa_N^t \mu_N \ell_0^{(N)} \\ \mu_D \ell_0^{(T)} \end{bmatrix}, \\
\beta^{(1)}_{W,t} & = & \begin{bmatrix} \mathbf{0}_{n_Z\times n_Z} & \mathbf{0}_{n_Z\times n_\eta} & \mathbf{0}_{n_Z\times(n_W-n_\eta)} \\ \mathbf{0}_{n_\eta\times n_Z} & \Phi_{n_\eta\times n_\eta} & \mathbf{0}_{n_\eta\times(n_W-n_\eta)} \\ \mathbf{0}_{(n_W-n_\eta)\times n_Z} & \mathbf{0}_{(n_W-n_\eta)\times n_\eta} & \mathbf{0}_{(n_W-n_\eta)\times(n_W-n_\eta)} \end{bmatrix} + \mu_D \begin{bmatrix} \mathbf{0}_{(n_Z+n_\eta)\times n_X} \\ \ell_1^{(D)\prime} \\ \mathbf{0}_{3\times n_X} \end{bmatrix} \\
& & + \kappa_N^t \mu_N \begin{bmatrix} \mathbf{0}_{(n_Z+n_\eta)\times n_X} \\ \mathbf{0}_{1\times n_X} \\ \ell_1^{(N)\prime} \\ \mathbf{0}_{2\times n_X} \end{bmatrix} + \mu_T \begin{bmatrix} \mathbf{0}_{(n_Z+n_\eta)\times n_X} \\ \mathbf{0}_{2\times n_X} \\ \ell_1^{(T)\prime} \\ \mathbf{0}_{1\times n_X} \end{bmatrix} + \mu_H \begin{bmatrix} \mathbf{0}_{(n_Z+n_\eta)\times n_X} \\ \mathbf{0}_{3\times n_X} \\ \ell_1^{(H)\prime} \end{bmatrix}.
\end{array}\right.$$

Proof. We have $W_t = [\eta_t', D_t, N_t]'$, where the dynamics of η, D_t and N_t are respectively defined by (II.2), (13), and (7). We have:

$$\mathbb{E}_t(W_{t+1}) = \mathbb{E}_t \begin{bmatrix} \Phi\eta_t + \varepsilon_{\eta,t+1} \\ D_{t+1} \\ N_{t+1} \\ T_{AT,t+1} \\ H_{t+1} \end{bmatrix} = \begin{bmatrix} \Phi\eta_t \\ \mu_D \left(\ell_0^{(D)} + \ell_1^{(D)\prime} X_t\right) \\ \kappa_N^t \mu_N \left(\ell_0^{(N)} + \ell_1^{(N)\prime} X_t\right) \\ \mu_T \left(\ell_0^{(T)} + \ell_1^{(T)\prime} X_t\right) \\ \mu_H \left(\ell_0^{(H)} + \ell_1^{(H)\prime} X_t\right) \end{bmatrix},$$

which gives the result. □

Proposition 5. *The conditional variance of W_{t+1}, given the information available at t, is given by:*

$$Vec\left(\mathbb{V}\mathrm{ar}_t(W_{t+1})\right) = \alpha_{W,t}^{(2)} + \beta_{W,t}^{(2)} X_t, \tag{II.11}$$

with

$$\begin{aligned}
\beta_{W,t}^{(2)} \;=\; & Vec\left(\begin{bmatrix} \mathbf{0}_{n_\eta \times n_\eta} & \mathbf{0}_{n_\eta \times 1} & \mathbf{0}_{n_\eta \times 1} & \mathbf{0}_{n_\eta \times 1} & \mathbf{0}_{n_\eta \times 1} \\ \mathbf{0}_{1 \times n_\eta} & 2\mu_D^2 & 0 & 0 & 0 \\ \mathbf{0}_{1 \times n_\eta} & 0 & 0 & 0 & 0 \\ \mathbf{0}_{1 \times n_\eta} & 0 & 0 & 0 & 0 \\ \mathbf{0}_{1 \times n_\eta} & 0 & 0 & 0 & 0 \end{bmatrix}\right) \ell_1^{(D)\prime} + \\
& Vec\left(\begin{bmatrix} \mathbf{0}_{n_\eta \times n_\eta} & \mathbf{0}_{n_\eta \times 1} & \mathbf{0}_{n_\eta \times 1} & \mathbf{0}_{n_\eta \times 1} & \mathbf{0}_{n_\eta \times 1} \\ \mathbf{0}_{1 \times n_\eta} & 0 & 0 & 0 & 0 \\ \mathbf{0}_{1 \times n_\eta} & 0 & 2\kappa_N^t \mu_N^2 & 0 & 0 \\ \mathbf{0}_{1 \times n_\eta} & 0 & 0 & 0 & 0 \\ \mathbf{0}_{1 \times n_\eta} & 0 & 0 & 0 & 0 \end{bmatrix}\right) \ell_1^{(N)\prime} + \\
& Vec\left(\begin{bmatrix} \mathbf{0}_{n_\eta \times n_\eta} & \mathbf{0}_{n_\eta \times 1} & \mathbf{0}_{n_\eta \times 1} & \mathbf{0}_{n_\eta \times 1} & \mathbf{0}_{n_\eta \times 1} \\ \mathbf{0}_{1 \times n_\eta} & 0 & 0 & 0 & 0 \\ \mathbf{0}_{1 \times n_\eta} & 0 & 0 & 0 & 0 \\ \mathbf{0}_{1 \times n_\eta} & 0 & 0 & 2\mu_T^2 & 0 \\ \mathbf{0}_{1 \times n_\eta} & 0 & 0 & 0 & 0 \end{bmatrix}\right) \ell_1^{(T)\prime} + \\
& Vec\left(\begin{bmatrix} \mathbf{0}_{n_\eta \times n_\eta} & \mathbf{0}_{n_\eta \times 1} & \mathbf{0}_{n_\eta \times 1} & \mathbf{0}_{n_\eta \times 1} & \mathbf{0}_{n_\eta \times 1} \\ \mathbf{0}_{1 \times n_\eta} & 0 & 0 & 0 & 0 \\ \mathbf{0}_{1 \times n_\eta} & 0 & 0 & 0 & 0 \\ \mathbf{0}_{1 \times n_\eta} & 0 & 0 & 0 & 0 \\ \mathbf{0}_{1 \times n_\eta} & 0 & 0 & 0 & 2\mu_H^2 \end{bmatrix}\right) \ell_1^{(H)\prime},
\end{aligned}$$

and

$$\alpha^{(2)}_{W,t} = Vec\left(\begin{bmatrix} \boldsymbol{Id}_{n_\eta\times n_\eta} & \mathbf{0}_{n_\eta\times 1} & \mathbf{0}_{n_\eta\times 1} & \mathbf{0}_{n_\eta\times 1} & \mathbf{0}_{n_\eta\times 1} & \mathbf{0}_{n_\eta\times 1} \\ \mathbf{0}_{1\times n_\eta} & 2\mu_D^2\ell_0^{(D)} & 0 & 0 & 0 & 0 \\ \mathbf{0}_{1\times n_\eta} & 0 & 2\kappa_N^t\mu_N^2\ell_0^{(N)} & 0 & 0 & 0 \\ \mathbf{0}_{1\times n_\eta} & 0 & 0 & 0 & 2\mu_T^2\ell_0^{(T)} & 0 \\ \mathbf{0}_{1\times n_\eta} & 0 & 0 & 0 & 0 & 2\mu_H^2\ell_0^{(H)} \end{bmatrix}\right).$$

Proof. The shocks being conditionally independent, we have:

$$\mathbb{V}\mathrm{ar}_t\left(W_{t+1}\right) = \begin{bmatrix} \mathbb{V}\mathrm{ar}_t(\eta_{t+1}) & 0 & 0 & 0 & 0 \\ 0 & \mathbb{V}\mathrm{ar}_t(D_{t+1}) & 0 & 0 & 0 \\ 0 & 0 & \mathbb{V}\mathrm{ar}_t(N_{t+1}) & 0 & 0 \\ 0 & 0 & 0 & \mathbb{V}\mathrm{ar}_t(T_{AT,t+1}) & 0 \\ 0 & 0 & 0 & 0 & \mathbb{V}\mathrm{ar}_t(H_{t+1}) \end{bmatrix}.$$

Using $\mathbb{V}\mathrm{ar}_t(\eta_{t+1}) = \mathbf{Id}_{n_\eta\times n_\eta}$, and

$$\begin{aligned} \mathbb{V}\mathrm{ar}_t(D_{t+1}) &= 2\mu_D^2\left(\ell_0^{(D)} + \ell_1^{(D)\prime}X_t\right) \\ \mathbb{V}\mathrm{ar}_t(N_{t+1}) &= 2\kappa_N^t\mu_N^2\left(\ell_0^{(N)} + \ell_1^{(N)\prime}X_t\right) \\ \mathbb{V}\mathrm{ar}_t(T_{AT,t+1}) &= 2\mu_T^2\left(\ell_0^{(T)} + \ell_1^{(T)\prime}X_t\right) \\ \mathbb{V}\mathrm{ar}_t(H_{t+1}) &= 2\mu_H^2\left(\ell_0^{(H)} + \ell_1^{(H)\prime}X_t\right) \end{aligned}$$

leads to the result. □

II.5. **Conditional mean and variance of $X_t = [Z_t', W_t']'$.**

Proposition 6. *The conditional mean of X_{t+h}, given the information available at t, is given by:*

$$\mathbb{E}_t(X_{t+h}) = \alpha^{(1)}_{t,h} + \beta^{(1)}_{t,h}X_t, \tag{II.12}$$

where

$$\begin{cases} \alpha^{(1)}_{t,h} &= \mu_{X,t+h-1} + \Phi_{X,t+h-1}\mu_{X,t+h-2} + \cdots + \Phi^{h-1}_{X,t+1}\mu_{X,t}, \\ \beta^{(1)}_{t,h} &= \Phi_{X,t+h-1}\Phi_{X,t+h-2}\ldots\Phi_{X,t}, \end{cases}$$

with

$$\begin{aligned} \mu_{X,t} &= \begin{bmatrix}\omega_{0,t+1}\\ \mathbf{0}_{n_W\times 1}\end{bmatrix} + \begin{bmatrix}\mathbf{0}_{n_Z\times n_Z} & \omega_{t+1}\\ \mathbf{0}_{n_W\times n_Z} & \boldsymbol{Id}_{n_W\times n_W}\end{bmatrix}\alpha^{(1)}_{W,t}, \quad \textit{and} \\ \Phi_{X,t} &= \begin{bmatrix}A_{1,t+1} & \mathbf{0}_{n_Z\times n_W}\\ \mathbf{0}_{n_W\times n_Z} & \mathbf{0}_{n_W\times n_W}\end{bmatrix} + \begin{bmatrix}\mathbf{0}_{n_Z\times n_Z} & \omega_{t+1}\\ \mathbf{0}_{n_W\times n_Z} & \boldsymbol{Id}_{n_W\times n_W}\end{bmatrix}\beta^{(1)}_{W,t}. \end{aligned}$$

Proof. Using (II.4), we have:

$$X_{t+1} = \begin{bmatrix} Z_{t+1} \\ W_{t+1} \end{bmatrix} = \begin{bmatrix} A_{1,t+1}Z_t + \omega_{0,t+1} + \omega_{t+1}W_{t+1} \\ W_{t+1} \end{bmatrix}, \tag{II.13}$$

and therefore

$$\mathbb{E}_t(X_{t+1}) = \begin{bmatrix} A_{1,t+1}Z_t + \omega_{0,t+1} \\ \mathbf{0}_{n_W \times 1} \end{bmatrix} + \begin{bmatrix} \mathbf{0}_{n_Z \times n_Z} & \omega_{t+1} \\ \mathbf{0}_{n_W \times n_Z} & \mathbf{Id}_{n_W \times n_W} \end{bmatrix} (\alpha^{(1)}_{W,t} + \beta^{(1)}_{W,t} X_t),$$

which gives the result for $h = 1$.

The law of iterated expectation implies that the conditional expectation $\mathbb{E}_t(X_{t+h})$ is given by:

$$\mathbb{E}_t(X_{t+h}) = \mu_{X,t+h-1} + \Phi_{X,t+h-1}\mathbb{E}_t(X_{t+h-1}),$$

which leads to the result. □

Proposition 7. *The conditional variance of X_{t+h}, given the information available at t, is given by:*

$$Vec\left(\mathbb{V}ar_t(X_{t+h})\right) = \alpha^{(2)}_{t,h} + \beta^{(2)}_{t,h} X_t, \tag{II.14}$$

where

$$\begin{cases} \alpha^{(2)}_{t,h} = \alpha^{(2)}_{t+h-1,1} + \beta^{(2)}_{t+h-1,1}\alpha^{(1)}_{t,h-1} + \left(\beta^{(1)}_{t+h-1,1} \otimes \beta^{(1)}_{t+h-1,1}\right)\alpha^{(2)}_{t,h-1} \\ \beta^{(2)}_{t,h} = \beta^{(2)}_{t+h-1,1}\beta^{(1)}_{t,h-1} + \left(\beta^{(1)}_{t+h-1,1} \otimes \beta^{(1)}_{t+h-1,1}\right)\beta^{(2)}_{t,h-1}, \end{cases} \tag{II.15}$$

with

$$\begin{cases} \alpha^{(2)}_{s,1} = \left(\Gamma_s \otimes \Gamma_s\right)\alpha^{(2)}_{W,t} \\ \beta^{(2)}_{s,1} = \left(\Gamma_s \otimes \Gamma_s\right)\beta^{(2)}_{W,t}, \end{cases} \tag{II.16}$$

where $\Gamma_s = \begin{bmatrix} \omega_{s+1} \\ \boldsymbol{Id}_{n_W \times n_W} \end{bmatrix}$.

Proof. Let us start with the case $h = 1$. Using (II.13), we have:

$$\mathbb{V}\mathrm{ar}_t(X_{t+1}) = \mathbb{V}\mathrm{ar}_t\left(\begin{bmatrix} \omega_{t+1} \\ \mathbf{Id}_{n_W \times n_W} \end{bmatrix} W_{t+1}\right) = \Gamma_t \mathbb{V}\mathrm{ar}_t(W_{t+1})\Gamma'_{t+1},$$

where $\mathbb{V}\mathrm{ar}_t(W_{t+1})$ is given by (II.11). This implies that:

$$Vec\left(\mathbb{V}\mathrm{ar}_t(X_{t+1})\right) = \left(\Gamma_{t+1} \otimes \Gamma_{t+1}\right) Vec\left(\mathbb{V}\mathrm{ar}_t(W_{t+1})\right) = \left(\Gamma_{t+1} \otimes \Gamma_{t+1}\right)\left(\alpha^{(2)}_{W,t} + \beta^{(2)}_{W,t} X_t\right),$$

where the last equality is obtained by applying Proposition 5. This proves (II.14) for $h = 1$ (using II.16). Let us make the inductive hypothesis that (II.14) holds for $h - 1$. More precisely,

assume that, for any date t:

$$\text{Vec}\left(\mathbb{V}ar_t(X_{t+h-1})\right) = \alpha^{(2)}_{t,h-1} + \beta^{(2)}_{t,h-1} X_t.$$

The law of total variance yields:

$$\mathbb{V}ar_t(X_{t+h}) = \mathbb{E}_t(\mathbb{V}ar_{t+h-1}(X_{t+h})) + \mathbb{V}ar_t(\mathbb{E}_{t+h-1}(X_{t+h})).$$

We get:

$$\begin{aligned}
&\text{Vec}\left(\mathbb{V}ar_t(X_{t+h})\right)\\
=\ &\mathbb{E}_t\Big(\underbrace{\alpha^{(2)}_{t+h-1,1} + \beta^{(2)}_{t+h-1,1} X_{t+h-1}}_{\text{using the inductive hypothesis}}\Big) + \text{Vec}\Big(\mathbb{V}ar_t\Big(\underbrace{\alpha^{(1)}_{t+h-1,1} + \beta^{(1)}_{t+h-1,1} X_{t+h-1}}_{\text{using (II.12)}}\Big)\Big)\\
=\ &\alpha^{(2)}_{t+h-1,1} + \beta^{(2)}_{t+h-1,1}\Big(\underbrace{\alpha^{(1)}_{t,h-1} + \beta^{(1)}_{t,h-1} X_t}_{\text{using (II.12)}}\Big) + \text{Vec}\Big(\beta^{(1)}_{t+h-1,1}\mathbb{V}ar_t(X_{t+h-1})\beta^{(1)\prime}_{t+h-1,1}\Big)\\
=\ &\alpha^{(2)}_{t+h-1,1} + \beta^{(2)}_{t+h-1,1}\alpha^{(1)}_{t,h-1} + \beta^{(2)}_{t+h-1,1}\beta^{(1)}_{t,h-1} X_t + \left(\beta^{(1)}_{t+h-1,1} \otimes \beta^{(1)}_{t+h-1,1}\right)\text{Vec}\left(\mathbb{V}ar_t(X_{t+1})\right)\\
=\ &\alpha^{(2)}_{t+h-1,1} + \beta^{(2)}_{t+h-1,1}\alpha^{(1)}_{t,h-1} + \beta^{(2)}_{t+h-1,1}\beta^{(1)}_{t,h-1} X_t + \left(\beta^{(1)}_{t+h-1,1} \otimes \beta^{(1)}_{t+h-1,1}\right)\left(\alpha^{(2)}_{t,h-1} + \beta^{(2)}_{t,h-1} X_t\right),
\end{aligned}$$

using (II.14) for $h = 1$.

To summarize, we have shown that: (II.14) is satisfied for $h = 1$, and we have shown that, if it is satisfied for $h-1$ (with $h \geq 2$), then it is also satisfied for h (see equation II.14). By induction, it comes that it is satisfied for any $h \geq 1$.

□

In practice, in order to use (II.15), we need:

- $\alpha^{(2)}_{t+k,1}$, $\beta^{(2)}_{t+k,1}$ for all k of interest, using (II.16);
- $\alpha^{(1)}_{t+k,1} \equiv \mu_{X,t+k}$, $\beta^{(1)}_{t+k,1} \equiv \Phi_{X,t+k}$ for all k of interest;
- $\alpha^{(1)}_{t,k}$, $\beta^{(1)}_{t,k}$ for all k of interest, using (II.12).

APPENDIX III. PRICING

III.1. Solving for the s.d.f.

Proposition 8. *In the context described by B.2.3, i.e., under (41), (17) and (18), and if, for $t \geq t_0$:*

$$\mu_{u,0,t} \equiv \mu_{u,0},\ \mu_{u,1,t} \equiv \mu_{u,1},\ \mu_{c,0,t} \equiv \mu_{c,0},\ \mu_{c,1,t} \equiv \mu_{c,1},\ \alpha_t(\bullet) \equiv \alpha(\bullet) \text{ and } \beta_t(\bullet) \equiv \beta(\bullet),$$

then we have:

$$u_t = c_t + \mu_{u,0,t} + \mu'_{u,1,t} X_t, \tag{III.1}$$

where

$$\begin{cases} \mu_{u,0,t} &= \delta(\mu_{u,0,t+1} + \mu_{c,0,t+1}) + \\ & \quad \frac{\delta}{1-\gamma}\alpha_t\{(1-\gamma)(\mu_{u,1,t+1} + \mu_{c,1,t+1})\} \\ \mu_{u,1,t} &= \frac{\delta}{1-\gamma}\beta_t\{(1-\gamma)(\mu_{u,1,t+1} + \mu_{c,1,t+1})\}, \end{cases} \tag{III.2}$$

and where, for $t \geq t_0$, $\mu_{u,1,t}$ solves:

$$\mu_{u,1} = \frac{\delta}{1-\gamma}\beta\{(1-\gamma)(\mu_{u,1} + \mu_{c,1})\}, \tag{III.3}$$

and $\mu_{u,0,t}$ satisfies:

$$\mu_{u,0} = \frac{\delta}{1-\delta}\mu_{c,0} + \frac{\delta}{1-\delta}\frac{1}{1-\gamma}\alpha\{(1-\gamma)(\mu_{u,1} + \mu_{c,1})\}. \tag{III.4}$$

Proof. We start by positing a specification for the log-utility of the form of (III.1). Our objective is to determine whether a utility of this form can satisfy (41), and the conditions that then have to be satisfied by $\mu_{u,0,t}$ and $\mu_{u,1,t}$. Under (III.1), we have:

$$\begin{aligned} & \mathbb{E}_t \exp\left[(1-\gamma)u_{t+1}\right] \\ = \ & \mathbb{E}_t \exp\left[(1-\gamma)(c_{t+1} + \mu_{u,0,t+1} + \mu'_{u,1,t+1}X_{t+1})\right] \\ = \ & \mathbb{E}_t \exp\left[(1-\gamma)(c_t + \Delta c_{t+1} + \mu_{u,0,t+1} + \mu'_{u,1,t+1}X_{t+1})\right] \\ = \ & \exp\left[(1-\gamma)(c_t + \mu_{u,0,t+1} + \mu_{c,0,t+1})\right] \times \mathbb{E}_t \exp\left[(1-\gamma)(\mu_{u,1,t+1} + \mu_{c,1,t+1})'X_{t+1}\right] \\ = \ & \exp\left[(1-\gamma)(c_t + \mu_{u,0,t+1} + \mu_{c,0,t+1})\right] \times \\ & \exp\left[\alpha_t\{(1-\gamma)(\mu_{u,1,t+1} + \mu_{c,1,t+1}) + \beta_t\{(1-\gamma)(\mu_{u,1,t+1} + \mu_{c,1,t+1})\}'X_t\right]. \end{aligned}$$

Substituting for $\mathbb{E}_t \exp\left[(1-\gamma)u_{t+1}\right]$ in (41) gives:

$$\begin{aligned} u_t \ = \ & c_t + \delta(\mu_{u,0,t+1} + \mu_{c,0,t+1}) + \\ & \frac{\delta}{1-\gamma}\Big(\alpha_t\{(1-\gamma)(\mu_{u,1,t+1} + \mu_{c,1,t+1})\} + \beta_t\{(1-\gamma)(\mu_{u,1,t+1} + \mu_{c,1,t+1})\}'X_t\Big). \end{aligned}$$

Therefore, for u_t to be equal to $c_t + \mu_{u,0,t} + \mu'_{u,1,t}X_t$, we need to have (III.2).

Equations (III.3) and (III.4) are obtained by setting $\mu_{u,1} = \mu_{u,1,t} = \mu_{u,1,t+1}$ and $\mu_{u,0} = \mu_{u,0,t} = \mu_{u,0,t+1}$ in (III.2). □

In practice, we start by solving (III.3); as a fixed-point problem, a good approximation to the solution is obtained in a few iteration.[41] This yields $\mu_{u,1}$. Then, we obtain $\mu_{u,0}$ by (III.4). Once $\mu_{u,0,t_0}$ $(= \mu_{u,0})$ and $\mu_{u,1,t_0}$ $(= \mu_{u,1})$ are known, one can deduce the previous $\mu_{u,i,t}$'s by backward computations. Specifically, knowing $\mu_{u,1,t+1}$, one can deduce $\mu_{u,1,t}$ by using the second equation of (III.2). And knowing $\mu_{u,0,t+1}$ and $\mu_{u,1,t+1}$, the first equation of (III.2) yields $\mu_{u,0,t}$.

Proposition 9. *We have:*

$$\mathcal{M}_{t,t+1} = \exp[-(\mu_{r,0,t+1} + \mu'_{r,1,t+1}X_t) + \Pi'_{t+1}X_{t+1} \underbrace{-\alpha_t(\Pi_{t+1}) - \beta_t(\Pi_{t+1})'X_t}_{=-\psi_t(\Pi_{t+1}),\ \textit{see Prop. 2}}],$$

with

$$\begin{cases} \Pi_{t+1} &= (1-\gamma)\mu_{u,1,t+1} - \gamma\mu_{c,1,t+1} \\ \mu_{r,0,t+1} &= -\log\delta + \mu_{c,0,t+1} + \alpha_t\{(1-\gamma)(\mu_{u,1,t+1} + \mu_{c,1,t+1})\} - \alpha_t(\Pi_{t+1}) \\ \mu_{r,1,t+1} &= \beta_t\{(1-\gamma)(\mu_{u,1,t+1} + \mu_{c,1,t+1})\} - \beta_t(\Pi_{t+1}), \end{cases} \tag{III.5}$$

where the (recursive) computation of $\mu_{u,1,t+1}$ results from Proposition 8.

The short-term risk-free rate, that is $-\log \mathbb{E}_t(\mathcal{M}_{t,t+1})$, is given by:

$$r_t = \mu_{r,0,t+1} + \mu'_{r,1,t+1}X_t.$$

Proof. When agents' preferences are as in (41), the s.d.f. is given by (e.g. Piazzesi and Schneider, 2007):

$$\mathcal{M}_{t,t+1} = \delta\left(\frac{C_{t+1}}{C_t}\right)^{-1} \frac{\exp[(1-\gamma)u_{t+1}]}{\mathbb{E}_t(\exp[(1-\gamma)u_{t+1}])}.$$

Therefore, we have:

$$\begin{aligned} \log\mathcal{M}_{t,t+1} &= \log\delta - \Delta c_{t+1} + (1-\gamma)u_{t+1} - \log\mathbb{E}_t(\exp[(1-\gamma)u_{t+1}]) \\ &= \log\delta - \Delta c_{t+1} + (1-\gamma)(c_t + \Delta c_{t+1} + \mu_{u,0,t+1} + \mu'_{u,1,t+1}X_{t+1}) \end{aligned}$$

[41] A relevant starting value is obtained by replacing function β, in (III.3), by its first-order Taylor expansion around zero: using Proposition 2, it can be seen that, when u is small, we have that $\beta(u) \approx Mu$ where

$$M = \begin{bmatrix} \begin{bmatrix} A'_1 \\ \mathbf{0}_{n_W \times n_Z} \end{bmatrix} & \mathbf{0}_{n_X \times n_W} \end{bmatrix} + \begin{bmatrix} \mathbf{0}_{n_X \times n_Z} & \begin{bmatrix} \mathbf{0}_{n_Z \times n_\eta} \\ \Phi' \\ \mathbf{0}_{(n_W - n_\eta)\times n_\eta} \end{bmatrix} & \mu_D \ell_1^{(D)} & \mu_N \kappa_N^t \ell_1^{(N)} \end{bmatrix} \cdot \begin{bmatrix} \mathbf{0}_{n_Z \times n_Z} & \mathbf{0}_{n_Z \times n_W} \\ \omega' & \mathbf{Id}_{n_W \times n_W} \end{bmatrix}.$$

Replacing the non-linear function $\beta\{(1-\gamma)(\mu_{u,1} + \mu_{c,1})\}$ with its linearized version—that is $M \cdot \{(1-\gamma)(\mu_{u,1} + \mu_{c,1})\}$—in (III.3) yields the (approximated) solution: $\mu^0_{u,1} = \delta(I - \delta M)^{-1}M\mu_{c,1}$.

$$
\begin{aligned}
& -(1-\gamma)(c_t + \mu_{u,0,t+1} + \mu_{c,0,t+1}) \\
& -\alpha_t\{(1-\gamma)(\mu_{u,1,t+1} + \mu_{c,1,t+1})\} - \beta_t\{(1-\gamma)(\mu_{u,1,t+1} + \mu_{c,1,t+1})\}' X_t \\
= \;& \log\delta - \mu_{c,0,t+1} - \alpha_t\{(1-\gamma)(\mu_{u,1,t+1} + \mu_{c,1,t+1})\} \\
& + \Big((1-\gamma)\mu_{u,1,t+1} - \gamma\mu_{c,1,t+1}\Big)' X_{t+1} - \beta_t\{(1-\gamma)(\mu_{u,1,t+1} + \mu_{c,1,t+1})\}' X_t,
\end{aligned}
$$

which leads to the result. □

III.2. **Generic pricing formulas.**

Proposition 10. *Consider an asset whose payoff, settled on date $t+h$, is $\exp(\omega' X_{t+h})$. The date-t price of this asset is given by:*

$$
\varphi_t^{(h)}(\omega) := \exp\left(\varphi_{0,t}^{(h)}(\omega) + \varphi_{1,t}^{(h)}(\omega)' X_t\right),
$$

where

$$
\left\{
\begin{array}{rcl}
\varphi_{0,t}^{(h)}(\omega) & = & -\mu_{r,0,t+1} - \alpha_t(\Pi_{t+1}) - \cdots - \mu_{r,0,t+h} - \alpha_{t+h-1}(\Pi_{t+h}) + \psi_{0,t}^{(h)}(u_1,\ldots,u_h) \\
\varphi_{1,t}^{(h)}(\omega) & = & -\mu_{r,1,t+1} - \beta_t(\Pi_{t+1}) + \psi_{1,t}^{(h)}(u_1,\ldots,u_h),
\end{array}
\right. \tag{III.6}
$$

where the $\mu_{r,0,t}$'s, the $\mu_{,r1,t}$'s and the Π_t's are defined in (III.5), where functions $\psi_{0,t}^{(h)}$ and $\psi_{1,t}^{(h)}$ are defined in (II.9) and where:

$$
u_k = \left\{
\begin{array}{ll}
-\mu_{r,1,t+1+k} - \beta_{t+k}(\Pi_{t+1+k}) + \Pi_{t+k} & \text{for} \quad k = 1,\ldots,h-1, \\
\Pi_{t+k} + \omega & \text{for} \quad k = h.
\end{array}
\right. \tag{III.7}
$$

Proof. The price of this asset is given by:

$$
\begin{aligned}
& \mathbb{E}_t\left(\mathcal{M}_{t,t+h}\exp(\omega' X_{t+h})\right) \\
= \;& \mathbb{E}_t\Big\{\exp\Big(-\left[\mu_{r,0,t+1} + \alpha_t(\Pi_{t+1}) + \{\mu_{r,1,t+1} + \beta_t(\Pi_{t+1})\}' X_t\right] \\
& - \left[\mu_{r,0,t+2} + \alpha_{t+1}(\Pi_{t+2}) + \{\mu_{r,1,t+2} + \beta_{t+1}(\Pi_{t+2})\}' X_{t+1}\right] + \Pi_{t+1}' X_{t+1} \\
& \cdots \\
& - \left[\mu_{r,0,t+h} + \alpha_{t+h-1}(\Pi_{t+h}) + \{\mu_{r,1,t+h} + \beta_{t+h-1}(\Pi_{t+h})\}' X_{t+h-1}\right] + \Pi_{t+h-1}' X_{t+h-1} \\
& + \Pi_{t+h}' X_{t+h} + \omega' X_{t+h}\Big)\Big\} \\
= \;& \exp(-\mu_{r,0,t+1} - \alpha_t(\Pi_{t+1}) - \cdots - \mu_{r,0,t+h} - \alpha_{t+h-1}(\Pi_{t+h})) \times \\
& \exp(-\{\mu_{r,1,t+1} + \beta_t(\Pi_{t+1})\}' X_t) \exp\left[\psi_{0,t}^{(h)}(u_1,\ldots,u_h) + \psi_{1,t}^{(h)}(u_1,\ldots,u_h)' X_t\right],
\end{aligned}
$$

where functions $\psi_{0,t}^{(h)}$ and $\psi_{1,t}^{(h)}$ are defined in (II.9) and the u_k's are given in (III.7). □

Corollary 2. *Consider an asset whose payoff, settled on date $t+h$, is $\omega' X_{t+h}$. The date-t price of this asset is:*

$$\widetilde{\varphi}_t^{(h)}(\omega) = \lim_{\varepsilon \to 0} \frac{\varphi_t^{(h)}(\varepsilon\omega) - \varphi_t^{(h)}(0)}{\varepsilon},$$

where the computation of $\widetilde{\varphi}_t^{(h)}(\omega)$ is given by Proposition 10.

Proof. The derivative of $\exp(x\omega' X_{t+h})$ w.r.t. x is $\omega' X_{t+h} \exp(x\omega' X_{t+h})$. Evaluated at $x = 0$, this derivative is equal to $\omega' X_{t+h}$, which leads to the result. □

Proposition 11. *Consider an asset whose payoff, settled on date $t+h$, is:*

$$\exp\left(\omega' X_{t+h}\right) \mathbb{1}_{\{a' X_{t+h} < b\}}.$$

The date-t price of this asset is given by:

$$\hat{\varphi}_t^{(h)}(\omega, a, b) = \frac{\varphi_t^{(h)}(\omega)}{2} - \frac{1}{\Pi} \int_0^\infty \frac{Im[\varphi_t^{(h)}(\omega + iax) \exp(-ibx)]}{x} dx,$$

where $Im(x)$ denotes the imaginary part of x and where function $\varphi_t^{(h)}$ is defined in Proposition 10.

Proof. This is a direct application of Proposition 2 (equation 2.12) of Duffie, Pan, and Singleton (2000). □

Corollary 3. *Consider an asset whose payoff, settled on date $t+h$, is:*

$$\omega' X_{t+h} \mathbb{1}_{\{a' X_{t+h} < b\}}.$$

The date-t price of this asset is:

$$\bar{\varphi}_t^{(h)}(\omega, a, b) = \lim_{\varepsilon \to 0} \frac{\hat{\varphi}_t^{(h)}(\varepsilon\omega, a, b) - \hat{\varphi}_t^{(h)}(0, a, b)}{\varepsilon},$$

where the computation of $\hat{\varphi}_t^{(h)}(\omega, a, b)$ is given by Proposition 11.

Proof. The proof is the same as that of Corollary 2. □

III.3. **Social cost of carbon.** This subsection describes the computation of the Social Cost of Carbon (SCC), as defined by:

$$SCC_t = -\frac{\partial U_t}{\partial M_{AT,t}} \Big/ \frac{\partial U_t}{\partial C_t}. \tag{III.8}$$

Note that (III.8) implies that the unit of the SCC is USD (of the initial period) per ton of Carbon since C_t is expressed in dollars of the initial period, and $M_{AT,t}$ is expressed in tons of Carbon.

As shown by Proposition 8, with preferences defined by (41), we have:

$$u_t = \log(U_t) = c_t + \mu_{0,u,t} + \mu'_{1,u,t} X_t,$$

or

$$U_t = C_t \exp\left(\mu_{0,u,t} + \mu'_{1,u,t} X_t\right). \tag{III.9}$$

In the Epstein-Zin context with unit EIS, we have:

$$\frac{\partial U_t}{\partial C_t} = (1-\delta)\frac{U_t}{C_t}.$$

Moreover, given (III.9), we have $\partial U_t / \partial M_{AT,t} = \mu_{1,u,t,6} U_t$ (because $M_{AT,t}$ is the 6^{th} component of X_t, see (II.1)). Therefore:

$$SCC_t = -\frac{1}{1-\delta}\mu_{1,u,t,6} C_t, \tag{III.10}$$

In other words, agents are willing to accept an increase in $M_{AT,t}$ of one unit if they are given an extra consumption of $|\mu_{1,u,t,6}|C_t$.

According to the World Bank, from 2015 to 2019, global final consumption expenditures (C_0) were of \$299tr (299×10^{12}). Therefore, if $M_{AT,t}$ is expressed in GtC, the social cost of carbon, expressed in dollars per ton of carbon, is given by:

$$|\mu_{1,u,t,6}| \times 299 \times 10^{12} / 10^9 = \frac{1}{1-\delta}|\mu_{1,u,t,6}| \times 299\,000.$$

Our framework also offers closed-form formulas for expectations of future SCCs. Indeed, using eq. (III.10), we get:

$$\begin{aligned}
\mathbb{E}_t(SCC_{t+h}) &= \frac{1}{1-\delta}|\mu_{1,u,t,6}|\mathbb{E}_t(\exp(c_{t+h})) \\
&= \frac{1}{1-\delta}|\mu_{1,u,t,6}|C_0\mathbb{E}_t(\exp(Cum_{\Delta c,t+h})), \quad \text{where } Cum_{\Delta c,t+h} = \textstyle\sum_{i=1}^{t}\Delta c_i \\
&= \frac{1}{1-\delta}|\mu_{1,u,t,6}|C_0\mathbb{E}_t(\exp(\omega'_c X_{t+h})),
\end{aligned}$$

where ω_c is such that $\omega'_c X_t = \log(C_t/C_0)$ (i.e., $\omega'_c X_t = Cum_{\Delta c,t}$, see eq. II.1). This conditional expectation can be computed using Corollary 1.

Furthermore, since:

$$\mathbb{1}_{\{SCC_{t+h}<x\}} = \mathbb{1}_{\left\{\frac{1}{1-\delta}|\mu_{1,u,t,6}|C_0\exp(\omega'_c X_{t+h})<x\right\}} = \mathbb{1}_{\left\{\omega'_c X_{t+h} < \log\left(\frac{(1-\delta)x}{C_0|\mu_{1,u,t+h,6}|}\right)\right\}},$$

it comes that the cumulative distribution function of future SCCs can be obtained by Fourier analysis.

APPENDIX IV. CALIBRATION

IV.1. **Outline of the calibration approach.** This appendix describes the calibration of three sets of parameters, which respectively characterize: damages (Subsection IV.2), the permafrost-related carbon release (Subsection IV.3), and sea level rise (Subsection IV.4). In these three cases, we adopt the same general approach. For a number k of parameters to calibrate, we consider k targeted moments and deduce the parameters so as to perfectly match these moments. The literature usually offers targets in the form of moments that are conditional on a given atmospheric temperature $T_{AT,t}$ on a given date ($t = t^*$, say). For instance, we may want our model to be such that global mean sea levels rise by X_1 meters if the atmospheric temperature is of T_1°C in 2100, and by X_2 meters if the temperature is of T_2°C. That is:

$$\mathbb{E}_0(H_{t^*}|T_{AT,t^*} = T_i) = X_i, \quad i \in \{1,2\}.$$

Even in a tractable model such as ours, the previous conditional expectation is complicated to calculate. But it becomes simple to compute if we do not condition only on the last temperature T_{AT,t^*}, but also on the previous ones, i.e., if we condition on $\underline{T_{AT,t^*}}$, with $\underline{T_{AT,t^*}} = \{T_{AT,0}, \ldots, T_{AT,t^*}\}$. Moreover, since temperatures only gradually move over time, this expectation is expected to be relatively close to the one conditional on a linear increase of $T_{AT,t}$ from $T_{AT,0}$ to T_{AT,t^*}, i.e., conditional on

$$T_{AT,i} = T_{AT,0} + \frac{i}{t^*}(T_{AT,t^*} - T_{AT,0}), \quad i \in \{0, \ldots, t^*\}. \tag{IV.1}$$

In the following, we explain how to obtain the distributions (and, therefore, moments) of cumulated damages, cumulated permafrost-related emissions, and sea level rises, conditional on such trajectories of atmospheric temperatures. Let us stress that these calibration approaches are immediate, contrary to simulation-based approaches.

IV.2. **Damages.** According to (13), and assuming that the shocks are independent of one another, we have:

$$D_1 + \cdots + D_{t^*}|\underline{T_{AT,t^*}} \sim \gamma_0\left(\frac{1}{\mu_D}\left[t^* a^{(D)} + b^{(D)}(T_{AT,0} + \cdots + T_{AT,t^*-1})\right], \mu_D\right).$$

Further, under (IV.1), we obtain:

$$D_1 + \cdots + D_{t^*}|\underline{T_{AT,t^*}} \sim \gamma_0\left(\frac{1}{\mu_D}\left\{t^* a^{(D)} + \frac{b^{(D)}}{2}\left[(t^*-1)T_{AT,t^*} + (t^*+1)T_{AT,0}\right]\right\}, \mu_D\right). \tag{IV.2}$$

This determines the distribution of $Cum_{D,t^*} := -D_1 - \cdots - D_{t^*}$, conditional on $\underline{T_{AT,t^*}}$. Using (34), we obtain the following Laplace transform for $Cum_{D,t}$:

$$\begin{aligned} & \mathbb{E}_0\left(\exp(uCum_{D,t^*})|\underline{T_{AT,t^*}}\right) \\ = \; & \exp\left(\frac{-u}{1+u\mu_D}\left(t^* a^{(D)} + \frac{b^{(D)}}{2}\left[(t^*-1)T_{AT,t^*} + (t^*+1)T_{AT,0}\right]\right)\right). \end{aligned} \tag{IV.3}$$

Assume we target a specific mean ($\overline{\mathbb{E}}_{0,D}$) and variance ($\overline{\mathbb{V}\text{ar}}_{0,D}$) of cumulated damages for a given trajectory of temperatures between dates 0 and t^*, i.e.,

$$\mathbb{E}_0\left(\exp(Cum_{D,t^*})|\underline{T_{AT,t^*}}\right) = \overline{\mathbb{E}}_{0,D}, \quad \text{and} \quad \mathbb{V}ar_0(\exp(Cum_{D,t^*})|\underline{T_{AT,t^*}}) = \overline{\mathbb{V}\text{ar}}_{0,D}.$$

It can be shown that this is satisfied for:[42]

$$\mu_D = \frac{2 - \frac{\log\left(\overline{\mathbb{V}\text{ar}}_{0,D} + \left[\overline{\mathbb{E}}_{0,D}\right]^2\right)}{\log\left(\overline{\mathbb{E}}_{0,D}\right)}}{2\left(\frac{\log\left(\overline{\mathbb{V}\text{ar}}_{0,D} + \left[\overline{\mathbb{E}}_{0,D}\right]^2\right)}{\log\left(\overline{\mathbb{E}}_{0,D}\right)} - 1\right)}.$$

Next, (IV.3) shows that, conditional on a given trajectory of temperatures, the (log) expected cumulated damages are linear in $\{a^{(D)}, b^{(D)}\}$. Hence, if we target two different conditional expectations, $\overline{\mathbb{E}}_{0,D,1}$ and $\overline{\mathbb{E}}_{0,D,2}$ (say) for two different terminal values of T_{AT,t^*} ($T_{AT,t^*,1}$ and $T_{AT,t^*,2}$), we simply obtain $\{a^{(D)}, b^{(D)}\}$ by solving a two-equation linear system:

$$\begin{bmatrix} a^{(D)} \\ b^{(D)} \end{bmatrix} = -(1+\mu_D)\begin{bmatrix} t^* & \frac{1}{2}\left[(t^*-1)T_{AT,t^*,1} + (t^*+1)T_{AT,0}\right] \\ t^* & \frac{1}{2}\left[(t^*-1)T_{AT,t^*,2} + (t^*+1)T_{AT,0}\right] \end{bmatrix}^{-1}\begin{bmatrix} \log(\overline{\mathbb{E}}_{0,D,1}) \\ \log(\overline{\mathbb{E}}_{0,D,2}) \end{bmatrix}.$$

IV.3. **Permafrost-related emissions.** According to (43), permafrost-related emissions are given by:

$$N_t|\underline{T_{AT,t}} \sim \gamma_0\left(\frac{\kappa_N^{t-1}}{\mu_N}\left[a^{(N)} + b^{(N)}T_{AT,t-1}\right], \mu_N\right).$$

This implies that:

$$N_t + \cdots + N_1|\underline{T_{AT,t}} \sim \gamma_0\left(\frac{1}{\mu_N}\left[\frac{1-\kappa_N^t}{1-\kappa_N}a^{(N)} + b^{(N)}\sum_{i=1}^{t}\kappa_N^{i-1}T_{AT,i-1}\right], \mu_N\right).$$

[42] Using that $\overline{\mathbb{E}}_{0,D} = \mathbb{E}_0\left(\exp(Cum_{D,t^*})|\underline{T_{AT,t^*}}\right)$ and that $\overline{\mathbb{V}\text{ar}}_{0,D} = \mathbb{E}_0\left(\exp(2Cum_{D,t^*})|\underline{T_{AT,t^*}}\right) - \overline{\mathbb{E}}_{0,D}^2$, we obtain $\overline{\mathbb{V}\text{ar}}_{0,D} + \left[\overline{\mathbb{E}}_{0,D}\right]^2 = \overline{\mathbb{E}}_{0,D}^{\frac{2(1+\mu_D)}{1+2\mu_D}}$, which gives the result.

Under (IV.1), we obtain:[43]

$$\begin{aligned} & N_{t^*} + \cdots + N_1 | \underline{T_{AT,t}} \\ \sim \; & \gamma_0 \left(\frac{1-\kappa_N^{t^*}}{\mu_N(1-\kappa_N)} \left(a^{(N)} + b^{(N)} T_{AT,0} \right) + \frac{b^{(N)} (T_{AT,t^*} - T_{AT,0})}{\mu_N t^*} \frac{\kappa_N + ((t^*-1)\kappa_N - t^*)\kappa_N^{t^*}}{(1-\kappa_N)^2}, \mu_N \right). \end{aligned}$$

As in Subsection IV.2, targeting a specific variance-to-expectation ratio, conditionally on a given trajectory of temperatures between dates 1 and t^*, gives μ_N. Indeed, using (35), we obtain:

$$\mu_N = \frac{\overline{\mathbb{V}ar}_0(N_1 + \cdots + N_{t^*} | \underline{T_{AT,t^*}})}{2\overline{\mathbb{E}}_0(N_1 + \cdots + N_{t^*} | \underline{T_{AT,t^*}})}. \tag{IV.4}$$

Moreover, $\mathbb{E}_0(N_1 + \cdots + N_{t^*} | \underline{T_{AT,t^*}})$ is a linear function of $\{a^{(N)}, b^{(N)}\}$:

$$\begin{aligned} \mathbb{E}_0(N_1 + \cdots + N_{t^*} | \underline{T_{AT,t^*}}) \;=\; & \frac{1-\kappa_N^{t^*}}{1-\kappa_N} \left(a^{(N)} + b^{(N)} T_{AT,0} \right) + \\ & b^{(N)} \times \frac{(T_{AT,t^*} - T_{AT,0})}{t^*} \frac{\kappa_N + ((t^*-1)\kappa_N - t^*)\kappa_N^{t^*}}{(1-\kappa_N)^2}. \end{aligned} \tag{IV.5}$$

Hence, for all other parameters given, one can solve for $\{a^{(N)}, b^{(N)}\}$ as soon as one targets a pair of conditional expectations (conditional on two different values of T_{AT,t^*}).

A last moment we want to match is the expected total amount of carbon trapped in the permafrost. Assuming that the temperature will stabilize relatively quickly, and for a long period of time around $\widetilde{T}_{AT}$, this amount should be close to $\lim_{t^*\to\infty} \mathbb{E}_0(N_1 + \cdots + N_{t^*} | T_{AT,1} = \cdots = T_{AT,t^*} = \widetilde{T}_{AT})$. According to (IV.5), this expectation is given by:

$$\lim_{t^*\to\infty} \mathbb{E}_0(N_1 + \cdots + N_{t^*} | T_{AT,1} = \cdots = T_{AT,t^*} = \widetilde{T}_{AT}) = \frac{1}{1-\kappa_N} \left(a^{(N)} + b^{(N)} \widetilde{T}_{AT} \right). \tag{IV.6}$$

To summarize, the set of parameters $\{\mu_N, \kappa_N, a^{(N)}, b^{(N)}\}$ is obtained as follows:

- Obtain μ_N through (IV.8).
- Consider a grid of values for κ_N. For each value:
  - Compute $a^{(N)}$ and $b^{(N)}$ using (IV.5).
  - Use (IV.6) to compute $\lim_{t^*\to\infty} \mathbb{E}_0(N_1 + \cdots + N_t^*)$.
- Select, within the grid, the value of κ_N that provides the best match of the targeted $\lim_{t^*\to\infty} \mathbb{E}_0(N_1 + \cdots + N_{t^*} | T_{AT,1} = \cdots = T_{AT,t^*} = \widetilde{T}_{AT})$, for the desired $\widetilde{T}_{AT}$ value.

[43] Using that $\sum_{i=0}^{n-1} i x^i = \frac{x + ((n-1)x - n)x^n}{(1-x)^2}$.

IV.4. **Sea levels.** Using the dynamics of global mean sea level H_t described by (8) and the approximate linear trajectory of $T_{AT,t}$ through time (eq. IV.1), we obtain:

$$H_{t^*} - H_0 | \underline{T_{AT,t^*}} \sim \gamma_0 \left(\frac{1}{\mu_H} \left\{ t^* a_H + \frac{b_H}{2} \left[(t^* - 1) T_{AT,t^*} + (t^* + 1) T_{AT,0} \right] \right\}, \mu_H \right). \tag{IV.7}$$

This implies in particular that

$$\mathbb{E}_0(H_{t^*}) \quad = \quad H_0 + t^* a_H + \frac{b_H}{2} \left[(t^* - 1) T_{AT,t^*} + (t^* + 1) T_{AT,0} \right].$$

Hence, $\mathbb{E}_0(H_{t^*})$ is an affine function of a_H and b_H. As a result, if we want to target two different sea levels ($\overline{H}_1$ and $\overline{H}_2$, say), for two different temperatures ($\overline{T}_{AT,t^*,1}$ and $\overline{T}_{AT,t^*,2}$, say), we obtain $\{a_H, b_H\}$ by solving a two-equation linear system:

$$\begin{bmatrix} a_H \\ b_H \end{bmatrix} = \begin{bmatrix} t^* & \frac{1}{2} \left[(t^* - 1) T_{AT,t^*} + (t^* + 1) T_{AT,0} \right] \\ t^* & \frac{1}{2} \left[(t^* - 1) T_{AT,t^*} + (t^* + 1) T_{AT,0} \right] \end{bmatrix}^{-1} \begin{bmatrix} \overline{H}_1 - H_0 \\ \overline{H}_2 - H_0 \end{bmatrix}.$$

Moreover, as above, if we target a specific variance-to-expectation ratio, conditionally a given trajectory of temperatures between dates 1 and t^*, we obtain μ_H since, using (35):

$$\mu_N = \frac{\overline{\mathbb{V}ar}_0(H_{t^*} | \underline{T_{AT,t^*}})}{2 \overline{\mathbb{E}}_0(H_{t^*} | \underline{T_{AT,t^*}})}. \tag{IV.8}$$

Appendix V. Power utility

This appendix develops a version of the model where agents feature time-separable power-utility preferences. Specifically, we consider the following time-separable intertemporal utility function:

$$U_t = \mathbb{E}_t \left(\sum_{k=0}^{\infty} \delta^k \frac{C_{t+k}^{1-\gamma}}{1-\gamma} \right). \tag{V.1}$$

V.1. **Consumption growth.** In that case, the Euler equation associated with capital is:

$$1 = \mathbb{E}_t \Big(\delta \left(\frac{C_{t+1}}{C_t} \right)^{-\gamma} \underbrace{\{(1 - \Lambda_{t+1}) A_{t+1} + 1 - dep\}}_{\approx \exp(\mu_{c,t+1} - \log \delta + \sigma_{c,t+1} \varepsilon_{A,t+1})} \exp(-D_{t+1} - b_{SK} \Delta H_{t+1}) \Big),$$

where $\mu_{c,t}$ and $\sigma_{c,t}$ are given in (17).

Hence, Δc_{t+1} must satisfy:

$$1 = \mathbb{E}_t \big(\exp(-\gamma \Delta c_{t+1} + \mu_{c,t+1} + \sigma_{c,t+1} \varepsilon_{A,t+1} - D_{t+1} - b_{SK} \Delta H_{t+1}) \big),$$

Therefore, a solution for consumption growth is given by $\Delta c_t = \mu_{c,0,t} + \mu'_{c,1,t} X_t$ where $\mu_{c,0,t}$ and $\mu_{c,1,t}$ are such that:

$$\Delta c_t = \mu_{c,0,t} + \mu'_{c,1,t} X_t := \frac{1}{\gamma} \left(\mu_{c,t+1} + \sigma_{c,t+1} \varepsilon_{A,t+1} - D_{t+1} - b_{SK} \Delta H_{t+1} \right).$$

V.2. **Solving for the utility function.** As in our baseline (Epstein-Zin) approach, agents determine the trajectory of mitigation rates on the initial date. Specifically, they solve (VI.2). We therefore need to compute the utility, which we obtain as follows:

$$\begin{aligned} U_t &= \frac{C_t^{1-\gamma}}{1-\gamma} \Bigg(1 + \sum_{k=1}^{\infty} \delta^k \exp((1-\gamma)(\mu_{c,0,t+1} + \cdots + \mu_{c,0,t+k})) \times \\ &\qquad \exp\left(\psi_{0,t}^{(k)}(u_1, \ldots, u_k) + \psi_{1,t}^{(k)}(u_1, \ldots, u_k)' X_t \right) \Bigg), \end{aligned} \tag{V.2}$$

with $u_k = (1-\gamma)\mu_{c,1,t+k}$, and where functions $\psi_{0,t}^{(k)}$ and $\psi_{1,t}^{(k)}$ are determined in Proposition 3.

V.3. **Social Cost of Carbon.** Eq. (V.2) implies, in particular, that the SCC is given by:

$$\begin{aligned} SCC_t &= -\frac{\partial U_t}{\partial M_{AT,t}} \Big/ \frac{\partial U_t}{\partial C_t} \\ &= \frac{C_t}{\gamma - 1} \sum_{k=1}^{\infty} \delta^k \psi_{1,t,M_{AT}}^{(k)}(u_1, \ldots, u_k) \exp((1-\gamma)(\mu_{c,0,t+1} + \cdots + \mu_{c,0,t+k})) \times \\ &\qquad \exp\left(\psi_{0,t}^{(k)}(u_1, \ldots, u_k) + \psi_{1,t}^{(k)}(u_1, \ldots, u_k)' X_t \right), \end{aligned}$$

where $\psi_{1,t,M_{AT}}^{(k)}(u_1, \ldots, u_k)$ denotes the component of vector $\psi_{1,t}^{(k)}((u_1, \ldots, u_k)$ associated with the carbon concentration $M_{AT,t}$.

Remark: It can be noted that, in the power-utility context (eq. V.1), we also have:

$$\begin{aligned} SCC_t &= -\frac{\partial U_t}{\partial M_{AT,t}} \Big/ \frac{\partial U_t}{\partial C_t} = -\mathbb{E}_t \left(\sum_{k=0}^{\infty} \frac{\partial C_{t+k}}{\partial M_{AT,t}} \delta^k C_{t+k}^{-\gamma} \right) \Big/ C_t^{-\gamma} \\ &= \mathbb{E}_t \left(\sum_{k=0}^{\infty} \mathcal{M}_{t,t+k} \mathcal{B}_{t,t+k} \right), \end{aligned} \tag{V.3}$$

where $\mathcal{B}_{t,t+k} = -\frac{\partial C_{t+k}}{\partial M_{AT,t}}$ is the consumption benefit, for date $t+k$, resulting from a one-ton reduction in carbon dioxide in the atmosphere on date t. Because $\mathcal{B}_{t,t+k}$ and $\mathcal{M}_{t,t+k}$ are correlated (conditional on the information available on date t), it comes that the SCC is different

from the net present value of future $\mathcal{B}_{t,t+k}$. More precisely, we have:

$$SCC_t = \underbrace{\sum_{k=0}^{\infty} \mathbb{E}_t\left(\mathcal{M}_{t,t+k}\right)\mathbb{E}_t\left(\mathcal{B}_{t,t+k}\right)}_{\text{net present value of future benefits}} + \underbrace{\mathbb{C}ov_t\left(\sum_{k=0}^{\infty}\mathcal{M}_{t,t+k}, \mathcal{B}_{t,t+k}\right)}_{\text{risk premiums}}. \tag{V.4}$$

When benefits tend to be higher in bad states of the work (states of high marginal utility of consumption; high SDF), then the covariance term is positive. In that case, the SCC is larger than the net present value of future benefits. This corresponds to a situation of negative climate beta (see Dietz et al., 2018; Lemoine, 2021).

V.4. **Stochastic discount factor and pricing.** The stochastic discount factor is given by $\mathcal{M}_{t,t+1} = \delta\exp(-\gamma\Delta c_{t+1})$. Using the same notations as in (20), we have:

$$\mathcal{M}_{t,t+1} = \exp[-(\mu_{r,0,t+1} + \mu'_{r,1,t+1}X_t) + \Pi'_{t+1}X_{t+1} \underbrace{-\alpha_t(\Pi_{t+1}) - \beta_t(\Pi_{t+1})'X_t}_{=-\psi_t(\Pi_{t+1}),\text{ see eq. (18)}}], \tag{V.5}$$

where

$$\begin{cases} \Pi_{t+1} &= -\gamma\mu_{c,1,t+1} \\ \mu_{r,0,t+1} &= -\log\delta + \gamma\mu_{c,0,t+1} - \alpha_t(\Pi_{t+1}) \\ \mu_{r,1,t+1} &= -\beta_t(\Pi_{t+1}). \end{cases} \tag{V.6}$$

Using these notations, all the pricing formulas presented in Appendix III remain valid.

V.5. **Model outputs.** Table V.1 shows model outputs based on the power-utility version of the model. This table can be compared with Table 3 in the main text.

It appears that, for risk aversion parameters that are substiantially above one, SCCs estimates are much smaller than with Epstein-Zin preferences. This essentially comes from the fact that, in the CRRA case, discount rates increase with risk aversion (see Panel D), which reduces the net present value of the future benefits associated with reductions of carbon in the atmosphere; this echoes the results of Daniel, Litterman, and Wagner (2019).

Panel C reports the difference between the SCC and the net present value of the benefits resulting from a reduction of one ton of carbon dioxide in the atmosphere. The sign of this object is the opposite of that of the climate beta (see remark below eq. V.3). Consistently with the analysis developed in Dietz et al. (2018) and Lemoine (2021), we find negative climate betas (i.e., positive risk premiums) when there is no uncertainty associated with the exogenous technological process ($\sigma_A = 0$, see eq. 10).

TABLE V.1. Sensitivity of SCC and risk premium estimates, power utility case

A. Social Cost of Carbon (in U.S. $ per ton of CO_2)						
Specification	$\gamma = 1.001$		$\gamma = 1.5$		$\gamma = 2.5$	
Baseline	**160**		**47**		**8**	
Deterministic model	157	*−2%*	45	*−3%*	8	*−5%*
No exog. techno. uncertainty ($\sigma_A = 0$)	160	*−0%*	47	*−0%*	8	*−1%*
No damage uncertainty ($\mu_D = 0$)	157	*−2%*	46	*−3%*	8	*−3%*
Small damages (twice lower)	77	*−52%*	21	*−54%*	4	*−54%*
No permafrost uncertainty ($\mu_N = 0$)	160	*−0%*	47	*−0%*	8	*−0%*
No permaf. releases ($a^{(N)} = b^{(N)} = 0$)	119	*−25%*	36	*−24%*	7	*−19%*
No sea-level uncertainty ($\mu_H = 0$)	160	*−0%*	47	*−0%*	8	*−0%*
No sea-level risks ($a^{(H)} = b^{(H)} = 0$)	86	*−46%*	24	*−48%*	4	*−48%*
B. Temperature risk premium (in °C)						
Specification	$\gamma = 1.001$		$\gamma = 1.5$		$\gamma = 2.5$	
Baseline	**0.005**		**-0.003**		**-0.036**	
Deterministic model	0.000	*−0.005°C*	0.000	*+0.003°C*	0.000	*+0.036°C*
No exog. techno. uncertainty ($\sigma_A = 0$)	0.011	*+0.005°C*	0.011	*+0.014°C*	0.011	*+0.047°C*
No damage uncertainty ($\mu_D = 0$)	0.005	*−0.000°C*	-0.004	*−0.001°C*	-0.037	*−0.001°C*
Small damages (twice lower)	-0.002	*−0.007°C*	-0.012	*−0.009°C*	-0.049	*−0.013°C*
No permafrost uncertainty ($\mu_N = 0$)	-0.005	*−0.010°C*	-0.013	*−0.010°C*	-0.046	*−0.010°C*
No permaf. releases ($a^{(N)} = b^{(N)} = 0$)	-0.006	*−0.011°C*	-0.014	*−0.011°C*	-0.046	*−0.010°C*
No sea-level uncertainty ($\mu_H = 0$)	0.005	*−0.000°C*	-0.003	*−0.000°C*	-0.036	*−0.000°C*
No sea-level risks ($a^{(H)} = b^{(H)} = 0$)	-0.001	*−0.006°C*	-0.011	*−0.008°C*	-0.047	*−0.011°C*
C. SCC minus NPV of benefits (expressed in percent of SCC)						
Specification	$\gamma = 1.001$		$\gamma = 1.5$		$\gamma = 2.5$	
Baseline	**-2.3**		**-1.1**		**-0.7**	
Deterministic model	-0.0	*+2.3 p.p.*	-0.0	*+1.1 p.p.*	-0.0	*+0.7 p.p.*
No exog. techno. uncertainty ($\sigma_A = 0$)	0.2	*+2.4 p.p.*	1.5	*+2.6 p.p.*	2.1	*+2.8 p.p.*
No damage uncertainty ($\mu_D = 0$)	-2.4	*−0.1 p.p.*	-2.2	*−1.1 p.p.*	-2.4	*−1.7 p.p.*
Small damages (twice lower)	-1.8	*+0.5 p.p.*	-1.7	*−0.5 p.p.*	-1.8	*−1.1 p.p.*
No permafrost uncertainty ($\mu_N = 0$)	-2.2	*+0.0 p.p.*	-1.3	*−0.2 p.p.*	-0.8	*−0.1 p.p.*
No permaf. releases ($a^{(N)} = b^{(N)} = 0$)	-1.7	*+0.6 p.p.*	-0.9	*+0.2 p.p.*	-0.6	*+0.1 p.p.*
No sea-level uncertainty ($\mu_H = 0$)	-2.3	*−0.1 p.p.*	-1.3	*−0.2 p.p.*	-1.0	*−0.3 p.p.*
No sea-level risks ($a^{(H)} = b^{(H)} = 0$)	-0.8	*+1.5 p.p.*	0.2	*+1.3 p.p.*	0.6	*+1.3 p.p.*
D. Long-term rate (in percent; maturity: 2100)						
Specification	$\gamma = 1.001$		$\gamma = 1.5$		$\gamma = 2.5$	
Baseline	**2.86**		**3.64**		**5.21**	
Deterministic model	2.88	*+2 bps*	3.68	*+3 bps*	5.27	*+7 bps*
No exog. techno. uncertainty ($\sigma_A = 0$)	2.87	*+1 bps*	3.66	*+2 bps*	5.26	*+5 bps*
No damage uncertainty ($\mu_D = 0$)	2.87	*+1 bps*	3.65	*+1 bps*	5.22	*+1 bps*
Small damages (twice lower)	2.99	*+14 bps*	3.78	*+13 bps*	5.34	*+13 bps*
No permafrost uncertainty ($\mu_N = 0$)	2.86	*+0 bps*	3.64	*+0 bps*	5.21	*+0 bps*
No permaf. releases ($a^{(N)} = b^{(N)} = 0$)	2.91	*+5 bps*	3.69	*+5 bps*	5.26	*+5 bps*
No sea-level uncertainty ($\mu_H = 0$)	2.86	*+0 bps*	3.65	*+0 bps*	5.21	*+0 bps*
No sea-level risks ($a^{(H)} = b^{(H)} = 0$)	2.96	*+10 bps*	3.75	*+10 bps*	5.31	*+10 bps*

Notes: This table illustrates the sensitivity of the SCC and of other model outputs. The SCC is expressed in U.S. $ per ton of carbon dioxide. The temperature risk premium corresponds to the difference between the risk-adjusted and physical expectations of temperature and SLR in 2100 (see Subsection 4.2.2). See Subsection V.5 for explanations regarding Panel C. The long-term rate (Panel D) is the model-implied 2020 real rate of maturity 2100. The deterministic model is a model where we remove all sources of uncertainty ($\mu_D = \mu_N = \mu_T = \mu_H = \sigma_A = 0$). Values in italics indicate changes from the baseline case. In the "Small damages" scenario, both $\lambda_{D,t}$ (eq. 13) and $\lambda_{H,t}$ (eq. 8) are divided by 2. "p.p." stands for percentage points; "bps" stands for basis points; "NPV" stands for net present value.

APPENDIX VI. ADDITIONAL RESULTS

VI.1. **Relationship between carbon concentrations and radiative forcing.** Following, e.g., Nordhaus (2017), we consider the following relationship between radiative forcing and carbon concentration:

$$F_t - F_{EX,t} = \tau \log_2 \left(\frac{M_{AT,t}}{M_{PI}} \right), \tag{VI.1}$$

where M_{PI} stands for preindustrial concentration of carbon in the atmosphere.

This formulation implies that τ corresponds to the increase in radiative forcing resulting from a doubling of atmospheric carbon concentration.

Linearizing (VI.1) at $\frac{M_{AT,t}}{M_{PI}} = m_0$ gives (4), that is:

$$F_t = \tau \log_2(m_0) + \frac{\tau}{\log(2) m_0} \left(\frac{M_{AT,t}}{M_{PI}} - m_0 \right) + F_{EX,t}.$$

In order to optimize the range of values of atmospheric carbon masses for which the linearization will be relevant, we take a value of m_0 that is consistent with the average carbon concentrations that will prevail between 2020 and 2100. More precisely, we take $m_0 = \frac{\overline{M}_{AT}}{M_{PI}}$, where $\overline{M}_{AT}$ is the 2020-2100 average of carbon masses underlying the RCP 4.5 and 6.0 scenarios established by the IPCC.

Panel (a) of Figure VI.1 compares (VI.1) to its linearized version (4). Panel (b) shows the model-implied distribution of carbon concentrations for two future dates, 2050 and 2100. Together, these two panels suggest that, for the most likely values of future carbon masses, the first-order approximation of (VI.1) is of good quality.

VI.2. **On the optimality of the mitigation process.** To get instant results, the agents are not allowed to re-optimize the mitigation rate μ_t on each date. Instead, they decide the mitigation rate path (μ_t) only once and for all on the initial date, and further commit to that parametric path. Formally, they solve

$$\{\theta_{a,opt}, \theta_{b,opt}\} := \underset{\theta_a, \theta_b}{\operatorname{argmin}}\ u_0[\mu_1(\theta_a, \theta_b), \ldots, \mu_k(\theta_a, \theta_b), \ldots], \tag{VI.2}$$

where the utility u is given in Proposition 8, and where the parametric form is (this is eq. 15):

$$\mu_t(\theta_a, \theta_b) = \min\left[\exp\left(-|\theta_a| + |\theta_b| \times t\right); 1\right], \quad t > 0.$$

This parametric time function is inspired by the usual forms of emission control rates obtained in standard IAMs (see, e.g., Cai and Lontzek, 2019, Figure 2.C). Panel (a) of Figure VI.1 displays our model-implied emission control rate μ_t (black solid line). For the sake of comparison, the figure also shows the emission control rate prevailing in the 2016 version of the DICE model (Nordhaus, 2017) (grey dashed line).

FIGURE VI.1. Relationship between radiative forcing and atmospheric carbon concentration

(a) Relationship between radiative forcings and atmospheric carbon concentration

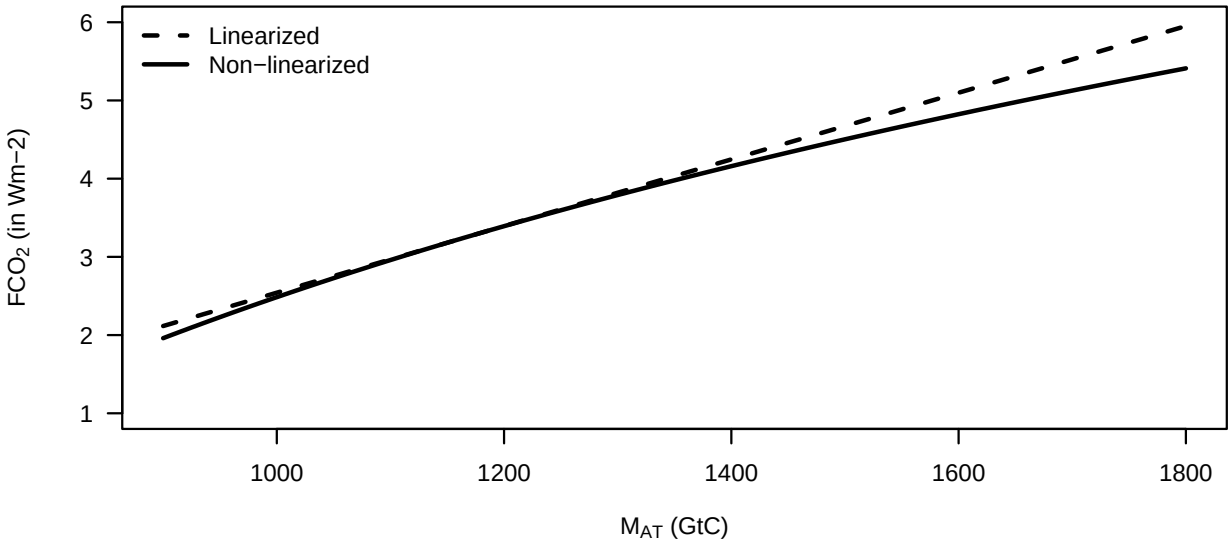

(b) Atmospheric carbon concentration p.d.f.

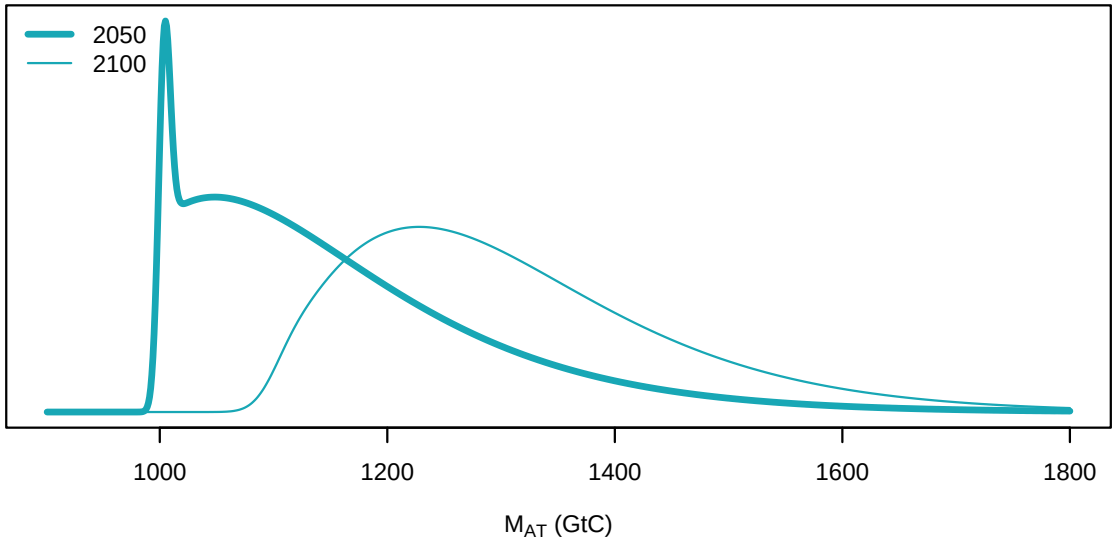

Notes: This figure illustrates the quality of the first-order approximation of (VI.1). In Panel (a), the solid line (respectively the dashed line) represents the conditional expectation $\mathbb{E}(F_t - F_{EX,t}|M_{AT,t})$ resulting from the non-linear equation (VI.1) (resp. from the equation 4, that is its first-order approximation at m_0). Panel (b) displays the distributions of $M_{AT,t}$ for two dates t (2050 and 2100).

Our approach does not allow abatement to respond to jumps in damages or emissions. Arguably, such a response would mitigate some of the risk studied here; moreover, it may introduce a policy component to risk, which is missing here. In order to assess these potential shortcomings, we proceed to two exercises:

FIGURE VI.2. Mitigation rate

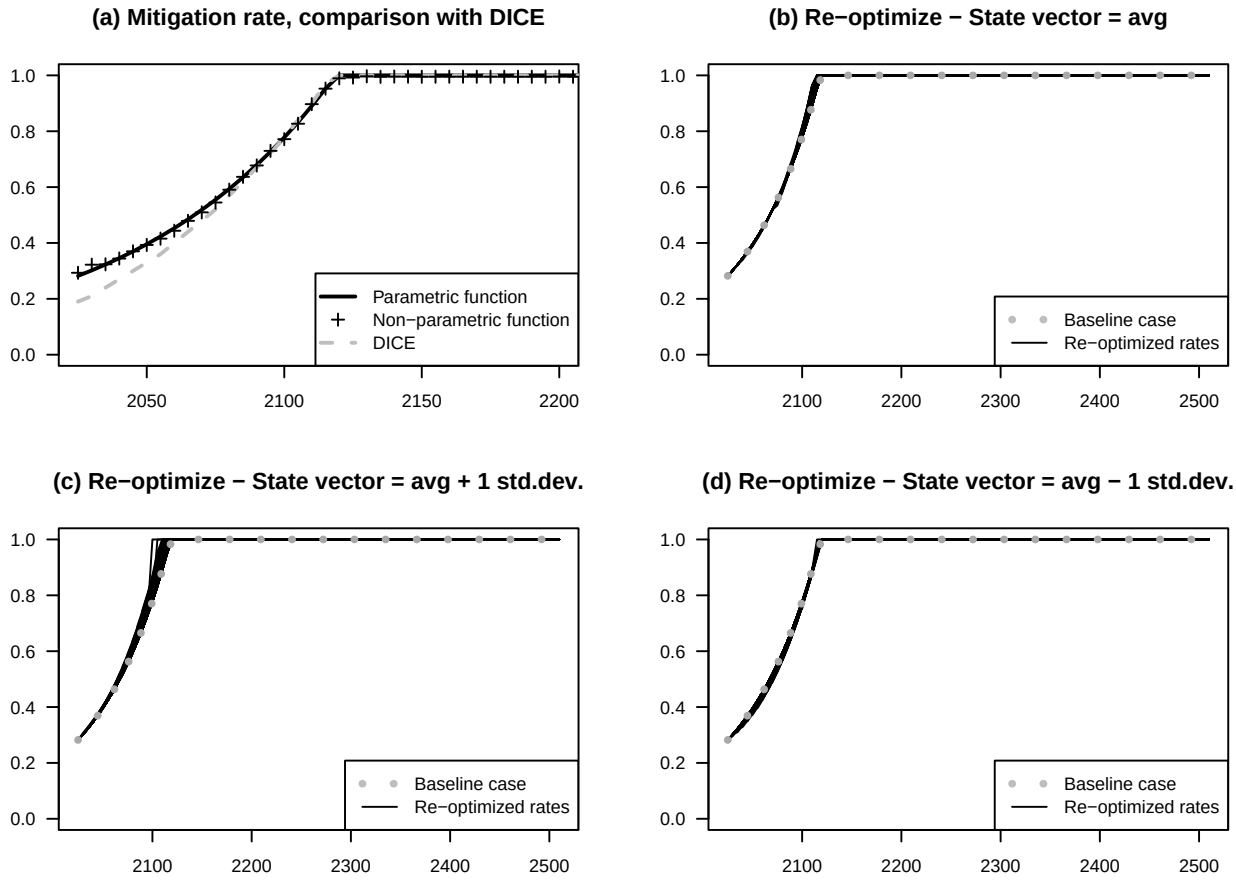

Notes: The grey dashed line in Panel (a) represents the mitigation rate of the 2016 version of the DICE (Nordhaus, 2017). In Panel (a), the black solid line is our baseline sequence of mitigation rates, resulting from problem (VI.2). The crosses are the solutions to the same type of problem, but without using a parametric formulation for the μ_t's (see problem VI.3). Panels (b) to (d) display the sequences of μ_t resulting from re-optimizations taking place at later periods: for each date t, we determine the pair $\{\theta_{a,opt}, \theta_{b,opt}\}_t$ that maximizes $u_t[\mu_{t+1}(\theta_a, \theta_b), \ldots, \mu_{t+k}(\theta_a, \theta_b), \ldots]$ (see problem VI.4). These optimizations depend on the value of the state vector on date t (X_t). We consider three cases: X_t is set at $\mathbb{E}_0(X_t)$ (Panel (b)); X_t is set at $\mathbb{E}_0(X_t) + SD_0(X_t)$ (Panel (c)); X_t is set at $\mathbb{E}_0(X_t) - SD_0(X_t)$ (Panel (d)), where $SD_0(X_t)$ denotes the vector of standard deviations of X_t, conditional on date 0.

(i) We replace the parametric function (15) with a complete sequence of μ_t's that the agents determine on date 0. That is, we replace (VI.2) with:

$$\{\mu_{1,opt}, \ldots, \mu_{k,opt}, \ldots\} := \underset{\mu_1, \ldots, \mu_k, \ldots}{\operatorname{argmin}} \; u_0[\mu_1, \ldots, \mu_k, \ldots]. \tag{VI.3}$$

(ii) We look at how agents would modify the future sequence of μ_t's if they were given the chance to, for dates $t > 0$. (On each instance, they think that is the last time they

can do so.) That is, we compute a sequence of pairs $\{\theta_{a,opt}, \theta_{b,opt}\}_t$ defined by:

$$\{\theta_{a,opt}, \theta_{b,opt}\}_t := \underset{\theta_a,\theta_b}{\operatorname{argmin}}\ u_t[\mu_{t+1}(\theta_a,\theta_b),\dots,\mu_{t+k}(\theta_a,\theta_b),\dots]. \tag{VI.4}$$

Note that the solution to the previous maximization problem depends on the state vector prevailing at date t (that is X_t). Our analysis considers three different cases: $X_t = \mathbb{E}_0(X_t)$, $X_t = \mathbb{E}_0(X_t) + SD_0(X_t)$, and $X_t = \mathbb{E}_0(X_t) - SD_0(X_t)$, where $SD_0(X_t)$ denotes the vector of standard deviations of X_t, conditional on date 0.

The results of these two exercises are displayed on Figure VI.2:

(i) Panel (a) of Figure VI.2 compares the baseline case (the solution to problem VI.2) with the "non-parametric" one (problem VI.3). The results appear to be very close.

(ii) Each Panel (b) to (d) shows the results of problem (VI.4), for $t \in \{1,\dots,40\}$ (i.e., 200 years). That is, each panel reports 40 trajectories (black lines) of mitigation rates. (Trajectory t is $\{\mu_{t+1}, \mu_{t+2}, \dots\}$). The three panels differ in the value of the initial state value: X_t is set at $\mathbb{E}_0(X_t)$ in Panel (b); X_t is set at $\mathbb{E}_0(X_t) + SD_0(X_t)$ in Panel (c); X_t is set at $\mathbb{E}_0(X_t) - SD_0(X_t)$ in Panel (d), where $SD_0(X_t)$ denotes the vector of standard deviations of X_t, conditional on date 0.
The results suggest that mitigation rate trajectories are relatively insensitive to the possibility of re-optimization over time.

VI.3. **SCC risk premiums versus temperature risk premiums.** Figure VI.3 complements Figure VI.4 by comparing our results, regarding the comparison of SCC and temperature risk premiums with those resulting from alternative approaches.

Figure VI.4 was showing that, in the context of our framework, we have a positive relationship between SCC risk premiums and temperature risk premiums when varying σ_A. We recall that we define the SCC risk premium as the difference between the SCC and the sum of discounted expected benefits associated with the removal of one ton of CO_2 from the atmosphere (see eq. V.4); the temperature risk premium is the difference between the risk-adjusted temperature and its physical counterpart, for a given horizon, see Subsection 4.2.2, and more particularly (30).

Figure VI.3 displays, in black, the three curves that appear in the three plots of Figure VI.4. Coloured lines correspond to alternative modeling approaches. They are all based on the general approach of Lemoine (2021), but with different damage specifications. Following Hambel et al. (2021), the figure's legend employs "G." and "L." to refer to damages that apply to consumption growth or level, respectively. Damage specifications are from: Dell, Jones, and Olken (2009), Nordhaus and Sztorc (2013), Weitzman (2012), Barnett, Brock, and Hansen (2020), Lemoine (2021).

We see that, in all considered cases, the relationship between the SCC risk premium and the temperature risk premium is positive, both metrics are the highest when $\sigma_A = 0$. In this case ($\sigma_A = 0$), both (a) the *capital accumulation channel* (temperature premium case) and (b) the *scaling channel* (SCC case) are switched off. (See Subsection 4.2.2 for the description of these channels.) This reduces the correlations between (a) consumption and temperature and (b) consumption and benefits associated with the removal of one ton of CO_2 from the atmosphere. This tends to augment (a) the SCC risk premium and (b) the temperature risk premium.

FIGURE VI.3. Social Cost of Carbon and temperature risk premiums

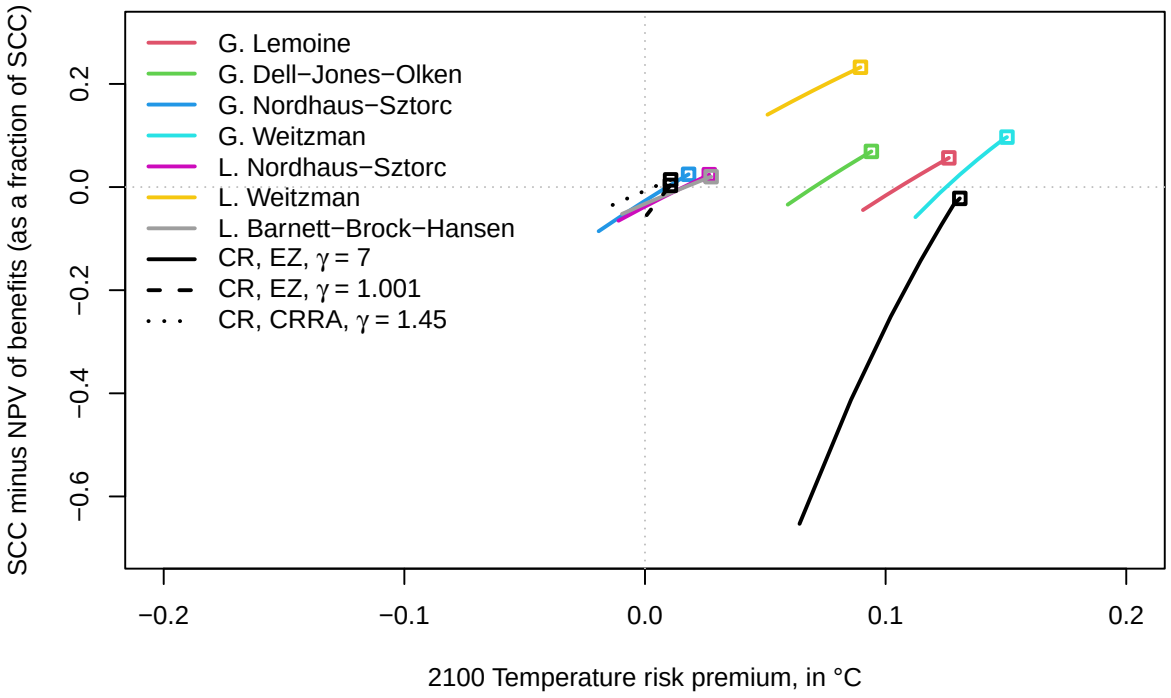

Notes: This figure shows the relationship between SCC and temperature risk premiums. The x-axis coordinates are 2100 temperature risk premiums—the difference between the risk-adjusted and the physical expectation of temperature. The y-axis coordinate is the difference between the SCC and the sum of discounted expected benefits associated with the removal of one ton of CO_2 from the atmosphere, expressed as a fraction of the SCC. Each line corresponds to one specific model, using varying degrees of consumption volatility, from zero (indicated with squares) to twice its baseline value (this volatility corresponds to parameter σ_A in our framework; see eq. 10). The black lines are obtained with our model, using Epstein-Zin or power-utility preferences (the black solid line corresponds to our baseline case). The coloured lines are based on Lemoine (2021)'s model (considering the 200-year SCC), but with different types of damage functions. Following Hambel et al. (2021), the "G." and "L." of the legend refer to damages applying to consumption growth or level, respectively. Growth-based damage specifications are as follows: $-0.00026T$ for Nordhaus and Sztorc (2013), $-0.0018T$ for Lemoine (2021), $-0.00137T$ for Dell et al. (2009), $-0.000075T^{3.23}$ for Weitzman (2012). Level-based damages take the form of multiplicative factors that reduce consumption; they are as follows: $1/(1+[T/20.64]^2+[T/6.081]^{6.754})$ for Weitzman (2012), $\exp(-0.0127T-0.0005T^2-0.005(T-2)_+^2)$ for Barnett et al. (2020), and $1/(1+0.00266T^2)$ for Nordhaus and Sztorc (2013).

VI.4. **Sensitivity analysis.** This subsection presents the results of an analysis where we examine the sensitivity of the main outputs of our study (Social Cost of Carbon, temperature risk premiums, long-term rates) to the model calibration.

As explained in Subsection 3.5 and in Supplemental Appendix IV, we calibrate our model by matching a set of moments (listed in Table 1, in italics). We proceed with the following exercise: we draw novel sets of targeted moments in uniform distributions with support of the form $[0.5 \times m_i, 1.5 \times m_i]$, where m_i is the i^{th} moment considered in the baseline calibration. For each novel set of targeted moments, we solve the model and compute measures of interest (SCC, risk premiums, and long-term real interest rate). We do that for four different pairs of risk aversion (γ) and preference for present (δ). Specifically, we consider two values of γ (the first is that used in the baseline calibration, 7, and the second is a smaller value, 2) and two values of δ (the first is based on the same annual rate of preference for present as in our baseline calibration, 1.5%, and the second is a smaller value, 1%).

The results are represented in Figure VI.4, in the form of boxplots. In line with the literature, the results suggest that the SCC is particularly sensitive to δ (the lower the rate of preference for present, the higher the SCC) and, to a lesser extent, to γ (the higher the risk aversion, the higher the SCC). Panels (b) and (c) show that the temperature and SLR risk premiums strongly depend on risk aversion; Panel (b) also shows that the temperature risk premium is negative for only a minority of calibrations.

VI.5. **Housing prices.** In this example, we use our framework to price housing at risk of sea level rise.[44] We follow Meese and Wallace (1994) or Clayton (1996) and compute the house price as the present discounted value of future imputed rents (akin to the classical valuation methodology of Gordon, 1962):

$$House_t = \sum_{h=1}^{\infty} \mathbb{E}_t(\mathcal{M}_{t,t+h} R_{t+h}), \tag{VI.5}$$

where R_t denotes the imputed rent yielded by this house. Considering coastal housing, we assume that R_t becomes null if H_t, the sea level, reaches a given threshold ($\overline{H}$, say). We further assume that, as long as $H_t < \overline{H}$, the log growth rate of R_t is affine in X_t, that is:

$$\log R_t = \log R_{t-1} + \mu_{R,0} + \mu'_{R,1} X_t.$$

[44] The literature on SLR and house prices is growing fast (See, e.g., Bernstein et al., 2019; Keys and Mulder, 2020; Murfin and Spiegel, 2020; Goldsmith-Pinkham et al., 2023).

FIGURE VI.4. Sensitivity analysis

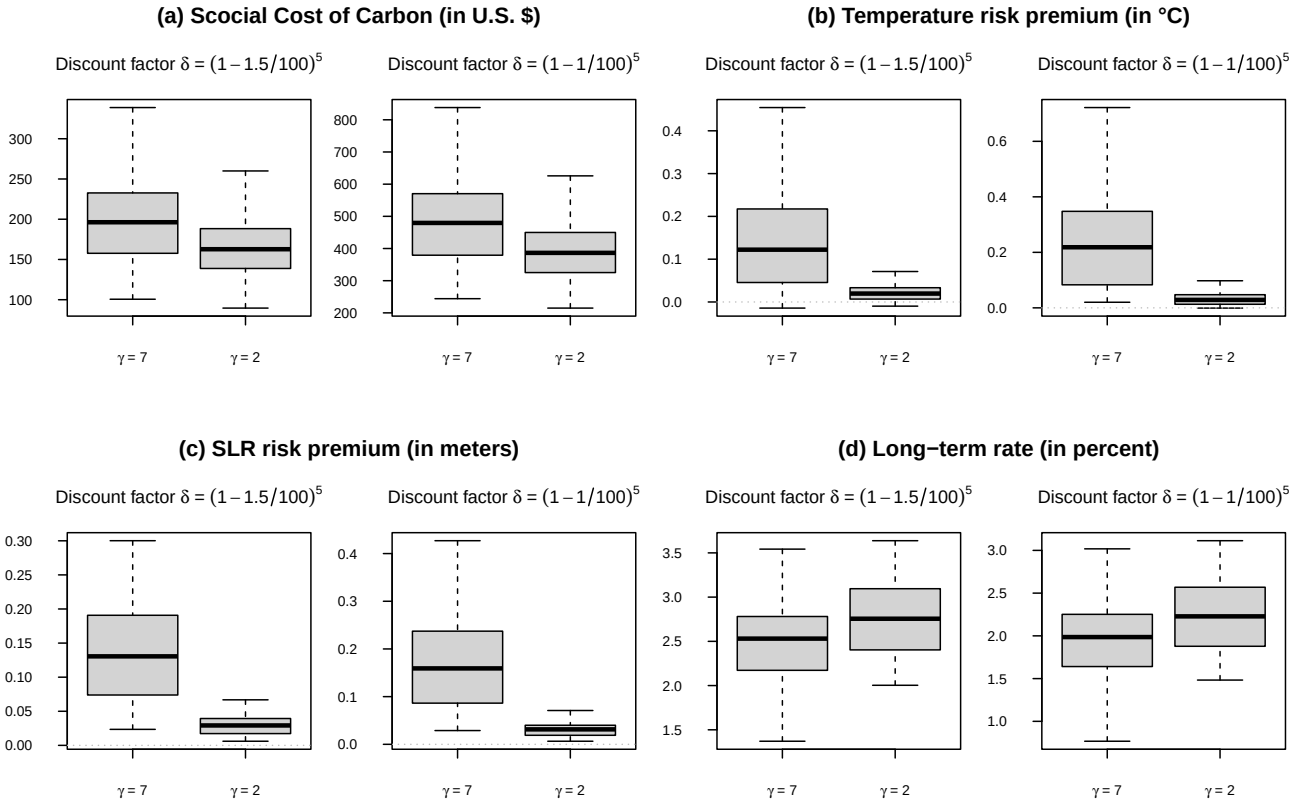

Notes: This figure illustrates the sensitivity of four model outputs to the calibration. See Subsection VI.4 for details regarding the simulation exercise. The social cost of carbon is expressed in U.S.$ per ton of carbon dioxide in 2020. The temperature and sea-level-rise risk premiums correspond to the difference between the risk-adjusted and physical expectations of temperature and SLR in 2100, respectively (see Subsection 4.2.2). The long-term rate is the model-implied 2020 real rate of maturity 2100. The grey box indicates the interquartile range (IQR, from the 25th to the 75th percentiles); the upper (respectively lower) whisker is located at the smaller (resp. larger) of the maximum (resp. minimum) value and $Q_3 + 1.5IQR$ (resp. $Q_1 - 1.5IQR$) where Q_1 and Q_3 respectively denote the 25th and 75th percentiles.

If $\log R_t = \mu_R' X_t$, equation (VI.5) then becomes:

$$\begin{aligned} House_t &= \sum_{h=1}^{\infty} \mathbb{E}_t \left(\mathcal{M}_{t,t+h} R_0 \exp(\mu_R' X_{t+h}) \mathbb{1}_{\{H_{t+h} < \overline{H}\}} \right) \\ &= R_0 \sum_{h=1}^{\infty} \hat{\varphi}_t^{(h)}(\mu_R, \mu_H, \overline{H}), \end{aligned}$$

where μ_H is the selection vector that is such that $H_t = \mu_H' X_t$.

Figure VI.5 presents the results of a numerical example where, for the sake of simplicity, we consider that imputed rents, excluding sea-level effects, simply grow at a constant real rate, of 2%, and $\mu_{R,1} = 0$. The orange line in Panel (a) shows how house prices depend on $\overline{H}$.

It is naturally increasing, since the higher $\overline{H}$, the lower the SLR exposure of the house. For high values of $\overline{H}$, the price converges to $House_{n.e.} = R_0 \sum_{h=1}^{\infty} \exp(h\mu_{R,0}) \mathbb{E}_t(\mathcal{M}_{t,t+h})$, that is the price of a house that is not exposed (n.e.) to SLR.[45] Panel (a) also shows, in blue, the sum of expected payoffs, discounted using the risk-free rates (blue line). If agents were not risk averse, or if the sea-level did not correlate with the SDF, the two lines would coincide. Alternatively put, the difference between the two curves captures housing SLR risk premiums. This premium is negative, reflecting the positive exposure of housing to SLR. Panel (b) of Figure VI.5 shows for instance that risk premiums reduce house prices by about 3% when $\overline{H} = 1$ meters. The share of housing SLR premiums diminishes and goes to zero since because both the blue and the orange lines converge to $House_{n.e.}$ for large values of $\overline{H}$.

On both panels of Figure VI.5, the dashed line correspond to a situation where sea level rise has a stronger adverse effect on capital—which we obtain by doubling b_{SK} in (12). House prices are then higher because growth is lower, which reduces discount rates. Panel (a) shows that risk premium are relatively more important in this situation; in this case, the covariance between imputed payoffs and SDF is higher.

[45] The convergence takes place for values of $\overline{H}$ that are larger than several meters, as the model predicts that such levels of SLR may be reached in the coming centuries. Comparable values are also obtained, e.g., by Garner et al. (2017), who consider horizons extending to 2300.

FIGURE VI.5. Sea level rise and housing prices

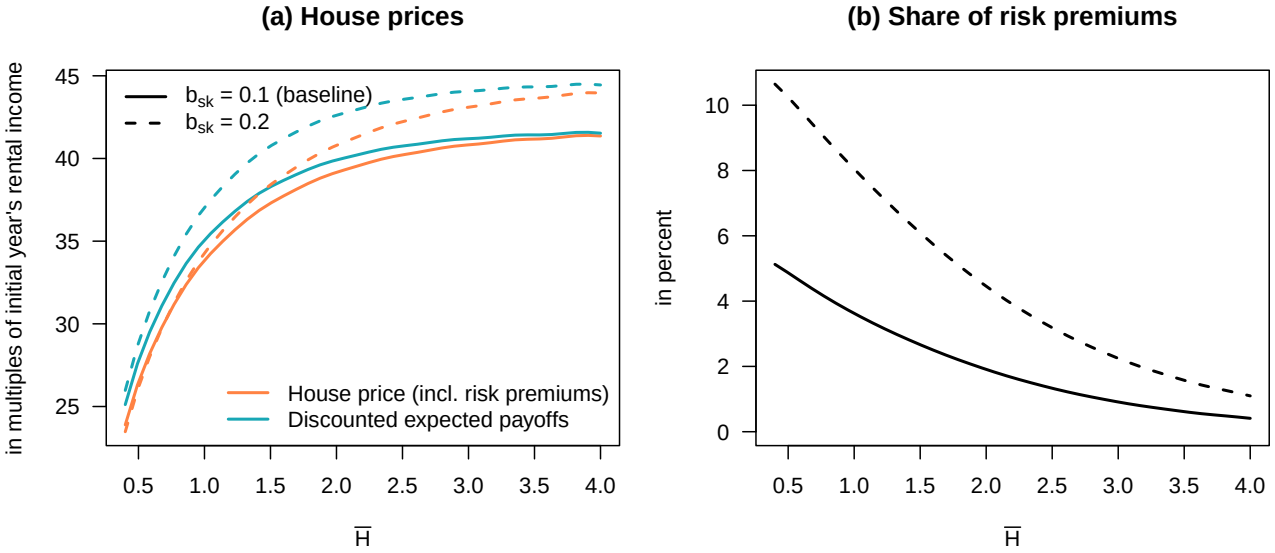

Notes: This figure illustrates the influence of sea level rise (SLR) on house prices. House prices (orange lines) are computed as the sums of discounted values of future of future imputed rents ($\sum_h^H \mathbb{E}_0(\mathcal{M}_{0,h} R_h)$, with $H = 500$ years, see eq. VI.5). Imputed rents (R_h) grow at a constant rate (set at the before-damage average growth rate of the economy) but drop to zero when $H_t > \overline{H}$. The blue line shows the sums of the discounted values of expected payoffs ($\sum_h^H \mathbb{E}_0(\mathcal{M}_{0,h})\mathbb{E}_0(R_h)$). The latter do not take into account the correlation between the SDF and sea level (that affects imputed rents). Accordingly, the difference between the blue and orange lines correspond to risk premiums; their relative importance is shown on the right hand-side plot. Dashed lines correspond to a situation where sea level has a stronger adverse effect on capital (higher b_{SK} parameter in eq. 12).